Technische Universität München
Fakultät für Maschinenwesen
Lehrstuhl für Carbon Composites

Process development and validation of thermoplastic complex shape thermoforming

Petra Fröhlich

Vollständiger Abdruck der von der Fakultät für Maschinenwesen
der Technischen Universität München zur Erlangung des akademischen Grades eines

Doktor-Ingenieurs

genehmigten Dissertation.

Vorsitzender: Univ.-Prof. Dr. Rafael Macián-Juan

Prüfer der Dissertation:

1. Univ.-Prof. Dr.-Ing. Klaus Drechsler
2. Univ.-Prof. Dr.-Ing. Peter Mitschang,
   Technische Universität Kaiserslautern

Die Dissertation wurde am 03.08.2015 bei der Technischen Universität München eingereicht
und durch die Fakultät für Maschinenwesen am 16.03.2017 angenommen.

Abstract

Thermoplastic composite materials are coming more into focus for future, high performance applications due to their potential for cost efficient manufacturing like short processing time and high level of automation. The application of the thermoforming process for structural parts requires enhanced design freedom regarding wall thickness to allow lightweight, local reinforced part design. In this thesis, the process design of complex thermoforming was studied and validated for wall thickness variations up to10mm.

A numerical tool for process design of parts with variable wall thicknesses was developed. Experimental investigations identified that the material temperature during processing is most critical due to the risk of unmelted and degraded areas across in one part at the same time. The numerical tool considers thermodynamic heat flow mechanisms, material parameters and process conditions. Thermoforming process conditions for a semi-crystalline polymer material with 2mm-10mm wall thickness can be derived using this tool. The material used in this work was continuous carbon fiber reinforced polyphenylene sulfide. The material temperature profile of the semi-crystalline polymer during processing impacts the mechanical performance of the finished product. The impact of temperature profile variations in one part due to variable wall thickness was investigated on experimental basis. Base of comparison was shear performance. An effect of temperature profile change was found for tool temperature and material temperature above degradation onset. Cooling rate, time in melt and temperature in melt were found to have no impact on shear performance. Temperature processing window during thermoforming processing from melting temperature +30K up to degradation onset temperature was identified.

Complex thermoforming requires the manufacture of a custom-made organo sheet including a previous consolidation step. The organo sheet manufacturing was optimized regarding consolidation time and consolidation pressure in comparison with standard press consolidation recommendations under the aspect of subsequent thermoforming. Base of comparison was interlaminar shear. As a result, consolidation time and consolidation pressure were significantly reduced.

A technology evaluation comparing complex thermoforming, RTM and prepreg manufacturing showed very high potential for automated, high volume complex thermoforming. Manufacturing process of a complex part, including separate manufacturing of four subcomponents and subsequent joining, was base of comparison. The complex thermoforming process was optimized. The optimization of the consolidation process resulted in a 10% overall thermoforming process time reduction, equivalent to 2% overall part cost reduction. Higher cost saving potential was found to be material costs which are dominating the part costs at increased manufacturing numbers. Material cost make up to 75% of the total part cost. In com-

parison with other technologies, complex thermoforming was found very time and most cost efficient for automated high volume manufacturing.

Zusammenfassung

Thermoplastische Verbundwerkstoffe werden aufgrund ihrer hervorragenden Eigenschaften zunehmend in zukunftsträchtigen Fertigungstechnologien verwendet. Ihr Vorteil liegt in ihrer kosteneffizienten Verarbeitung mit kurzen Zykluszeiten bei einem hohen Automatisierungsgrad. Die Nutzung des Thermoformprozesses zur Herstellung von Bauteilen variabler Wandstärke stellt diesen vor neue Herausforderungen. Variable Wandstärken und lokale Verstärkungen müssen zur Herstellung von optimierten Leichtbauteilen realisierbar sein. Ziel dieser Arbeit ist Erstellung von Prozessierungsrichtlinien für Bauteile mit Wandstärken bis 10mm.

Es wurde ein numerisches Modell zur Prozessdefinition für Bauteile mit variabler Wandstärke entwickelt. Anhand von experimentellen Untersuchungen wurde die Materialtemperatur im Vorheizprozess als kritischer Parameter beim komplexen Thermoformen identifiziert. Das gleichzeitige Auftreten von unaufgeschmolzenen oder degradierten Bereichen innerhalb eines Bauteils muss vermieden werden und stellt eine Herausforderung an die Prozessführung dar. Im Modell wurden Wärmeflüsse, Materialkennwerte und Prozessbedingungen berücksichtigt. Am Beispiel von endlos kohlenstofffaserverstärktem Polyphenylensulfid wurden Prozessbedingungen für teilkristalline Polymere im Thermoformprozess für den Wandstärkenbereich von 2-10mm untersucht. Die Temperaturführung im Thermoformprozess beeinflusst das mechanische Verhalten eines teilkristallinen Polymers nach dem Prozess und wurde experimentell untersucht. Als Vergleichsparameter wurde die Scherfestigkeit gewählt. Werkzeugtemperatur und Materialtemperaturen oberhalb des Degradationsbeginns konnten als Einflussparameter ermittelt werden. Ein Einfluss von Abkühlrate, Zeit in der Schmelze und Temperatur in der Schmelze auf die Scherfestigkeit konnte nicht festgestellt werden. Die Variation der Temperatur wurde durch Anpassung der Prozessbedingungen sowie Änderung der Wandstärke erreicht. Ein temperaturabhängiges Prozessfenster im Bereich von 30K oberhalb der Schmelztemperatur bis zum Beginn der Polymerdegradation konnte bestimmt werden.

Komplexes Thermoformen zur Herstellung dickenvariabler Bauteile benötigt individuell gefertigte Organobleche aus endlos-kohlenstofffaservestärkten Thermoplasten, welche in einem vorausgehenden Konsolidierungsschritt hergestellt werden. Bei der Herstellung der Organobleche konnten gegenüber Herstellerempfehlungen die Parameter Zeit und Druck deutlich reduziert werden, sofern ein anschließendes Thermoformen erfolgte.

Das Potential des entwickelten Prozesses wurde in einem kostenbasierten Rechenmodell mit dem von RTM- und Prepregverfahren verglichen. Basis war die Herstellung einer Baugruppe bestehend aus vier separat gefertigten Einzelteilen sowie deren Fügung. Bei hohen Stückzahlen erwies sich das komplexe Thermoformen als kosteneffizientester Prozess. Weiterhin konnte durch die Optimierung des Konsoliderungszyklus für komplexes Thermoformen eine zehnprozentige Zeiteinsparung im gesamten Herstellungsprozess erreicht werden, was einer zweiprozentigen Kostenersparnis entspricht. Größtes Einsparpotential wurde bei den Materialkosten gefunden, welche mit 75% die Bauteilkosten bei hohen Stückzahlen dominieren.

Komplexes Thermoformen ist ein im Vergleich zu RTM- und Prepregverfahren zeiteffizienter und günstiger Prozess bei automatisierter und hochvoluminger Fertigung.

Acknowledgements

This work has been made possible by the financial support of GE Global Research / Garching, which is gratefully acknowledged.

Especially I would like to thank my supervisor Prof. Dr.-Ing. Klaus Drechsler. He has inspired me to work in the field of composites and enabled me an early introduction into research and industry with my Diploma thesis. As the head of the Institute for Carbon Composites (LCC) he has enabled me to work with thermoplastic composites including their set-up at the newly founded institute. Furthermore I am very grateful for the opportunity to combine my career as a researcher with my family life over the past three years.

Furthermore, I would like to thank Prof. Dr.-Ing. Peter Mitschang for his acceptance to review this work. It is an honor to have such a well-known expert in the field of thermoplastic composites research as a reviewer to my doctoral thesis.

The head of the process technology for matrix systems group at LCC, Dipl.-Ing. Swen Zaremba has been a great support throughout this project. His constant support, inspiration, encouragement and the technical discussions over the past five years contributed a lot of value to this work.

I would like to thank Dr. mont. Elisabeth Ladstätter for co-reviewing my work and supporting me throughout the final phase.

Moreover, I would like to thank all colleagues at LCC. The support in technical and non-technical issues, the good working atmosphere, the supporting students, the workshop, the testing team and the administration have made this work possible and enjoyable.

Finally I would like to thank my family. My parents Roswitha and Hermann Frohnapfel for their constant support within my academic career and for the many hours (and weeks) of childcare. My husband Felix and my sisters Bettina und Anja for endless support, goal-oriented discussions and the ability to keep an eye on essential things of this work and after work. And finally Leonard, Anna and Johann for distracting me from too much work and putting a smile on my face when things were rough at work.

Table of Contents

1. Introduction 1

2. State of the art 7
   - 2.1. Continuous carbon fiber reinforced thermoplastics 7
   - 2.2. Consolidation 9
   - 2.3. Thermoforming 11
   - 2.4. Impact of temperature on mechanical performance 14
     - 2.4.1. Degree of crystallization 14
     - 2.4.2. Degradation 19
   - 2.5. Heat flow during infrared heating 20
     - 2.5.1. Radiation 20
     - 2.5.2. Free convection 23
     - 2.5.3. Heat conduction 25
   - 2.6. Test specifications 26
     - 2.6.1. Flexural strength 26
     - 2.6.2. Interlaminar shear strength 27
     - 2.6.3. Curved beam strength 27
     - 2.6.4. Thermal analysis 29

3. Complex Thermoforming 31
   - 3.1. Geometry definition 32
   - 3.2. Demonstrator processing 35
     - 3.2.1. Consolidation 36
     - 3.2.2. Thermoforming 38
   - 3.3. Conclusions 43

4. Experimental investigation 45
   - 4.1. Consolidation 45
     - 4.1.1. Processing 46
     - 4.1.2. Results 48
   - 4.2. Thermoforming 54
     - 4.2.1. Processing 55
     - 4.2.2. Results 57
   - 4.3. Conclusions 62

5. Numerical tool development for thermoforming process definition 65
   - 5.1. Assumptions 66
     - 5.1.1. General 66
     - 5.1.2. Heating method specific 69

5.2. Numerical approach 72
5.2.1. Radiation heating 72
5.2.2. Free convection 78
5.2.3. Heat conduction 80
5.3. Validation 85
5.4. Evaluation 90
5.5. Conclusions 94
6. Economic tool development for cost efficiency evaluation 97
6.1. Assumptions 97
6.1.1. Processing 100
6.1.2. Cost determination 103
6.2. Evaluation 107
6.3. Conclusions 117
7. Summary 119
A. Supervised student thesis 123
B. Technology evaluation 125
C. Index of Symbols 135
D. List of Abbreviations 139
E. List of Figures 141
F. List of Tables 145
G. References 147

1. Introduction

With the growth of the global aviation market, the carbon footprint and sustainability of airplanes become more important [1–3]. Any weight savings in aviation result in reduced airplane weight, hence fuel saving or room for additional transport weight [4]. Therefore, the demand for enhanced material increases [5]. High potential is seen in fiber reinforced composites due to their ability for weight efficient design [6]. The amount of additional 500€/kg manufacturing cost can be applied in aviation per kg weight saving [7]. New developed aircrafts from leading manufacturers Airbus and Boeing have a material weight share for composite materials over 50% (Figure 1.1) [8,9].

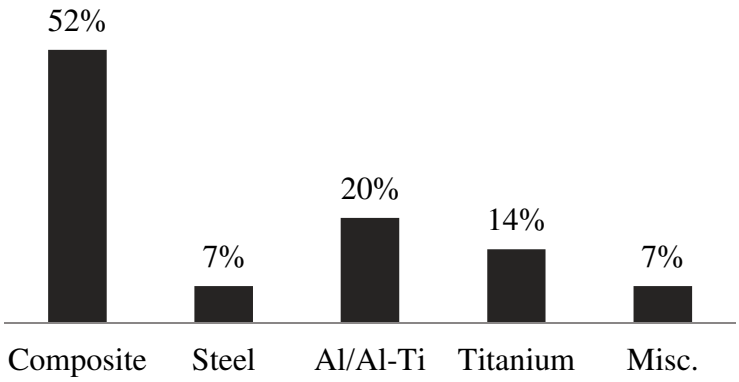

Figure 1.1 Material breakdown of A350-900 XWB, numbers from [8]

The need for cost reduction in aviation leads to research towards the production of structural composite parts in higher volumes. For the A380 vertical tail plane 10-15% less cost along with a weight saving was achieved. The component was redesigned from aluminum towards composite materials [4]. Engine turbine manufacturers General Electric have introduced and Rolls Royce plan to introduce more composite parts in their turbines for additional weight reduction [10,11].

A further example for research on composite applications in engine turbines is the European Environmentally Friendly Aero Engine (VITAL) project. Amongst others, structural vane demonstrators from engine bypasses were designed and manufactured. Beside the using prepreg technology, thermoplastic material with focus on material performance is investigated [12,13].

Fiber reinforced composites can be divided into two main material classes according to their matrix material: thermoset and thermoplastic. Thermoset polymers represent the majority. Their processing involves a curing process during manufacturing as the polymer builds up a three-dimensional molecular structure. Thermoplastics polymers have a two-dimensional molecular structure held together by secondary bonding [14].

The composite manufacturing process is chosen in dependence of the matrix material. Thermoplastic matrix materials require high processing temperatures as they have to be molten during processing. Thermoplastic polymers do not chemically react during processing, and therefore can be processed very time efficient. Their long molecular chains are already built up. Potential of thermoplastic composites lies within the opportunity for automated and cost efficient processing (Figure 1.2).

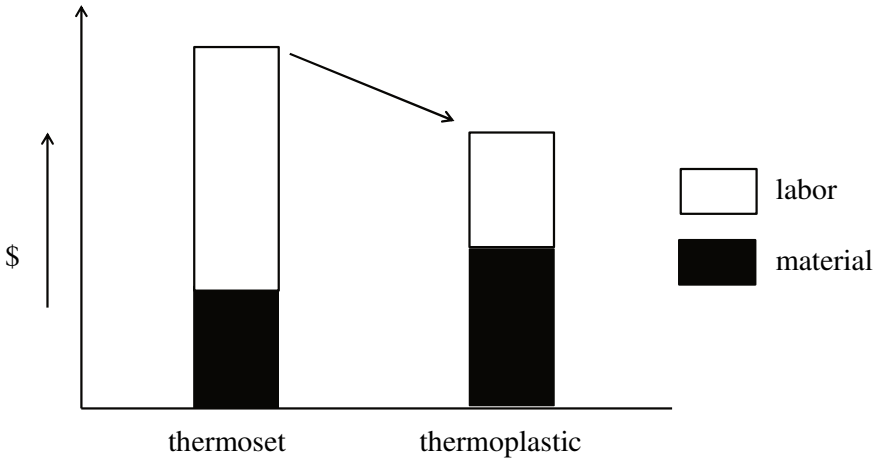

Figure 1.2 Cost advantage of thermoplastic composites [15]

Due to their excellent media resistance (fire, smoke, toxicity) and short processing times, thermoplastic composites are widely used in aircraft interior applications. More than 1500 different parts used in Airbus aircrafts are made from material of thermoplastic material supplier Tencate Advance Composites [16]. First introduction of thermoplastic composites in aviation was in the 1980's in vertical fins (CF/PEEK) and in floor panels (CF/PEI) [17]. First primary thermoplastic composite structure was built in mid-1990s in Gulfstream business jets (CF/PEI) (Figure 1.3) [18].

High potential parts for thermoplastic reinforced composites are wings (torsion boxes), fuselage, tail surfaces, pylons and doors [19,20]. Breakthrough for thermoplastic composite application was the implementation of welding for the A380 J-nose ribs to the outer structure in series [21]. Thermoplastic welding is a joining technique which does require neither curing nor additional riveting. A welding, hence joining cycle is done within minutes [15].

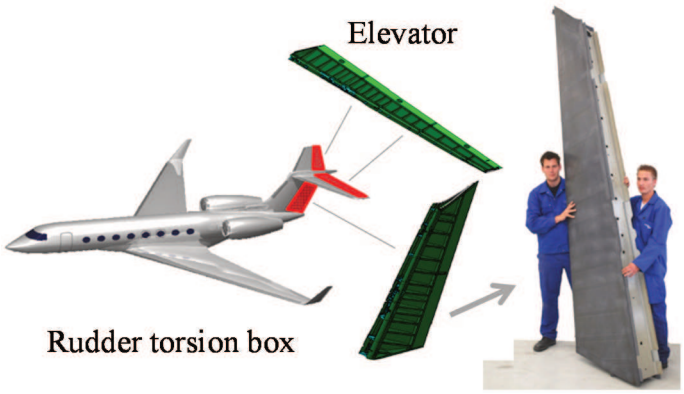

Figure 1.3 Primary thermoplastic composite structures in Gulfstream [22]

A common process for thermoplastic composite manufacturing is the thermoforming process. Thermoforming is a stamp forming process with the ability for automated, high volume production. Material is heated up to melting and subsequently formed and cooled in an adjacent press. Process time is within minutes. Thermoforming is able to manufacture high performance parts [23]. Performance of thermoformed thermoplastic composites for structural aviation application is investigated and proven in research EU-projects (TAPAS, VITAL) and applications (DO 328 flap ribs, A380 J-Nose ribs, A350XWB clips) [13,20,24–26].

Application range for thermoplastic composites using thermoforming is still limited due to the limitation of preform design freedom regarding geometry and wall thickness. In state of the art processes constant, limited wall thickness organo sheets are processed. These thermoformed parts are mainly used for joining onto larger structures. Process recommendations and set-up have been developed for these thin-walled, constant wall thickness parts.

Aviation parts require part design in dependence of function and loads. The possibility for complex geometry design including variable and local high wall thickness is required. The ability to process more complex structural parts would open the potential for a wider range of producible geometries and parts manufactured by the thermoforming process. Processing complex parts arises several challenges on the thermoforming process regarding temperature control and process efficiency. Therefore, process control and efficiency regarding complex shape processing must be investigated and defined.

Objective of this work is the generation of a basic understanding of the processing challenges and potentials of complex thermoforming. Complex thermoforming describes the thermoplastic composites part manufacturing with variable wall thickness up to 10mm. The specific process conditions provided by the material supplier cannot be fulfilled with complex geometries. Organo sheets of variable wall thickness require an enhanced range of processing temperatures. A process design in dependence of wall thickness is necessary. A process chart of the complex thermoforming process is given in Figure 1.4. Geometric details for complex geometry thermoforming are defined. A generic geometry will be defined and the process chain from organo sheet manufacturing to the final part will be studied.

Focus of the experimental part of this work is the optimization of consolidation process of the complex organo sheet manufacturing and investigation of temperature impact during infrared heating phase of thermoforming. A process window defining infrared heating temperature limits is derived from the results. Further, a numerical tool is developed to predict material temperature development during infrared heating in dependence of wall thickness within the process window. Additionally, an economic efficiency evaluation tool is set up to compare the thermoforming manufacturing process.

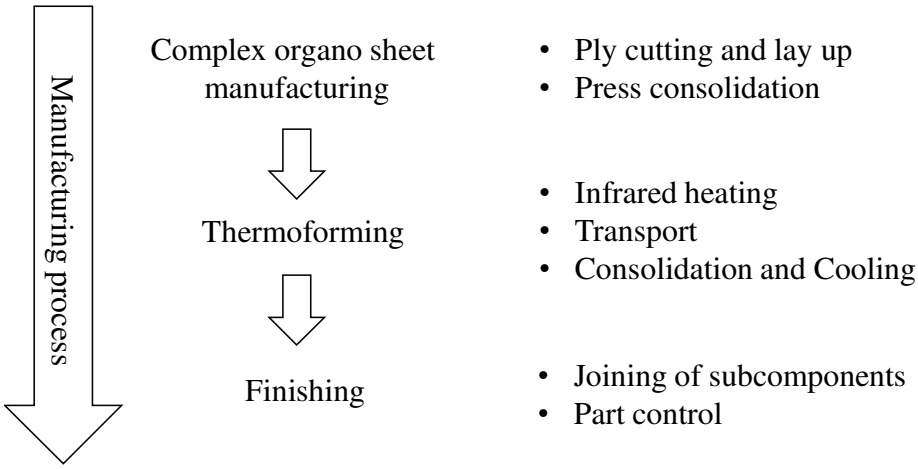

Figure 1.4 Process chart of the complex thermoforming process

Complex organo sheet consolidation is performed prior to thermoforming to generate the custom made preform which is used in the thermoforming process. This processing step has to be taken into account for complex thermoforming as state of the art, constant wall thickness organo sheets cannot be used here. By studying general consolidation process parameters, the consolidation process itself shall be optimized towards time and cost efficient conditions.

Temperature history is very important for a semi-crystalline polymer as it has significant impact on its mechanical performance. On experimental basis different effects of thermal history are studied and rated to define temperature dependent processing recommendations of thick walled organo sheets. Complex organo sheets have a local increased wall thickness and cannot be processed according to recommendations for standard, thin-walled parts. Material temperatures during preheating of thick walled organo sheets are studied and a process window is determined.

A numerical process definition tool is set up, to ensure material temperatures within the process window determined during preheating phase. A numiercal approach is chosen for efficient determination of suitable processing conditions for complex organo sheets during preheating. Heat flow from the infrared heater, free convection as a result from the arising temperature delta and material convection needs consideration. A through thickness temperature profile is required to determine the material temperature range at a certain time. Minimum and

maximum wall thicknesses illustrate processing limitations to avoid material damage caused by preheating temperatures.

To determine process efficiency an economic evaluation tool is developed. On basis of pure part manufacturing cost, complex geometry manufacturing is studied for various manufacturing numbers, processes and processing conditions.

2. State of the art

Complex thermoforming consists of two main process steps: consolidation and thermoforming. During consolidation, raw material use in the thermoforming process, so called organo sheets, is manufactured. An organo sheet is a consolidated stack of plies made from fabric or UD fiber material already coated with the thermoplastic matrix material. Thermoforming itself is a stamp forming process shaping the final part geometry.

In aviation carbon fiber reinforced composites are used for structural parts due to their excellent specific stiffness and strength properties. Polyphenylene sulfide (PPS), polyetherimide (PEI), polyetheretherketone (PEEK) and polyetherketoneketone (PEKK) are thermoplastic polymer materials used in aviation. Besides PEI all polymers have a semi-crystalline structure. Temperature processing conditions occurring during complex thermoforming have an impact on the degree of crystallinity of a semi-crystalline polymer. In turn, the degree of crystallinity affects the mechanical performance of a polymer. Effects on the degree of crystallinity caused by temperature during processing have been reported in literature. The impact of processing parameters is evaluated via mechanical testing and thermal analysis. Test standards are chosen to verify these impacts and to allow literature comparison. Thermal analysis is used to determine the degree of crystallization.

2.1. Continuous carbon fiber reinforced thermoplastics

A composite material is made up from fiber and matrix. Material properties of a composite are superposed from their component properties. A large variety among composite materials exists. Continuous carbon fiber reinforced thermoplastics are made from continuous carbon fiber and a thermoplastic polymer matrix. The carbon fiber significantly impacts tensile strength and stiffness in direction of the carbon fiber. The matrix material is important for load introduction and the transfer of off axis loads and to prevent fiber buckling. Furthermore, temperature application range, media resistance, processing conditions, storage and handling requirements depend on the matrix material.

Polymers used in aviation applications have an increased service temperature along with excellent material properties and good solvent resistance in common. Further advantages of continuous fiber reinforced thermoplastic composites have an unlimited shelf life, recyclability, provide cost efficient processing, and excellent toughness as well as damage tolerance. As adhesive joining is used for thermoset composite joining, this technique requires additional

riveting. Thermoplastic composites can be joined via welding and do not need riveting. This does result in weight savings and the potential for process optimization. [15,27]

An overview of properties of polymers used in aviation is given in Table 2-1.

Table 2-1 Overview of high performance thermoplastic matrices [28]

	PEI	PPS	PEEK	PEKK
Morphology	amorphous	semi-crystalline	semi-crystalline	semi-crystalline
T_G [°C]	217	90	143	156
Typical process temperature	330	325	390	340
+	High temperature Moderate processing temperature	Excellent environmental resistance Moderate processing temperature	Extensive database Excellent environmental resistance High toughness	Excellent environmental resistance High toughness Lower process temperature than PEEK Bonding and painting
-	Environmental resistance	Low T_G Low toughness Poor paint adhesion	High process temperature High polymer cost	Limited database in composite form

In this thesis, PPS reinforced composites are used. PPS is a polymer synthesized by the reaction of p-dichlorobenzene with sodium sulfide (2.1 and Figure 2.1) which was first developed at Phillips Petroleum Company in the 1960s [29].

$$ClC_6H_4Cl + Na_2S \rightarrow 1/n[C_6H_4S]_n + 2NaCl \qquad 2.1.$$

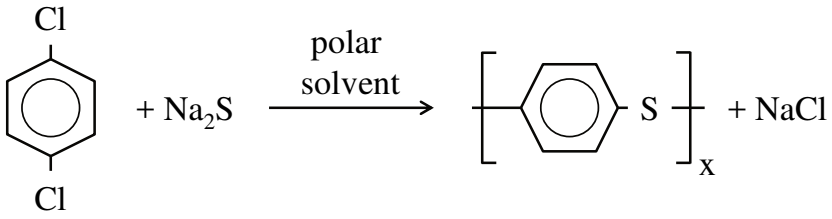

Figure 2.1 Synthesis of Polyphenylene Sulfide [30]

PPS is especially popular for its inherent fire resistance, excellent solvent resistance and chemical resistance. The application range of thermoplastic composites depends on the polymer. The application range of PPS ranges from -60°C to T_G (~90°C) without a significant loss of shear properties. In aviation, a low service temperature is important due to conditions at high altitude. Depending on the specific application and property required, PPS may be used at temperatures above T_G up to 120°C. [19,31]

2.2. Consolidation

Thermoplastic polymers are solid at room temperature. They have to be heated and molten for processing. Even in the molten stage their viscosity is about 100 times higher than an average uncured thermoset. The impregnation of dry fibers with thermoplastic matrix involves temperatures above melt temperature and additional pressure over a certain time period to ensure a good consolidation [32]. Therefore consolidation is done in a previous step.

During consolidation organo sheets are manufactured. Organo sheets are used in the thermoforming process. The pre-impregnation of the organo sheets is important for the rapid thermoforming process time.

There are two methods for the manufacturing of organo sheets: using prepreg materials and direct processing. Figure 2.2 gives an overview over the manufacturing techniques. The technique chosen depends on the fiber type and matrix state used. Direct processing is the standard manufacturing technique for organo sheets used during thermoforming for high volume applications. Direct preform manufacturing includes both impregnation and consolidation of the material. Many configurations of fiber and matrix combinations are possible. Organo sheets are available in any desired fiber orientation in large scale blanks which are cut in shape before thermoforming. Standard organo sheets made via direct processing have a constant wall thickness.

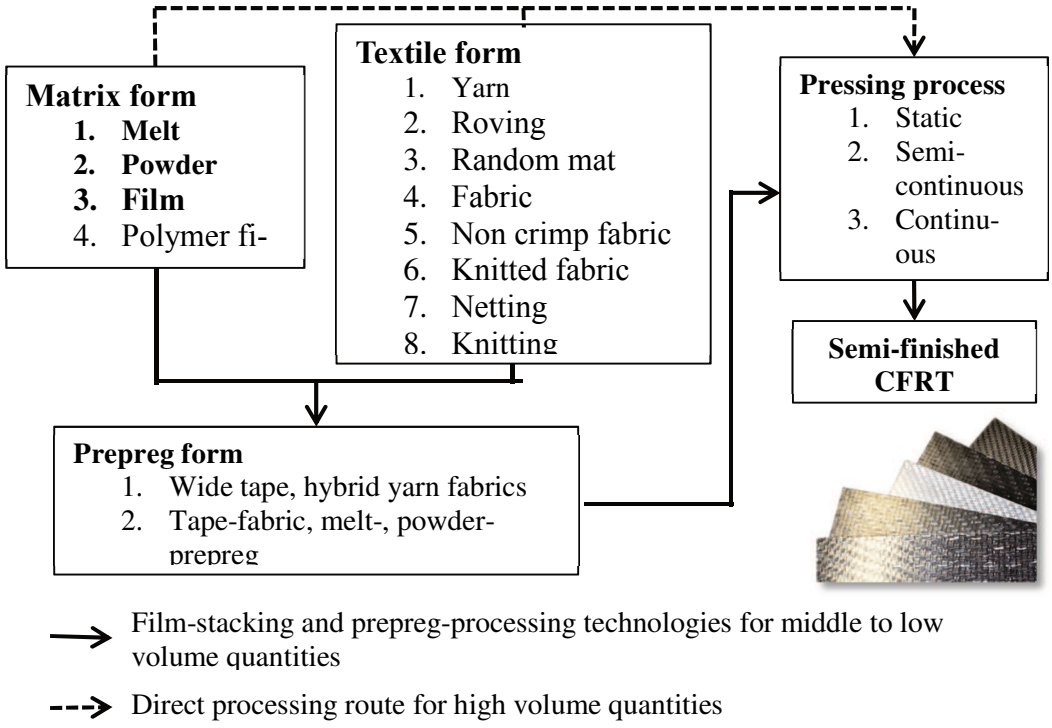

Figure 2.2 Manufacturing chains for continuous carbon fiber reinforced thermoplastic material [33]

Custom made organo sheets can be manufactured from a prepreg material. Prepreg material is a single ply material already impregnated. Individual fiber plies are attached or mixed with polymer matrix. The material is then called tape, prepreg, or semi-preg and available as rolled goods [34]. To manufacture an organo sheet, a desired number of prepreg material layers have to be consolidated.

Film prepreg material is arranged like a sandwich having dry fiber material in the center and matrix layers on either side. A calendar for film impregnation process and a coating for powder-prepreg impregnation process are used [34]. Tape prepreg material is impregnated via solvent impregnation. Solvent impregnation is done in a bath with solved thermoplastic material, followed by material drying, consolidation and heating [35]. Tape prepreg material is available in variable widths up to 10''. At room temperature, it is bendable in two dimensions. These materials are usually used for autoclave and press consolidation part manufacturing and for new developed placement processes.

Consolidation of a prepreg preform is done using a press or an autoclave. All prepreg material is fully molten and the organo sheet is created. At room temperature an organo sheet can be stored at environmental conditions. Process recommendations for prepreg press consolidation can be found in literature. Recommended consolidation times spread from 15min to 30min.

The processing temperature range for PPS composites is usually around 315-360°C [36]. Recommended pressure levels range from 5bar [37] and 14bar to 17bar. [38,39]

Process recommendations for autoclave consolidation are also found in literature. The pressure level ranges from 6-10bar for a consolidation time of 20-50min at a temperature level of 300-310°C for PPS. During heating and cooling, pressure is applied. [39]

Table 2-2 shows the process recommendation for the fiber reinforced thermoplastic material (CF/PPS) used in a press process. Heating of the material occurs without pressure, only by contact heating until the temperature reaches melting temperature (~285°C). A high pressure of 17bar is then applied for 30min. During subsequent cooling is pressure is still maintained.

Table 2-2 Consolidation recommendation for CF/PPS tape by TenCate [39]

Heat to 330°C-360°C
Wait at contact pressure until material reaches temperature
Increase pressure to 17bar
Hold for 30min
Cool to room temperature under pressure

2.3. Thermoforming

Thermoforming is a manufacturing process including heating and forming of a fiber reinforced thermoplastic composites into a defined shape. The thermoforming process is divided into two main phases having two separate areas: Infrared heating and forming and cooling (

Figure 2.3). The infrared heating area rapidly melts the preform material and the forming and cooling area press forming and cooling is done. In between the two working areas an automated transport system allows rapid and gentle transport of the organo sheet. Rapid transport is necessary to ensure the material temperature stays above melting for the following forming step.

organo sheet surface is ensured, when the size of the infrared heater is significantly bigger than the size of the organo sheet [24].

The overall processing time for a thermoforming process is within minutes. The process time depends on material type and organo sheet wall thickness. For both, heating and forming phase, several variations exist.

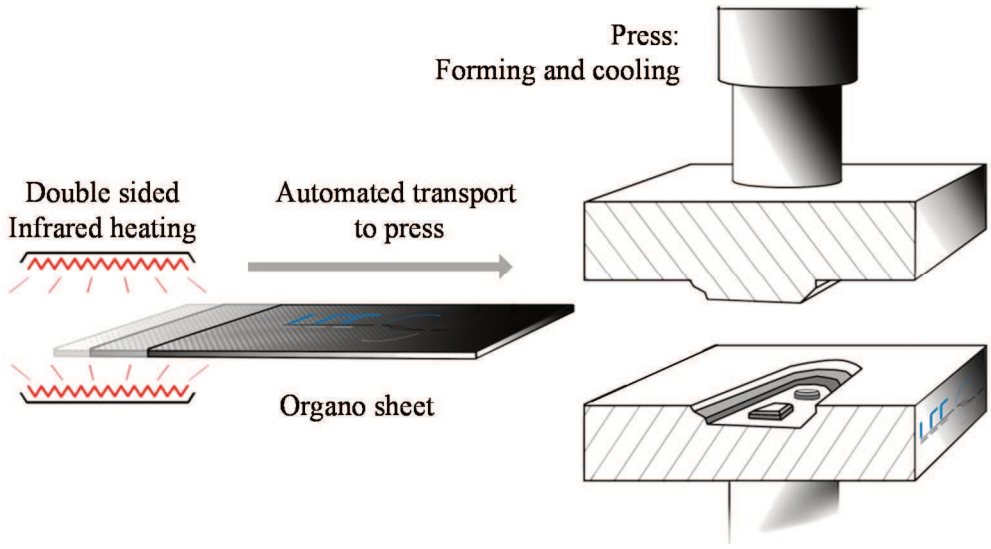

Figure 2.3 Thermoforming process [40]

Thermoplastic composites need to be heated above polymer melting temperature in the heating station. Different techniques such as contact, convection or induction heating are used. Most common method is infrared heating. Infrared heating is economic, flexible, contactless, reliable, and fast [24,41]. A homogenous temperature distribution on In the forming station, the material is rapidly formed, consolidated and cooled while applying pressure. The forming process is done via diaphragm or press forming. Diaphragm uses vacuum and optional pressure for forming with a flexible membrane. Thermoforming is done in a press using a rubber-mold or two-sided metal tooling. Different sub-versions of both tooling versions exist. [41]

After a defined period of time (consolidation time) the pressure is released and the formed part can be demolded. Temperature and pressure development during thermoforming processing time is shown in Figure 2.4.

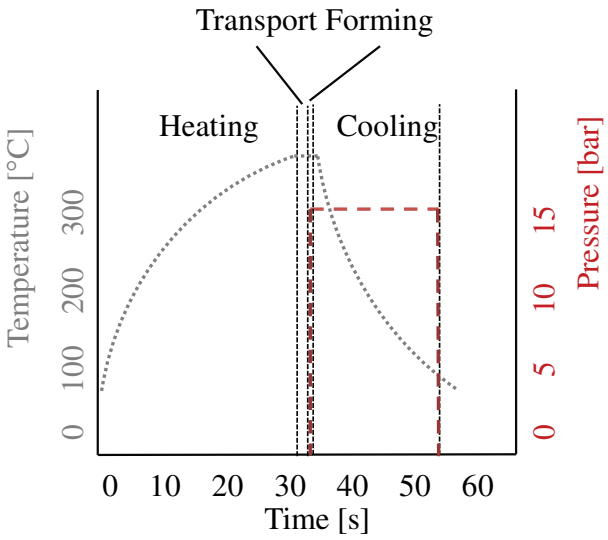

Figure 2.4 Typical thermoforming process

Interest of recent research include process conditions during thermoforming, ideal thermoplastic processing conditions, and process optimization for standard part processing [23,36,41,42]. Recommendations for thermoforming process conditions for standard part processing can be found in literature [36,39,43]. Table 2-3 gives an overview of standard process recommendations.

Table 2-3 Thermoforming parameters for CF/PPS by Tencate [39]

Maximum heater temperature [°C]	360
Material forming temperature [°C]	330
Tool temperature [°C]	170
Consolidation pressure [bar]	10-40
Consolidation time [min]	1-3

The thermoforming process is limited to stamp forming geometries. Standard part wall thickness ranges from 1-4mm [36,43,44]. Typical parts being thermoformed are ribs, stiffeners, floor panels and clips.

Since the 1980s thermoformed thermoplastic composites have been used in aviation [44]. An early thermoformed part was the Dornier Do228 flap rip [24]. More recent parts manufactured via thermoforming are the A380 J-Nose rib and A350 XWB clips. Parts are shown in Figure

2.5. All parts are of a U-shape derived geometry having a constant wall thickness and are needed at high numbers. The A350 XWB requires about 1500 clips per airplane. Manufacturing numbers of 10-13 planes per month are planned [26]. A fully automated process chain has been developed [45].

Figure 2.5 Donier flap rib (1989), A380 rib, A350XWB clip [24–26]

2.4. Impact of temperature on mechanical performance

Complex thermoformed parts will have a different material temperature profile in comparison to state of the art parts. Temperature profile of complex parts will vary with the temperature range. The temperature profile caused by complex thermoforming impacts the degree of crystallization of a semi-crystalline polymer and hence the material properties. An overview of conditions that affect the degree of crystallization is given on the basis of PPS. The work focuses on the impact of conditions that occur as a result of increasing the temperature processing window.

2.4.1. Degree of crystallization

Interest on the relation between the mechanical behavior and temperature history of thermoplastic polymers arose in the 1960s and 1970s [46],[30]. Detailed investigation, especially regarding crystallinity continued in the 1990s [47,48]. Detailed investigation regarding the impact of thermoforming on semi-crystalline polymers started the 1980s [49]. Thermoplastic fiber reinforced composites became matter of interest when impact of processing and fiber reinforcements was studied [38,50,51]. A comprehensive review on crystallization behavior of carbon fiber reinforced PPS is given by Spruiell [52].

PPS polymer properties are strongly related to the crystalline structure [30]. Crystalline sections have the polymer chains lined up side by side, whereas amorphous sections are in disorder. The amount of crystalline structure varies according to the processing temperature profile.

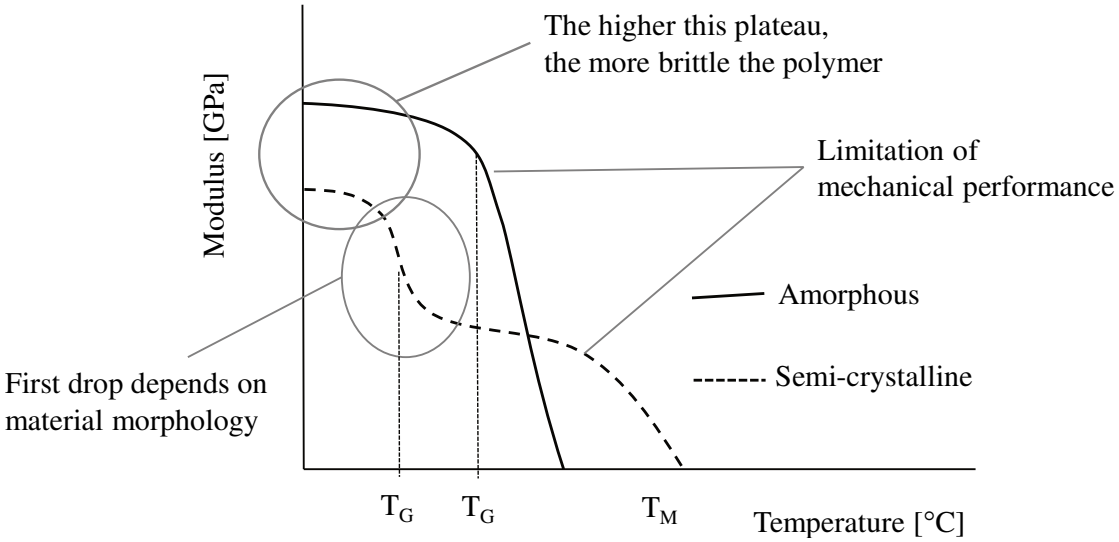

Figure 2.6 Temperature dependent behavior of semi-crystalline and amorphous polymers [53]

Amorphous bonds are loosened around glass transition temperature T_G, crystalline structures loosen at melting temperature. Application temperature for amorphous polymers is below T_G. Semi-crystalline polymers are used also above T_G (Figure 2.6). The crystalline phase contributes to stiffness, tensile strength and solvent resistance; amorphous phase improves impact resistance [52]. A dependence of degree of crystallization from thermoforming process conditions was found by McCool [36].

To rate the crystallization behavior, crystallization half time $C_{half\ time}$ is used as value. Crystallization half time is defined as the time $t_{C\ 50\%}$ needed to build 50% of possible crystallization over the time $t_{C\ max}$ to build maximum possible crystals. A short crystallization half time represents fast crystallization reaction. [54]

$$C_{half\ time} = \frac{t_{C\ 50\%}}{t_{C\ max}} \qquad 2.2.$$

Impact of processing conditions on the degree of crystallization is found in three process parameters of the thermoforming process: Infrared heating condition (time and temperature in melt), tool temperature (isothermal crystallization), and cooling rate (non-isothermal crystallization) (Table 2-4). [50,55]

The impact of time and temperature in melt for pure PPS on crystallization half time is shown in Figure 2.7. Storage time in melt from 10s to 1000s (~17min) is shown on the x-axis. In the

graph, different lines represent temperatures of melt from 317°C to 377°C. Both, increase in time in melt and increase in melt temperature lead to longer crystallization half times. [55]

Table 2-4 Impact factors for crystallization during thermoforming

Impact factor	Relevant process parameter
Time and temperature in melt [55]	Infrared heating conditions
Isothermal crystallization [50]	Tool temperature
Non-isothermal crystallization [50]	Cooling rate

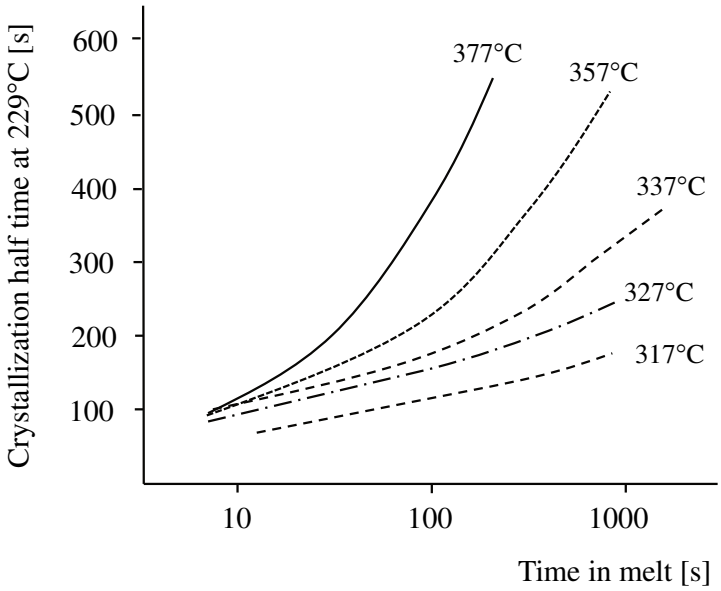

Figure 2.7 Impact of time and temperature in melt on crystallization half time [55]

Isothermal crystallization depends on the tool temperature. During thermoforming the material is rapidly cooled to this temperature and consolidated. Crystallization speed depends on the tool temperature. Figure 2.8 shows the PPS crystallization half time in dependence of crystallization temperature.

At minimum crystallization half time of 170°C crystals grow about twice as large compared to a 30K temperature offset [56]. To ensure dimensional stability of the part before demolding, the consolidation time in the tool should be above crystallization time of the polymer. [54]

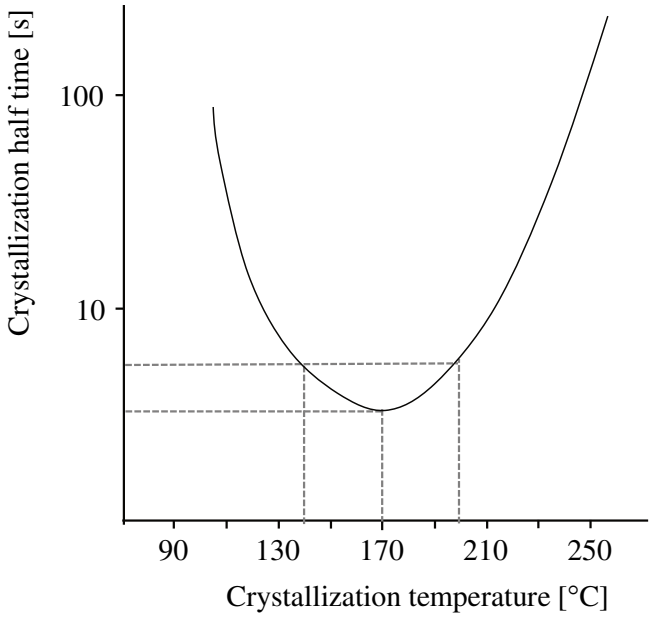

Figure 2.8 Crystallization half time over isothermal crystallization temperature [54]

McCool studied the impact of tool temperature during thermoforming towards lower temperatures. The recommended tool temperature of 170°C for PPS composites was compared to low tool temperatures of 110°C and 50°C. The dependence of degree of crystallinity on mechanical performance (flexural strength) was shown (Figure 2.9). [36].

Rapid cooling of the polymer to an ambient temperature above glass transition temperature for consolidation during thermoforming results in non-isothermal crystallization [50]. Density, heat distortion temperature and flexural strength increase while tensile strength decreases during very low cooling rates (annealing) [30]. Increasing cooling rate results in decrease in degree of crystallinity [38,50,52]. The lower degree of crystallinity is caused by the decrease in polymer chain mobility and the decreasing ability to diffuse to the growing crystal front. Figure 2.10 shows the dependence of cooling rate for different PPS blends on the resulting degree of crystallinity. Low cooling rate leads to high degree of crystallinity. High cooling rates result in lower crystallization levels. A minimum of crystallization half time can be seen at 170°C. Both an increase and decrease of crystallization temperature lead to an increase in crystallization half time, hence a decrease in crystallization rate. Crystallization half time is at 170°C about 3,5s and at 140°C and 200°C it increases to about 5,5s. [54]There are two competing mechanisms during fast cooling: high residual stresses of the amorphous phase and only little crystallization and residual stresses of crystalline phase [57].

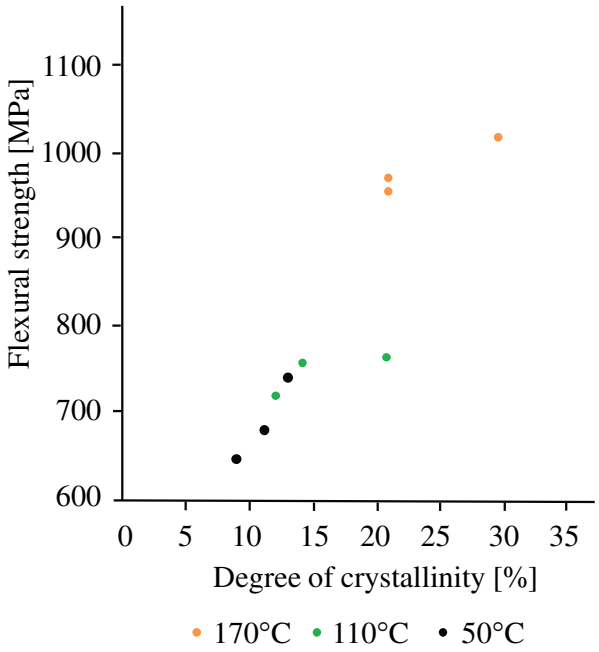

Figure 2.9 Impact of degree of crystallization on flexural strength in dependence of tool temperature [36]

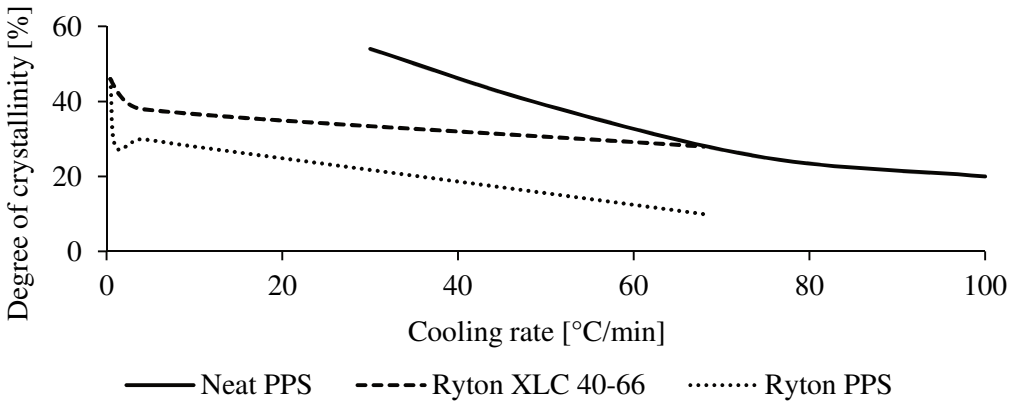

Figure 2.10 Dependence of degree of crystallinity on cooling rate [38,50]

The effects introduced above impact the degree of crystallinity of a semi-crystalline polymer during thermoforming process. Their impact on mechanical behavior under thermoforming process conditions for complex organo sheets will be studied in this work.

2.4.2. Degradation

Above a certain temperature, polymer degradation occurs. Material damage due to degradation can be determined via thermal analysis or weight loss measurements [58,59]. A PPS degradation temperature of 420°C was found by Ning [60].

Day et. al measured the weight loss for PPS over temperatures up to 600°C. Results are shown in Figure 2.11. The onset of weight loss (>0,1%/°C) is at about 410°C. Further temperature increase results in an increase in weight loss up to 1%/°C at about 500°C. At 600°C polymer weight loss increased to more than 60%. [59]

The onset of weight loss as described above depends on the heating rate. Figure 2.12 shows the dependence of weight loss per degree Celsius over temperature in dependence of heating rate.

In general, a trend for increase in heating rate shifts the onset of weight loss towards higher temperatures and the weight loss per degree Celsius decreases. Fast heating of 5°C/min shift the degradation onset up to about 470°C, whereas very low heating rates at 0,03°C/min result in an early onset of weight loss significantly below 400°C. Hence, temperature level, heating rate and time in melt as resulting factors influence the onset of material degradation.

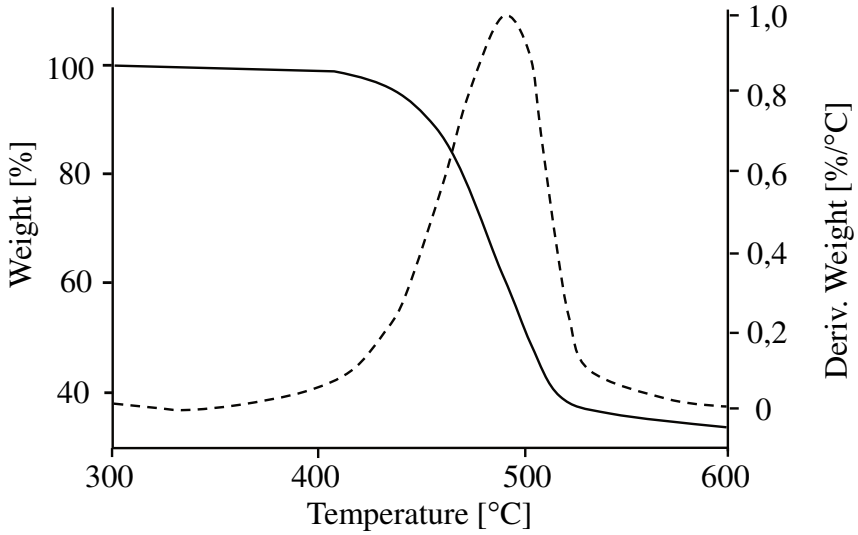

Figure 2.11 Impact of temperature on weight loss of PPS [59]

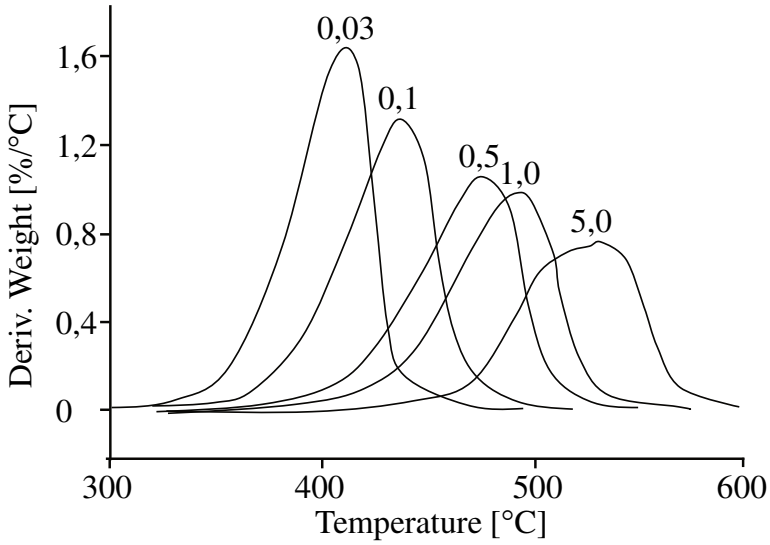

Figure 2.12 Impact of heating rate [°C/min] on onset of material weight loss (degradation) [59]

2.5. Heat flow during infrared heating

During the infrared heating phase of the thermoforming process, material is brought above melt temperature. Material is heated using an infrared heater. The heat flow during infrared heating needs to be understood to determine suitable heating conditions for complex organo sheets. Relevant heat flow is generated by radiation, convection, and conduction. Following, the thermodynamic background is introduced.

2.5.1. Radiation

Atoms of a body at a temperature above absolute zero move. The higher the body temperature of an object, the more intense the atoms move. Due to the movement of the atoms, electromagnetic waves are emitted. Electromagnetic waves heat an object by causing the object's atoms to oscillate. The oscillation energy increases the atom temperature and in consequence the object's temperature. Every body emits electromagnetic waves, hence emits energy. The emission of electromagnetic waves is called radiation. An infrared heater emits waves of a certain wavelength.

The Stefan-Boltzmann-Law describes the dependency of the power (energy over time) $\dot{E}$ emitted from the body temperature T and a specific Stefan-Boltzmann constant σ_B. [61]

$$\dot{E}(T) = \sigma_B * T^4 \qquad 2.3.$$

For determination of the heat flow $\dot{Q}$ of a panel (organo sheet), a material dependent emission coefficient ε and the surface area A have to be considered. The heat flow from the organo sheet towards its surrounding area can be determined by:

$$\dot{Q} = A * \varepsilon * \sigma_B * T^4 \qquad 2.4.$$

The heat flow of the infrared heater is determined differently, as the heater is actively emitting radiation. Infrared radiation is electromagnetic radiation of a certain wavelength. Infrared radiation is located in the electromagnetic wave spectra between visible light and microwave radiation (Figure 2.13). An infrared heater is actively emitting radiation. Radiation sent out during infrared heating increases temperature of a body that absorbs the radiation. [62]

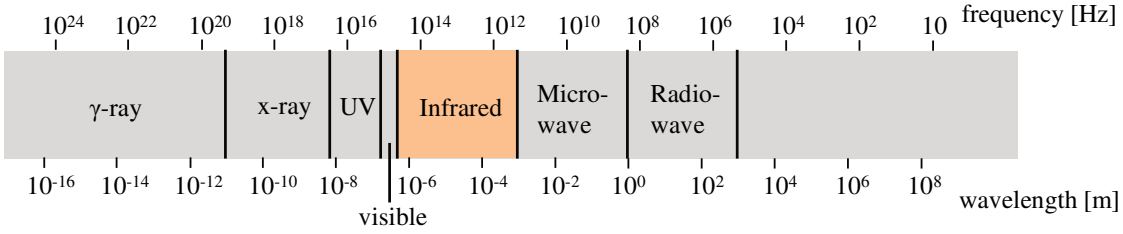

Figure 2.13 Infrared radiation within the electromagnetic wave spectra [63]

Radiation heat flow of an infrared heater $\dot{Q}_{IR,H}$ towards a heated object's surface depends on the heater's size A_H, the view factor from heater surface F_{H-La} to object and the power density L_H.

$$\dot{Q}_{IR,H} = F_{H-La} * A_H * L_H \qquad 2.5.$$

The view factor describes the amount of radiation exchanged between two surfaces separated by a transparent medium [64]. View factors are dependent on the geometry of the surfaces relative to each other.

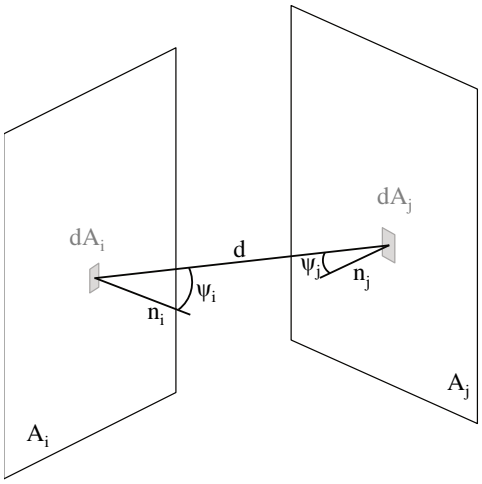

Figure 2.14 View factor relations

Figure 2.14 shows the geometrical relations needed to determine the view factor. The view factor dF_{di-dj} of the element dA_i towards the element dA_j is dependent on the distance d and the angles ψ_i and ψ_j between the perpendiculars n_i and n_j.

The differential view factor dF_{di-dj} is the described by:

$$dF_{di-dj} = \frac{cos\psi_i \cdot cos\psi_j}{\pi \cdot d^2} \cdot dA_j \qquad 2.6.$$

The integration of the differential view factor over the surfaces dA_i and dA_j gives the view factor F_{i-j} of the surface A_i towards the surface A_j.

$$F_{i-j} = \frac{1}{A_i} \int_{A_i} \int_{A_j} \frac{cos\psi_i \cdot cos\psi_j}{\pi \cdot d^2} \cdot dA_j dA_i \qquad 2.7.$$

The power density L_H depends on the heater source and current heater temperature. The power density in relation to the heater temperature is usually provided by the heater manufacturer. Power density is given in power per area. The temperature development curve of the heater is needed for accurate determination of time (temperature) dependent emitted power density.

On basis of heater temperature, the radiated heat flow from heater towards the organo sheet can be determined using equation 2.5.

2.5.2. Free convection

Free convection is caused by a temperature gradient within a fluid. It occurs in air (fluid) during infrared heating phase when infrared heater and the laminate heat up. The transfer of power caused by free convection $\dot{Q}_{Con}$ is dependent on the heat transfer coefficient α, the temperature difference between wall T_W and fluid T_∞ (not near wall in boundary layer) and the surface area A. [61]

$$\dot{Q}_{Con} = \alpha\, A\, (T_W - T_\infty) \qquad 2.8.$$

The heat transfer coefficient α depends on thermodynamic effects that are described by dimensionless numbers, summarized by the Nusselt relations [65]. Those are Nusselt number, Grashof number, Rayleigh number and Prandtl number.

The Nusselt number Nu describes the ratio of convective to conductive heat transfer at a material interface. It is dependent on the heat transfer coefficient, the ratio from area A over compass C (equivalent the characteristic length L_C) for a surface and the thermal conductivity of the fluid λ_{Fl}. Grashof number Gr approximates the ratio of buoyancy forces to viscous forces in the fluid. It is determined from gas coefficients, geometry and temperature delta. The Rayleigh Ra number is the product of Grashof number Gr and Prandtl number Pr_{Fl} and important for determining whether conduction or convection occurs. The Prandtl number describes the ratio of viscous diffusion rate ν_{Fl} to thermal diffusion rate a_{Fl}.

$$Nu = \frac{\alpha \cdot L_C}{\lambda_{Fl}} \qquad 2.9.$$

$$Gr = \frac{\beta \cdot g \cdot (T_w - T_\infty) \cdot L_C^3}{{\nu_{Fl}}^2} \qquad 2.10.$$

$$Ra = Gr \cdot Pr_{Fl} \qquad 2.11.$$

$$Pr_{Fl} = \frac{\nu_{Fl}}{a_{Fl}} \qquad 2.12.$$

Convection flow depends on the surface temperature. There are two types of free convection for a horizontal panel. Convection can move freely when occurring on the upper side of a panel, compared to the bottom side (Figure 2.15).

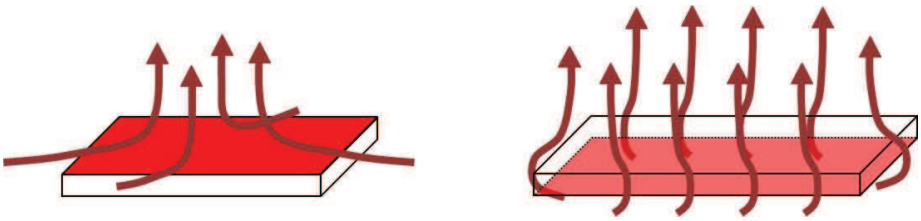

Figure 2.15 Free convection of surface (left) and bottom (right) heated panel

Therefore two categories are defined for convection calculation:

- Energy emission on the top side and absorption on the bottom side
- Energy absorption on the top side and emission on the bottom side

Two Prandtl functions, depending on the convection type are needed to determine the Nusselt number, can be solved to a constant. [61]

$$f_1(Pr) = (1 + 0{,}671 \cdot Pr^{-\frac{9}{16}})^{-\frac{16}{9}} = 0{,}3409 \quad 2.13.$$

$$f_2(Pr) = (1 + 0{,}536 \cdot Pr^{-\frac{11}{20}})^{-\frac{20}{11}} = 0{,}3973 \quad 2.14.$$

For energy absorption of organo sheet downside and energy emission on organo sheet upside it is important whether the heat flow is laminar or turbulent. [61]

A laminar heat flow occurs when

$$Ra \cdot f_2(Pr) \leq 7 \cdot 10^4 \quad 2.15.$$

The Nusselt number is then determined by

$$Nu = 0{,}766 \cdot [Ra \cdot f_2(Pr)]^{1/5} \quad 2.16.$$

A turbulent heat flow occurs when

$$Ra \cdot f_2(Pr) > 7 \cdot 10^4 \quad 2.17.$$

The Nusselt number is then determined to

$$Nu = 0{,}15 \cdot [Ra \cdot f_2(Pr)]^{1/3} \quad 2.18.$$

For energy absorption on organo sheet upside and energy emission on organo sheet downside only a laminar solution is available, when

$$10^3 \leq Ra \cdot f_1(Pr) \leq 10^{10} \quad 2.19.$$

The Nusselt number is then determined to

$$Nu = 0{,}6 \cdot [Ra \cdot f_1(Pr)]^{1/5} \quad 2.20.$$

Using formulas 2.9-2.20 the free convection heat flow according to 2.8 can be determined.

2.5.3. Heat conduction

Heat conduction describes the energy transport between different molecules. In case of a temperature gradient within a material, heat conduction occurs.

The temperature of a body ϑ dependents on time t and position x, y, z:

$$\vartheta = \vartheta(x, y, z, t) \quad 2.21.$$

The temperature field of a body is described by a partial differential equation over time *t* in dependence of position and temperature conduction a. [63]

$$\frac{\partial \vartheta}{\partial t} = a\left(\frac{\partial^2 \vartheta}{\partial x^2} + \frac{\partial^2 \vartheta}{\partial y^2} + \frac{\partial^2 \vartheta}{\partial z^2}\right) \quad 2.22.$$

Fourier's law ("law of heat conduction") describes the relation of power transfer $\dot{Q}$ through wall thickness in relation to temperature delta (proportional to negative delta T). [66]

$$\dot{Q}(z,t) = \dot{Q}_z(z,t) = -\lambda A \frac{\partial \vartheta(z,t)}{\partial z} \quad 2.23.$$

On basis of radiation power and convection power, the surface temperature of the organo sheet can be determined. From the resulting temperature gradient, the material temperature can be determined using 2.23 in dependence of time and position.

2.6. Test specifications

The impact of processing on mechanical performance has to be evaluated to be able to determine a processing window for complex thermoforming. Relevant test standards with focus on matrix dominated failure behavior and comparison with experimental data provided in literature are chosen. The evaluation method for determination of degree of crystallinity using thermal analysis is introduced.

2.6.1. Flexural strength

DIN EN ISO 14125 is a standard for flexural strength determination. Flexural strength is determined using a three point bending test set up. Tests will be conducted according to DIN EN ISO 14125 [67]. A three point bending test initiates complex stress conditions with a mixture of normal stress, shear stress and compression stress in the specimen. As this standard test method is widely used for quality control, it is here applied for comparison with experimental data from literature. The flexural strength σ is determined from the maximum load F at first failure and bearing distance l over width b by thickness d squared.

$$\sigma = \frac{2}{3} * \frac{F * l}{b * d^2} \quad 2.24.$$

Comparing mechanical performance of specimens manufactured under variable conditions might require normalization of test data. Failure mode during three point bending is fiber dominated. Data normalization is required for a composite specimen if actual fiber content varies from the defined common fiber volume content. The normalized value is determined from the test value $X_{measured}$ multiplied by the fraction of normalized fiber volume content $FVC_{normalized}$ over the specimen specific fiber volume content $FVC_{specimen}$. [68]

$$X_{normalized} = X_{measured} * \frac{FVC_{normalized}}{FVC_{specimen}} \quad 2.25.$$

2.6.2. Interlaminar shear strength

Inter-laminar shear- strength is measured using DIN EN 2563 [69]. The standard defines interlaminar shear strength as the maximum shear stress occurring in the mid plane of the specimen at first failure. Interlaminar shear strength rates the fiber matrix bonding of the material. Interlaminar shear strength τ is determined from the maximum load F at first failure over the cross section of the specimen (width b, thickness d).

$$\tau = \frac{3}{4} * \frac{F}{b * d} \quad 2.26.$$

In case of plastic failure of the specimen, the value determined is no true shear stress failure and can only be used for comparison within the test series and is not valid for comparison with data from literature.

2.6.3. Curved beam strength

ASTM D 6415 allows the determination of the curved beam strength (CBS) of a bended composite specimen. Further radial stress for a curved beam under pure bending can be determined. The maximum radial stress calculated from the curved beam strength is equivalent to the interlaminar shear strength of the specimen. [70]

The standard allows a four-point-bending testing of a formed V-shaped specimen at variable thickness. Figure 2.16 shows a sketch of the testing set up.

During testing a constant bending moment is applied on the curved section, a complex, out of plane tensile stress is applied. As the failure is interlaminar, it is impacted by processing quality issues like fiber-matrix-bondage and material quality, which are dependent on degree of crystallinity and potential degradation.

Level of comparison is the radial stress σ_r. The radial stress σ_r for a curved beam with inner radius r_i and outer radius r_o is calculated via

$$\sigma_r = -\frac{CBS}{r_0^2 \cdot g} * \left[1 - \frac{1-\rho^{\kappa+1}}{1-\rho^{2\kappa}} * \left(\frac{r_m}{r_0}\right)^{\kappa-1} - \frac{1-\rho^{\kappa-1}}{1-\rho^{2\kappa}} \cdot \rho^{\kappa+1} * \left(\frac{r_0}{r_m}\right)^{\kappa+1}\right] \quad 2.27.$$

with

$$g = \frac{1-\rho^2}{2} - \frac{\kappa}{\kappa+1} * \frac{(1-\rho^{\kappa+1})^2}{1-\rho^{2\kappa}} + \frac{\kappa * \rho^2}{\kappa-1} * \frac{(1-\rho^{\kappa-1})^2}{1-\rho^{2\kappa}} t \quad 2.28.$$

$$\kappa = \sqrt{\frac{E_\theta}{E_r}} \quad 2.29.$$

$$\rho = \frac{r_i}{r_o} \quad 2.30.$$

and

$$r_m = \left[\frac{(1-\rho^{\kappa-1}) * (\kappa+1) * (\rho * r_o)^{\kappa+1}}{(1-\rho^{\kappa+1}) * (\kappa-1) * {r_o}^{-(\kappa-1)}}\right]^{\frac{1}{2\kappa}} \quad 2.31.$$

The curved beam strength CBS is calculated from the maximum force F and the angle from to horizontal to the specimen legs Φ

$$CBS = \left(\frac{F}{2 \cdot b \cdot cos(\Phi)}\right) * \left(\frac{d_x}{cos(\Phi)} + (D+t) \cdot tan(\Phi)\right) \quad 2.32.$$

with

$$d_y = d_x * tan(\Phi_i) + \frac{D+d}{cos(\Phi_i)} - \Delta \quad 2.33.$$

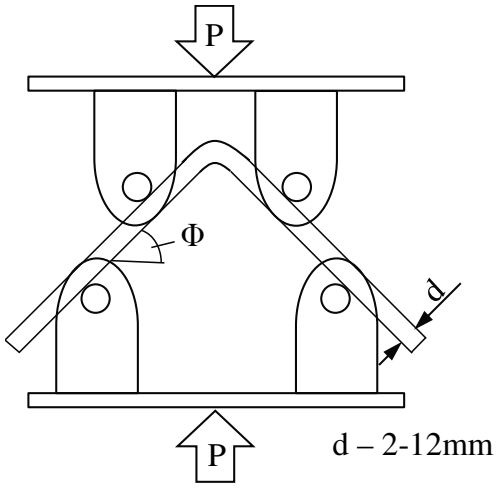

Figure 2.16 Curved Beam in Four-Point Bending [70]

2.6.4. Thermal analysis

Thermal analysis describes methods for determination of physical and chemical properties of a material as a function of time or temperature after treating the material with a defined temperature cycle. [71]

Differential scanning calorimetry (DSC) is one method used for thermal analysis. A sample and a reference undergo a temperature cycle while the heat flow is measured. DSC can be used for determining the degree of crystallinity. The degree of crystallinity of a polymer describes the amount crystalline structure in a polymer. The degree of crystallinity is determined from the melt enthalpy curve.

Crystallization enthalpy is determined according to DIN 53 765 [72]. The degree of crystallinity X_C is determined from melt enthalpy ΔH_{melt} and cold crystallization enthalpy ΔH_{CC} over the enthalpy at maximum crystallization enthalpy ΔH_{max} . Cold crystallization describes the material crystallization during material heating between glass transition temperature and melting temperature. For a composite material the matrix material weight share δ_M has to be taken into account.

$$X_C = \frac{\Delta H_{CC} + \Delta H_{melt}\ [J/g]}{\delta_M * \Delta H_{max}\ [J/g]} \qquad 2.34.$$

Determination of degree of crystallinity is difficult as different references for maximum degree of crystallinity values occur in literature. Values from 80J/g to 150J/g are found for the

enthalpy of maximum crystallization for PPS [30,47,52,58]. Most common reference value is 112J/g determined by Cebe [47]. The fiber volume content of the evaluated sample is often taken as average value from the test panel.

Through thickness change in degree of crystallinity for thick materials was investigated by [73]. A measurable change in degree of crystallinity due to cooling rate variations during processing could not be determined for wall thickness below 50mm.

3. Complex Thermoforming

Complex thermoforming enables the manufacturing of parts having geometries of variable wall thickness and three-dimensional shape. Those geometries cannot be realized by standard thermoforming. Complex thermoforming increases the part design freedom regarding wall thickness and wall thickness variation. Studied wall thickness variation is from 2-10mm.

Every forming process is only capable of limited wall thickness. Material thickness beyond 10mm results in very high forming forces of intraply shear and interlaminar slip. A part wall thickness above 10mm only occurs on a small number of highly loaded parts. Therefore, if wall thickness above 10mm is required, alternative manufacturing including thermoplastic joining technologies should be considered.

Table 3-1 opposes complex and standard thermoforming to clarify differences regarding geometry limitations. Standard thermoforming uses constant thin-wall thickness organo sheets from suppliers. Custom made organo sheet manufacturing is part of the complex thermoforming process. Standard constant wall thickness organo sheets cannot be used for complex thermoforming. The complex geometry thermoforming includes variable single ply geometries and local reinforcements. A three dimensional geometry profile (2D profile changing over the length of the organo sheet) is possible. The organo sheet is custom made and is dependent on the specific geometry. Therefore, consolidation of the preform ply stack is part of the complex thermoforming process. This section introduces a demonstrator geometry implying complex geometry challenges. Consolidation and thermoforming processes are studied.

Table 3-1 Comparison of standard and complex thermoforming

	Standard thermoforming	Complex thermoforming
Local reinforcement	Not possible	Possible
Organo sheet	From supplier	Custom made
Separate material consolidation	Not necessary	Necessary
Wall thickness	1-4mm	2-10mm
Part dimensions	2D and 3D	2D and 3D

3.1. Geometry definition

A demonstrator geometry having a variable wall thickness is defined for consolidation and thermoforming study.

A generic complex geometry was designed. The geometry chosen was an airfoil geometry (main section) having flanges on both sides (Figure 3.1). Airfoil geometry was derived from a structural airfoil in aircraft engines.

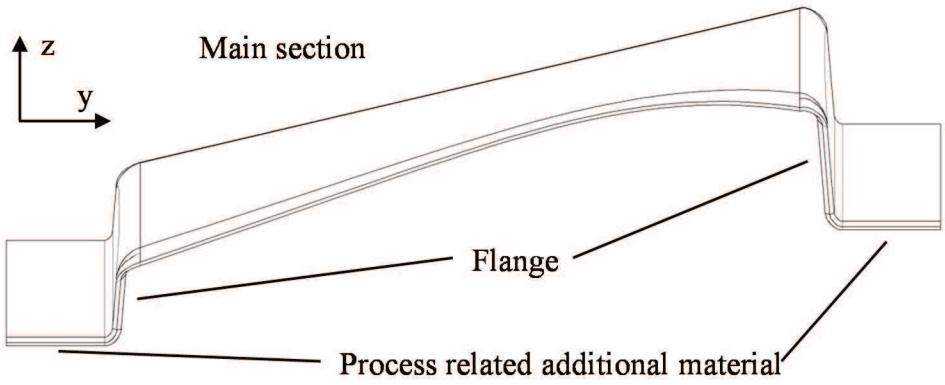

Figure 3.1 Airfoil demonstrator geometry

Main section of the geometry has an aerodynamic profile changing along the airfoil length. Wall thickness from about 2-10mm is realized resulting in local ply numbers from 13-56. Leading and trailing edge are defined and spline shaped. High forming angles of flanges towards main section occur. Flanges have a constant, still increased wall thickness and a high forming angle of 85° (5°draft angle). Geometric requirements are summarized in Figure 3.2.

The length of the main section along y-axis is about 400mm. Flanges represent joining sections towards larger structures. Flange length (depth) in z-direction is about 50mm. Width of the geometry in x-direction is roughly 150mm. Airfoil geometry has an off set over the length (y-axis) in z-direction of 65mm (Figure 3.1) and an offset along y-axis in x-direction of 36mm (Figure 3.3).

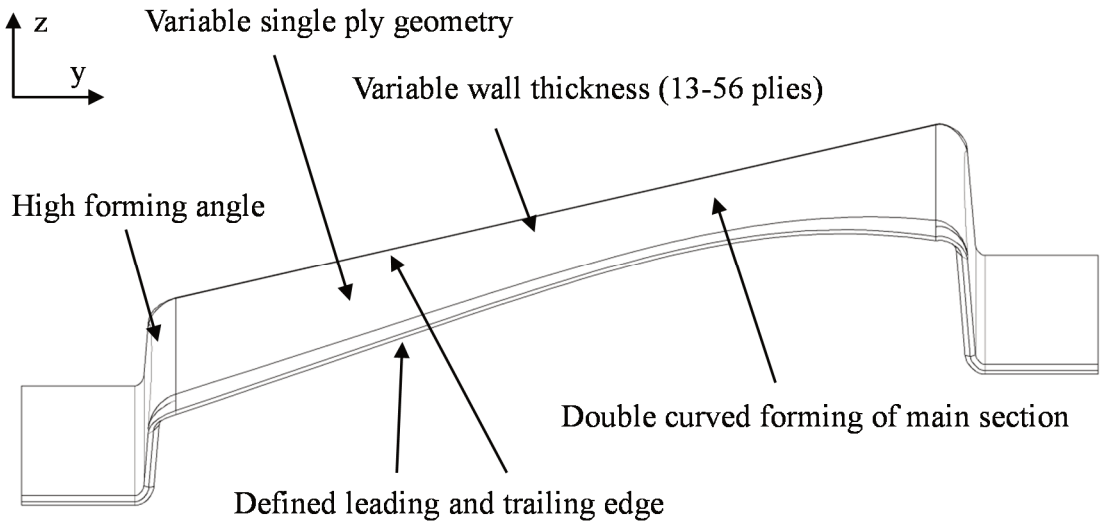

Figure 3.2 Complex geometry challenges

Total airfoil bending radius curvature is from 125mm to 300mm. Forming of flanges occurs from this curvature. Forming radius is variable from 5mm – 12mm. Leading edge of the airfoil has a curvature (Figure 3.3 right) and trailing edge is straight (Figure 3.3 left). Airfoil width narrows down to 83% (134mm) from its maximum width of 162mm.

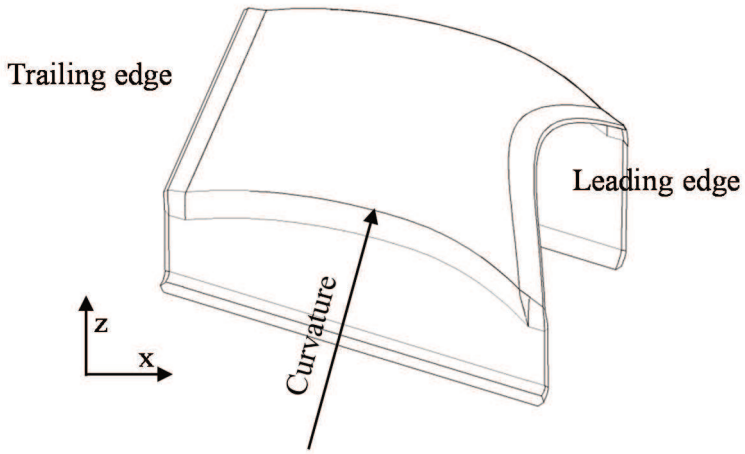

Figure 3.3 Side view over demonstrator geometry

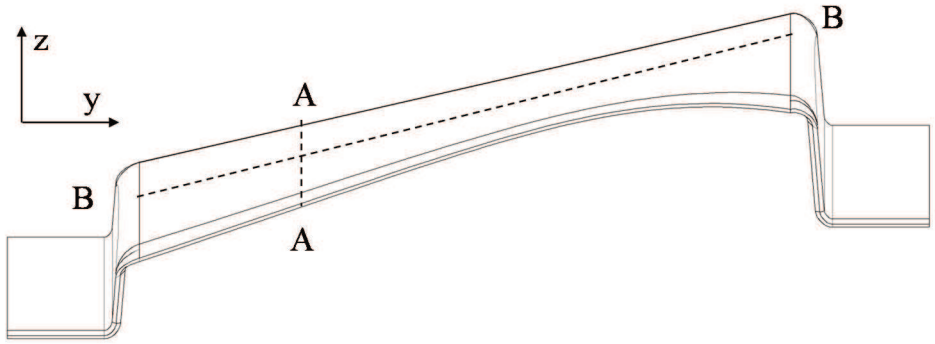

Figure 3.4 Axis A-A and B-B of wall thickness variation across demonstrator

Across the main section, wall thickness is variable from 2mm to 9mm. The local variation of wall thickness is shown along two axis of the airfoil as marked in Figure 3.4 for cuts along A-A and B-B. Figure 3.5 shows the change in wall thickness along x-axis (A-A). Figure 3.6 shows the wall thickness change along y-axis (B-B). Wall thickness changes from 7,7mm to 8,7mm along the chosen line.

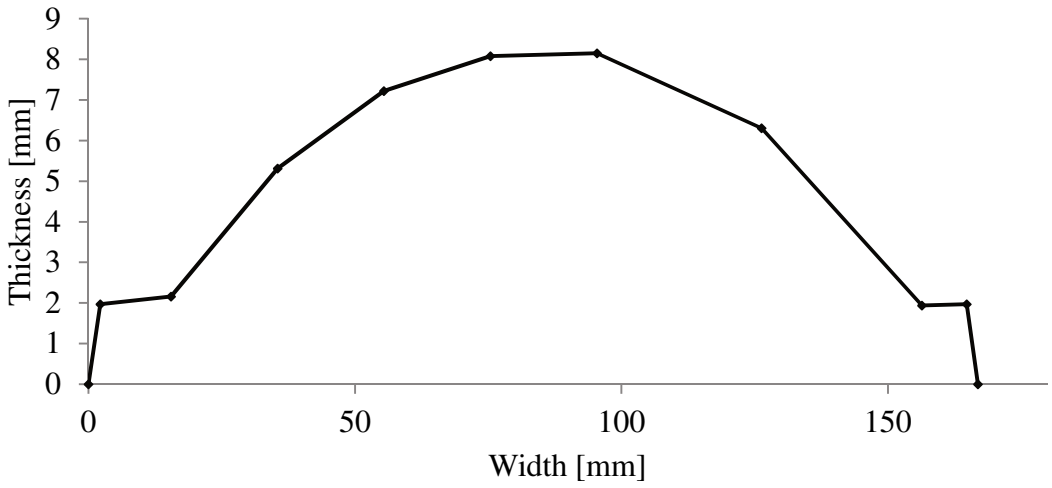

Figure 3.5 Complex preform wall thickness variation over width (A-A)

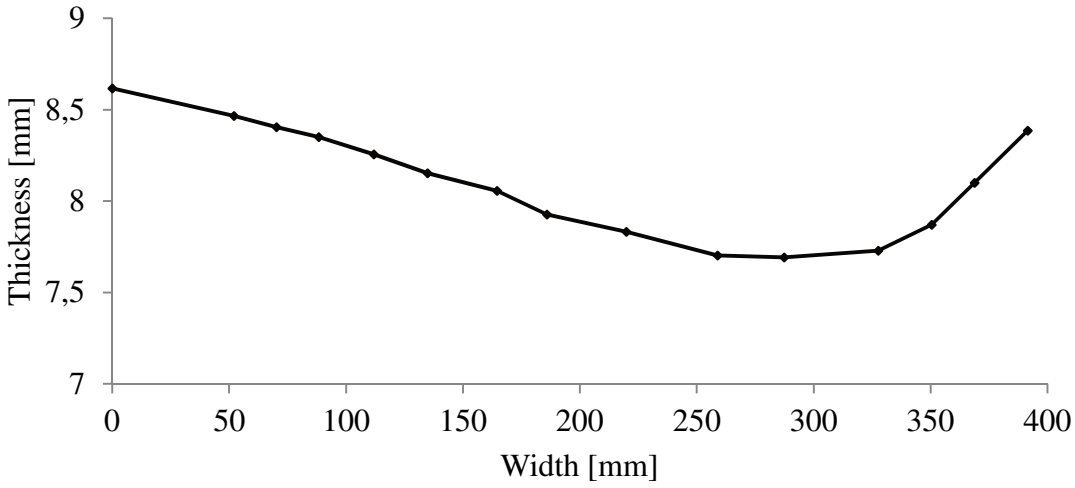

Figure 3.6 Preform maximum wall thickness over length of main section (B-B)

Process related additional material as shown in Figure 3.1 is needed for preform clamping during forming. Contact of clamping system and tool during thermoforming must be avoided to prevent tool and organo sheet from potential damage. After thermoforming, finishing is required to achieve the exact demonstrator contour.

3.2. Demonstrator processing

During complex thermoforming both, consolidation and thermoforming processes are carried out. Figure 3.7 shows the process chain of complex thermoforming. Consolidation of the custom made organo sheet requires previous preform lay-up (“Preforming”). Thermoforming follows consolidation. After thermoforming the part requires finishing.

Figure 3.7 Process chain of complex thermoforming

3.2.1. Consolidation

Custom made preforms need consolidation before thermoforming. Material used for the demonstrator was a 10” UD carbon fiber tape material from Ticona [74] and a satin semi-preg carbon fiber fabric material from Tencate [75]. Semi-preg was used for outer plies to improve impact resistance. Inner layup was multi axial with a majority of 0° (y-axis) layers.

Figure 3.8 Preform - without cover layer (left) / with cover layer (right)

Figure 3.8 shows the preforming lay-up of the demonstrator. Maximum number of plies was 56. Single layers were cut automatically using a cutter. Lay-up was done manually using a template for positioning and an ultrasonic welding unit for fixation. Fabric layers were used as outer layers for coverage. Preform was extended on both sides with additional material for clamping. Flange area had in increased number of plies compared to the area of additional material for clamping (not to be distinguished in the figure). Clamping was done only on additional material. Main section could be clearly distinguished as wall thickness variation occurred mainly here and ply mounting was clearly visible.

For a smooth and even surface contour, an additional two layers of tape were used on the preform topside besides the cover fabric layer. Imprint of variable layer geometry on to the surface was avoided.

Ply stacks were consolidated in an autoclave bagging set-up. An overview on autoclave consolidation parameters is given in Table 3-2. Conditions were chosen according to process recommendations (2.2). Consolidation time was 30min at 315°C. Consolidation pressure of 6bar was applied during heating, consolidation and cooling. Heating and cooling rate were at 15K/min. Autoclave cycle time was 66min. Additional time was needed for bagging and process preparation. The custom made organo sheet before and after consolidation is shown in Figure 3.9.

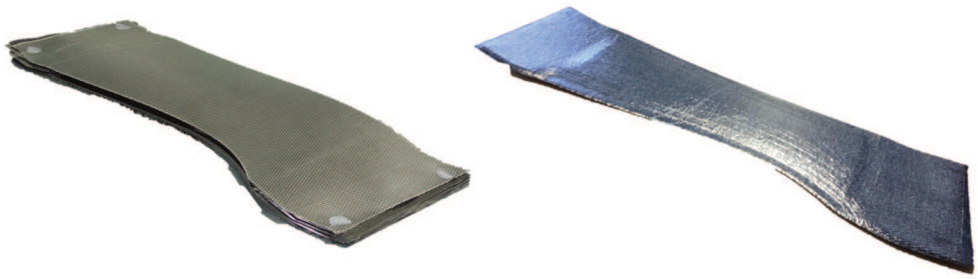

Figure 3.9 Demonstrator before (left) and after (right) consolidation

Table 3-2 Demonstrator autoclave consolidation parameters

Consolidation temperature	315°C
Consolidation time [min]	30
Consolidation pressure [bar]	6
Heating rate [K/min]	15
Cooling rate [K/min]	15

Table 3-3 Demonstrator vacuum consolidation parameters

Consolidation temperature	315°C
Consolidation time [min]	30
Consolidation pressure [bar]	1
Heating rate [K/min]	15
Cooling rate [K/min]	15

As alternative manufacturing method, vacuum consolidation on a heated press plate was carried out. No additional consolidation tool was required as vacuum bagging was possible. Heating was done via contact heating. Pressure applied was vacuum pressure. Consolidation using a heated press plate avoids the use of an autoclave for consolidation. Autoclave consolidation is expensive in comparison with vacuum consolidation.

An overview on selected process parameters during vacuum consolidation is given in Table 3-3. No significant difference in organo sheet suitability for subsequent thermoforming regarding preform fitting, processing or handling was found.

3.2.2. Thermoforming

Thermoforming process was done according to process recommendations (2.3). Not all process settings are defined in recommendations and were set according to experience. An overview on process parameters is given in Table 3-4.

Preform was heated via infrared heating above melting temperature. Infrared heaters were switched out at an early stage to allow through thickness temperature increase towards recommended temperature level. Preform was transported in the press and formed into the heated tool of 170°C. Thermoforming was done into a double sided metal tool. Figure 3.11 shows the organo sheet in press just before thermoforming. Figure 3.11 shows the formed part in press after thermoforming. Tool was heated via contact heating from the press plates. After a three minute consolidation phase, the formed demonstrator was demolded. Trimming finished the demonstrator building (Figure 3.12). In total, ten demonstrator parts were manufactured.

Table 3-4 Thermoforming parameters for CF/PPS by Tencate [39]

Maximum heater temperature [°C]	360
Total heating time [min]	5,5
Heater distance [mm]	200
Material forming temperature [°C]	330
Tool temperature [°C]	170
Consolidation pressure [bar]	10-40
Consolidation time [min]	3

Figure 3.10 Organo sheet in press before thermoforming

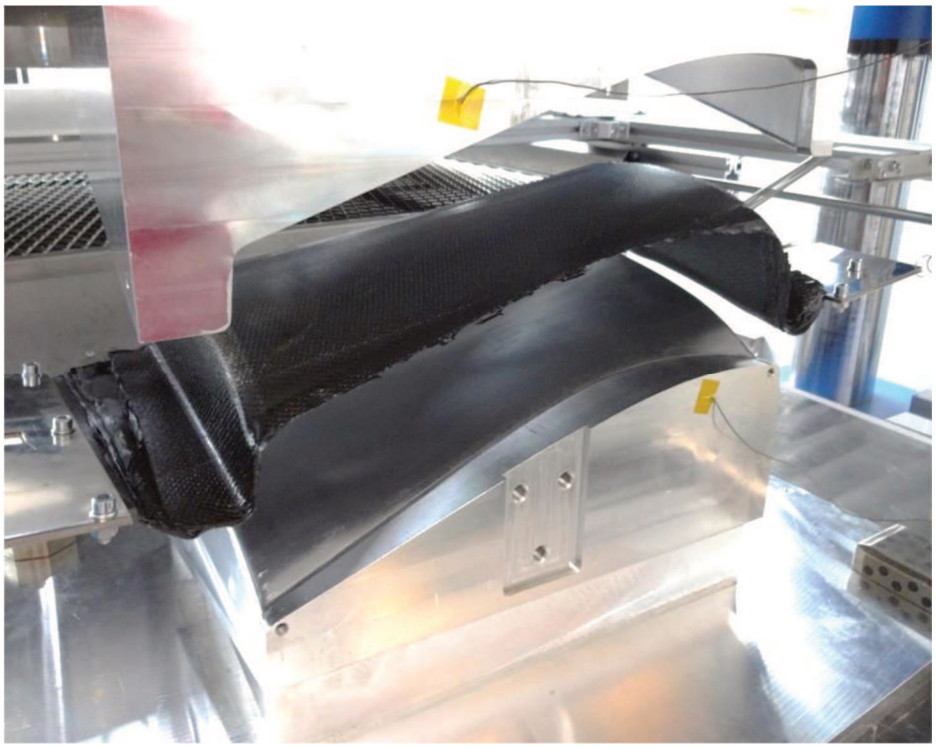

Figure 3.11 Part in press after thermoforming

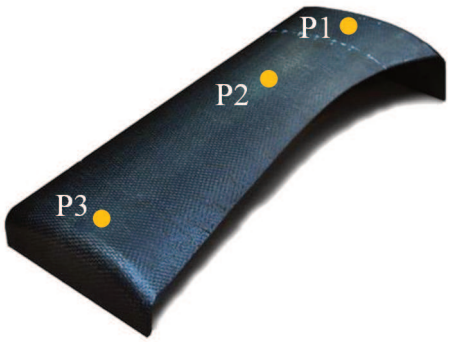

Figure 3.12 Final demonstrator part with marked positions of DSC evaluation

Characterization of formed demonstrators was done on basis of thermal analysis and optical evaluation. During complex thermoforming special attention needs to be drawn on material temperature as temperature history of a polymer is relevant for its performance (2.4.1). Throughout a complex preform temperature history varies locally.

Effect of this temperature history on the material was evaluated using thermal analysis measurements via DSC (2.6.4). DSC allows the determination of melt enthalpy. Potential material degradation due to temperature processing during thermoforming was derived by comparison of melt enthalpy curves. Samples of about 10mg are heated at 20°C/min up to 330°C and cooled down afterwards. An enlarged melt enthalpy zone indicates material degradation due to too hot processing [58].

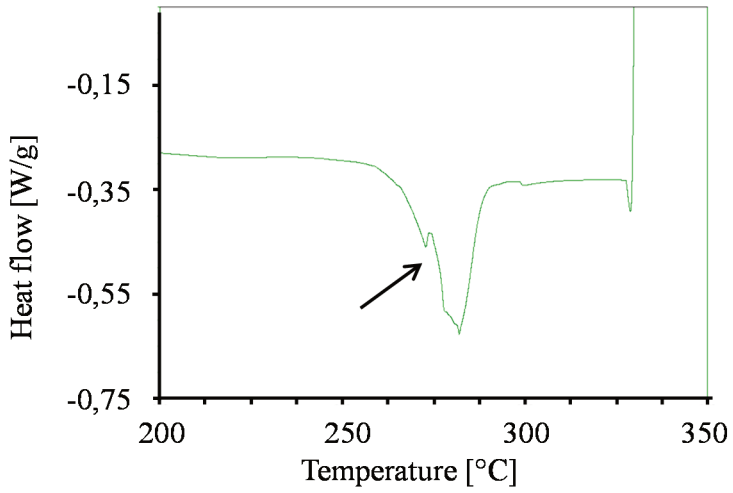

Figure 3.13 DSC plot of demonstrator sample – degraded material

Melt enthalpy is derived from heat flow curves. Heat flow curves were determined for three positions P1-P3 along the main section (y-axis, see Figure 3.12). Figure 3.13 shows a heat

flow curve from P2 during DSC analysis. The double enthalpy melting peak (see pointing arrow) is an indicator for material damage. For comparison, a standard material heat flow curve from DSC analysis is shown in Figure 3.14. Locally, maximum material temperature must have been above material degradation temperature.

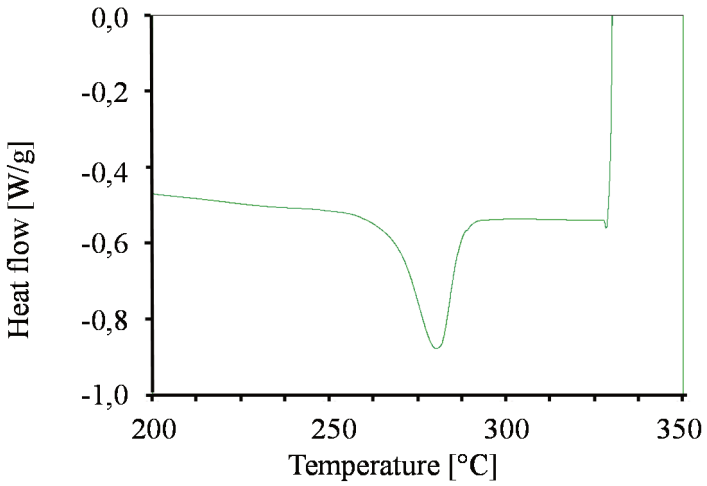

Figure 3.14 DSC plot of demonstrator sample - standard material

Optical evaluation of the demonstrator was done. At standard thermoforming process conditions an unmelted zone could be detected after thermoforming. The unmelted zone correlated with the thickest section of the demonstrator. The thermoforming process was repeated and heater distance was reduced from 200mm to 100mm. The unmelted zone on part bottom side could not be detected after thermoforming anymore. Figure 3.15 shows the demonstrator after standard condition thermoforming (left) and after decreased heater distance (right). A reduced heater distance lead to increased surface temperatures on bottom-side.

Figure 3.15 Demonstrator bottom-side comparison

Following, temperature development in dependence of wall thickness and heater distance was studied. Material surface temperature depends on the local wall thickness. Figure 3.16 shows

the surface temperature development of organo sheets of thickness *d* 2mm and 10mm at maximum heater temperature of 400°C. The surface temperature of the 2mm organo sheet heated up much faster than the surface of the 10mm organo sheet.

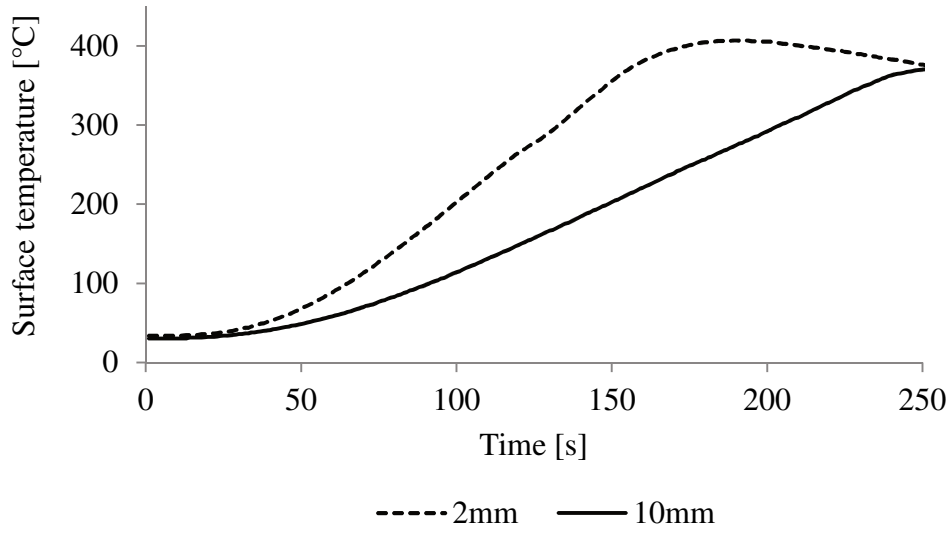

Figure 3.16 Impact of organo sheet thickness d on surface temperature

As a result from the dependence of surface temperature on wall thickness, mid temperature development also depends on wall thickness. Figure 3.17 shows the mid temperature development of organo sheets of 2mm, 6mm and 10mm from 130°C to melt temperature. Heating rate decreased from 2.9K/s to 1.3K/s with increasing wall thickness from 2mm to 10mm.

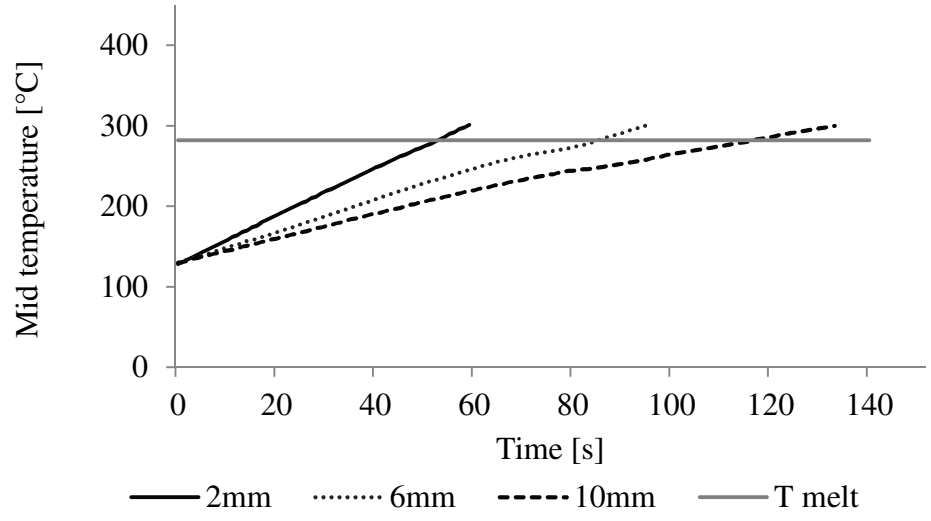

Figure 3.17 Variation of heating rate due to variable wall thickness

Figure 3.18 shows the surface temperature development on 2mm organo sheets for a heater distance a of 100mm and 350mm An increase in heater distance leads to decreased surface temperature heating rates.

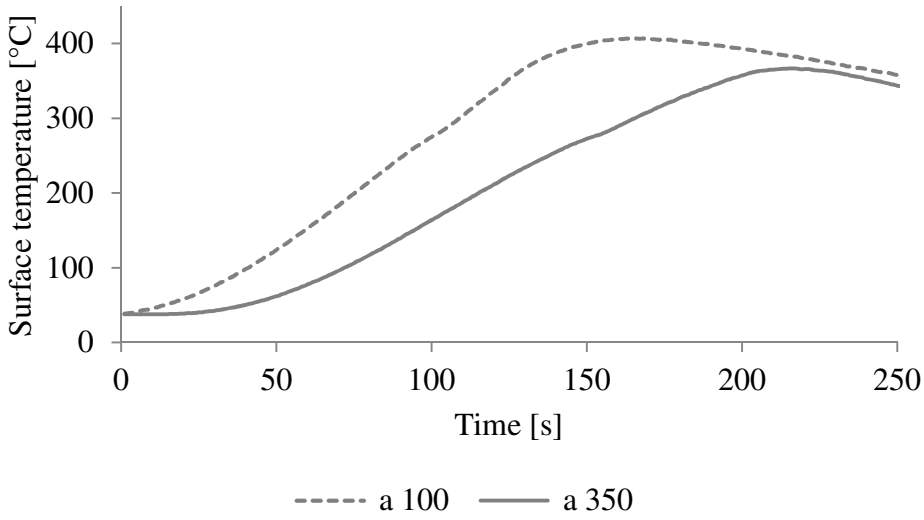

Figure 3.18 Impact of heater distance a on surface temperature

3.3. Conclusions

In this section complex thermoforming was defined and studied. Main aspect of complex thermoforming is the variable wall thickness from 2-10mm for 3-dimensional forming of structural parts. Organo sheet material for this process need to be custom made. Hence, consolidation and thermoforming have to be considered for the complex thermoforming process.

Complex geometry design was derived from an engine turbine airfoil at an approximate size of 400mm x 200mm x 50mm. It has a defined variable wall thickness from 2-9mm having local reinforcements and an aerodynamic profile from leading to trailing edge. Leading and trailing edge are defined and bent. A high flange forming angle of 95° occurs towards the main section around a curved edge. Forming was done in a double sided metal tool using a standard state of the art thermoforming process. Carbon fiber reinforced PPS which is used in structural aviation application was chosen.

Consolidation was carried out according to process recommendation using an autoclave process. The consolidation process took 66min. Consolidation is very time intense comparing the further processing. Thermoforming process time was below 10min. An efficient process development regarding complex thermoforming is required. For comparison, vacuum consolidation was done. No difference regarding preform fitting, processing or handling was deter-

mined. Highest potential regarding time efficiency lies within the consolidation process. The temperature history during process is relevant for the composite polymer, but consolidation is a previous step before final material temperature treatment. Details of the process optimization with focus on consolidation process optimization have to be studied.

Demonstrator thermoforming was done according to process recommendations. Evaluation of temperature impact was done on basis of thermal and optical evaluation. Indicators for local material damage were found during thermal analysis. At the same time, unmelted sections on the part downside were detected. Along local increased wall thickness, temperature did not exceed melting temperature and no forming along tool geometry occurred. An increase in minimum material temperature on bottom side was achieved by reducing heater distance.

Process constraints for complex thermoforming were derived from demonstrator forming results. Complex thermoforming requires temperature process control. For application in structural parts, the process conditions must not impact material performance. Potentials of the complex thermoforming process depend on the understanding of temperature behavior throughout the process and its control within a processing window. Control and definition of temperature history during complex thermoforming is the key for high quality complex manufacturing. General processing guidelines are needed with respect to wall thickness variation.

4. Experimental investigation

During experimental investigations, consolidation and thermoforming were studied separately.

Preform consolidation is a necessary, previous processing step for any type of custom made organo sheet used for complex thermoforming. Within the whole thermoforming processing chain, consolidation is an important process step to enable rapid heating during thermoforming. Consolidation is time intense according to general recommendations [39]. During demonstrator building, different process variations for consolidation of complex organo sheets were investigated and no difference in preform handling, processing or tool fitting was found. In this section, consolidation process variations for press consolidation were studied and evaluated with respect to resulting organo sheet thickness and mechanical performance.

Complex thermoforming demonstrator building further showed that temperature control throughout the thermoforming process is essential for successful part forming without causing material degradation. Processing complex parts needs a defined and enlarged temperature process window in comparison with standard thermoforming. This is to ensure highest material performance standards. For semi-crystalline polymers, temperature history is directly linked to polymer structure and material properties [30]. Complex geometries cannot be processed within recommended thermoforming conditions. Impact of resulting process conditions due to variable wall thickness on mechanical performance was studied. Process impact factors were rated to judge process drift from ideal thin-walled material processing towards complex part processing conditions.

Material used in this thesis is Celstran® CFR-TP PPS CF 60-01 from Ticona GmbH [74]. The Thermoforming unit KV 289, Rucks Maschinenbau GmbH, Glauchau at the Institut for Carbon Composites at the Technische Universität München is used for all experimental work.

4.1. Consolidation

Complex thermoforming requires custom made preforming built up from thermoplastic reinforced tape and fabric material. This material needs to be pre-processed before thermoforming in a so-called consolidation process. Fast heating process during thermoforming requires a consolidated preform stack to ensure rapid heat conduction along material through thickness. Without sufficient consolidation, even material temperature distribution during heating is not possible. Lack of heat conduction is caused by insulation behavior of large voids.

In this section, consolidation process variation for organo sheet manufacturing is done via press consolidation. Consolidation was carried out using organo sheets of constant wall thickness to allow mechanical testing according to standards. Impact of consolidation was determined after consolidation and after subsequent thermoforming.

During consolidation pressure and temperature and defined cooling are applied. Process recommendations for consolidation are made for press forming processes without subsequent thermoforming. Thermoforming heating is done via infrared, hence pressure-less and subsequent forming, consolidation and cooling are done in one processing step. Pressure-less heating can increase the void content of a thermoplastic composite up to 40% [37,76].

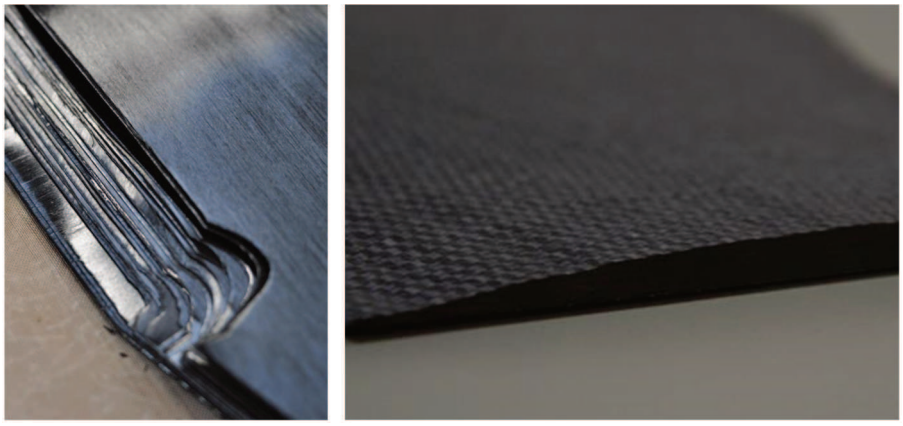

Figure 4.1 Preform stack before (left) and after (right) consolidation

4.1.1. Processing

Key parameters during consolidation are pressure and time. Processing guidelines can be found for consolidation or press forming of thermoplastic tape and fabric material (2.2) [39,77].

To optimize the consolidation process the impact of reduction in consolidation time and pressure was studied as shown in Table 4-1. Consolidation temperature was not varied, and held constant at 330°C for all variations. Consolidation time was varied in two steps from the basis of 30min to 15min and 5min. Consolidation pressure was varied from 1,9bar to 3,8bar and 7,5bar. Recommended pressure level for press consolidation is 17 bar. Heating and cooling rate was set constant on 15K/min. Consolidation was done in a closed mold in a heated press (Figure 4.2). Sealing of the consolidation tool was very important to avoid material flow during consolidation, especially for high pressure and long consolidation times. A high temperature sealing tape was used.

Table 4-1 Consolidation parameters

Consolidation temperature		330°C	
Consolidation time [min]	5	15	30
Consolidation pressure [bar]	1,9	3,8	7,5
Heating rate [K/min]		15	
Cooling rate [K/min]		15	

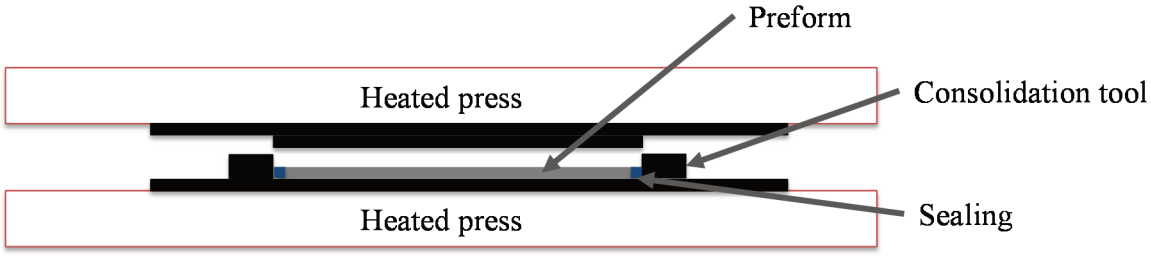

Figure 4.2 Consolidation tool

Consolidation pressure was applied when material temperature reached 310°C. Consolidation time started when pressure was applied. Cooling was done under pressure as well.

For each set of consolidation parameters two identical organo sheets were manufactured. One organo sheet was evaluated directly; the second one was thermoformed before evaluation.

Conditions of subsequent thermoforming were chosen close to the standard Tencate processing recommendation [77] applicable for thin walled structures and are shown in Table 4-2. Maximum infrared temperature was set at 360°C. This is 30K above maximum organo sheet mid temperature of 330°C. Recommended tool temperature was 170°C. Thermoforming was done in a V-shaped tool, for details see 4.2.1. Thermoforming pressure of 50bar (equivalent of 70bar / projected area) was slightly above Tencate recommendations. Time in mold was defined 1,5min. This was to ensure sufficient material cooling and dimensional stability before demolding.

Table 4-2 Thermoforming parameters

Maximum heater temperature [°C]	360
Material forming temperature [°C]	330
Tool temperature [°C]	170
Thermoforming pressure [bar]	50
Time in mold [min]	1,5

Organo sheets had a symmetric, 13 cross ply lay-up, having 0° layer on top, bottom and middle. According to single ply thickness of 0,156mm, organo sheets of 2mm reference wall thickness were manufactured and tested according to standards (2.6).

Two mechanical tests were carried out for determination of flexural strength and interlaminar shear strength. Flexural strength is a value often compared in literature and was therefore used to range and compare material quality of this work with data from literature. Interlaminar shear strength is a matrix specific value that was chosen to illustrate the impact of consolidation process variation on interlaminar shear strength.

Flexural strength was determined via a three point bending test according to DIN EN ISO 14125 (2.6.1) [67]. Specimen dimension was 100x10x2mm, bearing distance L was at 80mm. Ratio of bearing distance L over material thickness d was at 40. Inter-laminar shear- strength was measured via DIN EN 2563 (2.6.2) [69].Specimens of 20x10x2mm were three-point-bended at bearing distance of 10mm. Ratio of bearing distance L over material thickness d was at 5. Test speed was at 1mm/min. All testing was performed at a universal testing machine Inspekt 100, Hegewald & Peschke GmbH, Nossen with a 10kN load cell. At least five samples were tested.

4.1.2. Results

Evaluation of the manufactured panels was done after consolidation and after thermoforming. Seven different consolidation conditions varying pressure and time were investigated. Lowest and highest pressure levels of 1,9bar and 7,5bar were each used for consolidation times of 5min, 15min and 30min. Intermediate pressure level of 3,8bar was studied at 15min consolidation time.

First reference value for comparison was panel thickness after consolidation and after thermoforming. Figure 4.3 shows the panel thickness according to consolidation conditions. Con-

solidation conditions were varied according to x-axis labels (see also Table 4-1). Thermoforming conditions were identical for all panels according to Table 4-2 and are not shown in Figure 4.3. Black columns represent consolidated specimen results; grey columns represent results after consolidation and subsequent thermoforming. Consolidation processing conditions are equivalent to consolidation time and consolidation pressure values naming each set of columns. Theoretical panel thickness according the suppliers cured ply thickness is 2,03mm and is illustrated by the dashed line.

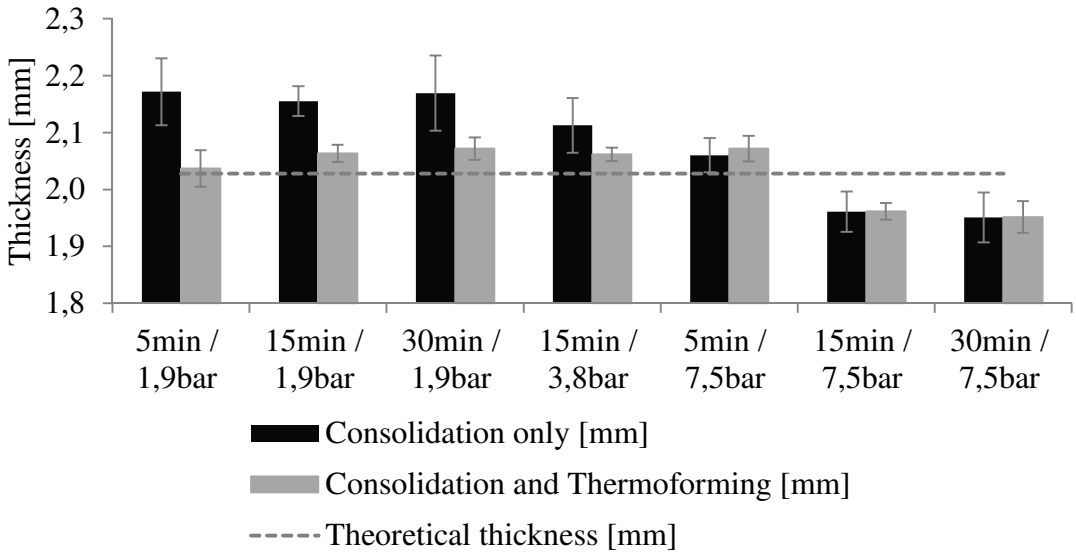

Figure 4.3 Panel thickness according to consolidation conditions after consolidation and after consolidation and thermoforming

For pressure of 1,9bar and 3,8bar a decrease in panel thickness from consolidation to thermoforming was determined. A post-compaction during thermoforming occurred. For a pressure of 7,5bar wall thickness level hardly changed from consolidation to thermoforming. Wall thickness tended to increase within the deviation limits and no further compaction was achieved via thermoforming. Long consolidation time of 15min and 30min at a consolidation pressure of 7,5bar resulted in a panel thickness below reference thickness.

In general, deviation decreased from consolidation towards thermoforming from 4% down to 2%. Average panel thickness decreased from consolidation towards thermoforming from 2,08mm to 2,03mm.

Low consolidation pressure went along with increased panel thickness. After thermoforming, the difference in wall thickness could not be shown anymore. Consolidation time did not have a similar impact as consolidation pressure (Figure 4.3).

Tool sealing during high pressure consolidation especially at high consolidation times was an important and hard to handle issue. High pressure allowed material flow into very small holes, resulting in local material flow acceleration out of the tool.

Flexural strength results were gained from a three point bending according to DIN EN ISO 14125 (2.6.1). The overall range of flexural strength from different sources is shown in Figure 4.4. Reference data from Tencate [78] and McCool [36] was used. Material supplier Tencate gives a range of 0,83MPA – 1,04MPa in its Cetex Material Data Sheet. McCool used Tencate Material for thermoforming tool temperature variation investigations. McCool tested according to ASTM D790 with a flexural stress range from 0,7-1GPa. Low flexural strength values from McCool resulted from very low tool temperatures during processing which was studied in this work. Results from consolidation impact study are shown in the last column. The range includes all results after consolidation only and after both consolidation and thermoforming. Flexural Strength range was from 0,9-1GPa.

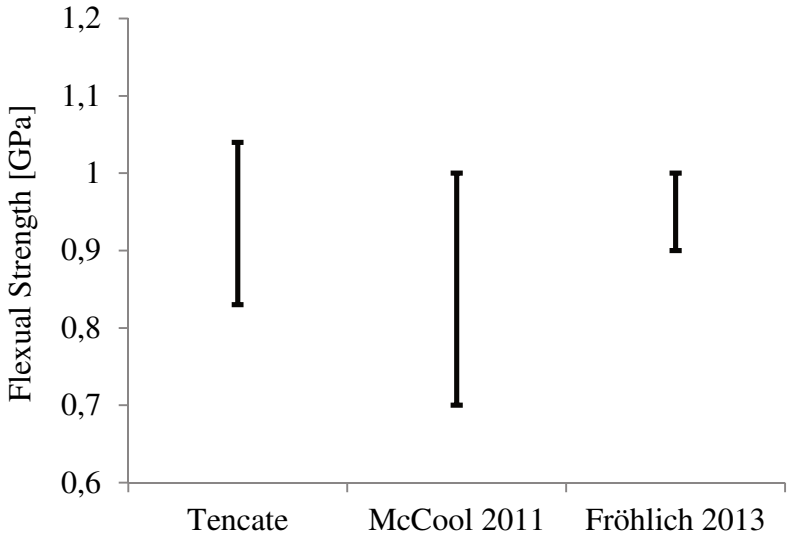

Figure 4.4 Comparison of Flexural Strength Results

Generated data had in comparison with other data a low overall variation in the upper half of the literature values. Therefore, general specimen quality was defined good as material performance was at a competitive level.

Figure 4.5 shows a detailed analysis of the flexural strength over processing conditions. Overall average flexural strength was at 952MPa. Average flexural strength after consolidation was at 948MPa (deviation 68MPa / 7%), average flexural strength after thermoforming was at 955MPa (deviation 93MPa / 10%). Flexural strength values after thermoforming increased slightly by 0,7% (deviation increased by 3%) in comparison with flexural strength after consolidation.

No clear trend for processing impact within consolidation variation or from subsequent thermoforming could be derived. An increase of failure at a bending distance of 8,3-8,33mm was found. 46% of the specimens tested after thermoforming failed at this bending distance and 16% of the consolidated specimens. This was the maximum bending distance measured. Failure mechanism were fiber dominated (fiber fracture). Shear failure was not determined until bending limit. Fiber matrix bond seemed to be improving after thermoforming in comparison to consolidation as higher bending angles were achieved.

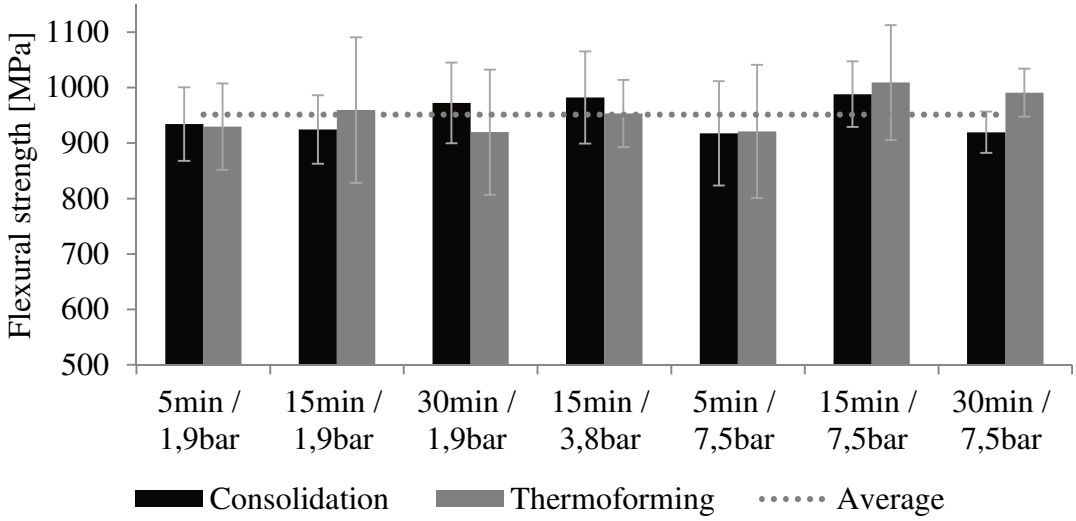

Figure 4.5 Maximum bending stress after consolidation and subsequent thermoforming

Interlaminar shear strength (ILSS) determined the maximum shear at the time of first failure on behalf of a three-point-bending test set-up (2.6.2). Interlaminar shear strength is influenced by matrix and fiber-matrix-interface.

Figure 4.6 shows the force-distance-curve during ILSS testing for a sample specimen. The failure behavior during ILSS testing was plastic having a clear maximum. According to the standard interlaminar shear strength can only be detected when the failure behavior is an interlaminar single or multiple shear with a sharp force drop. Still relative comparison was possible due to the repeatable behavior and is allowed in the standard. Shear strength τ determined from the generated ILSS testing data was not true interlaminar shear strength. Therefore, plastic interlaminar shear strength represented by $\tau_{plastic}$ is introduced.

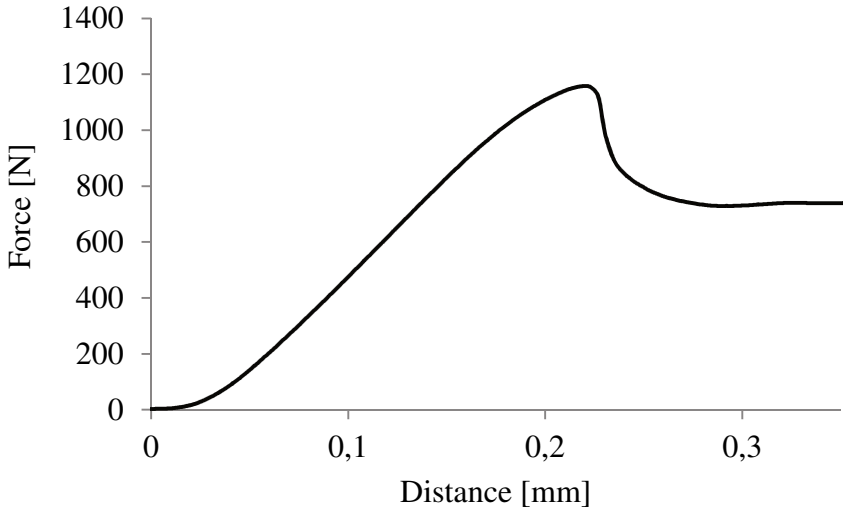

Figure 4.6 Applied force over bending distance during ILSS testing

Values for plastic interlaminar shear strength after consolidation are shown in Figure 4.7. Consolidation conditions are shown along the x-axis. Plastic interlaminar shear strength ranged from 20MPa (15min at 1,9bar consolidation) to 34MPa (5min at 7,5bar consolidation). Minimum value was only at 60% of the maximum value, deviation within single test series varied from 1% to 9%. A trend for high plastic interlaminar shear strength at higher consolidation pressure could be derived from results. An impact of consolidation time variation could not be derived.

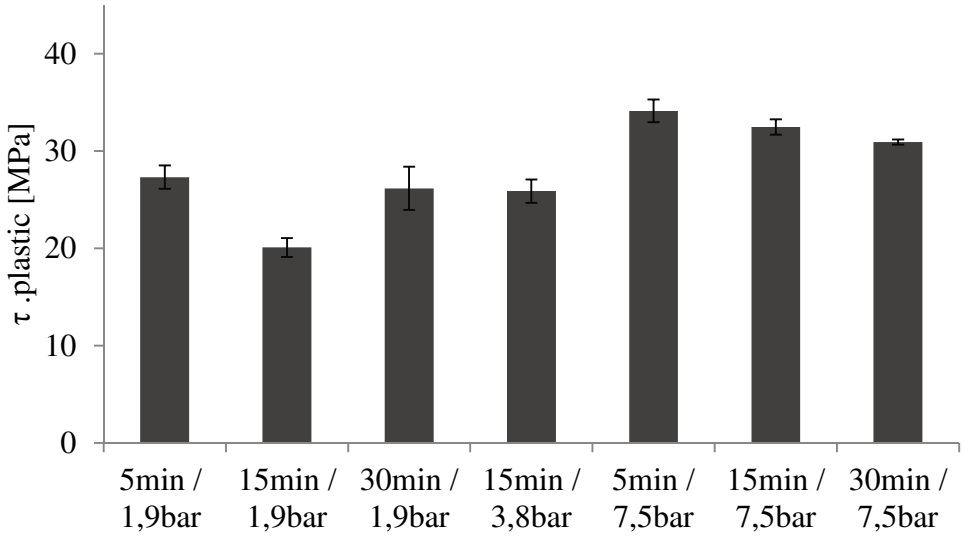

Figure 4.7 Plastic interlaminar shear strength after consolidation only

Figure 4.8 shows the plastic interlaminar shear strength after consolidation and thermoforming. Consolidation conditions are shown along the x-axis. Thermoforming conditions were kept constant according to Table 4-2. Values for $\tau_{plastic}$ ranged from 38,5MPa to 43,3MPa. Minimum value was at 88% of the maximum value. Standard deviation maximum was at 6%. Among the thermoforming results no performance trend regarding impact of former consolidation processing was seen.

The comparison of $\tau_{plastic}$ from consolidated specimens towards thermoformed specimens showed an increase in average shear strength level from 28,1MPa to 40,4MPA. Standard deviation from consolidation towards thermoforming over all tests decreased from 16% down to 3%.

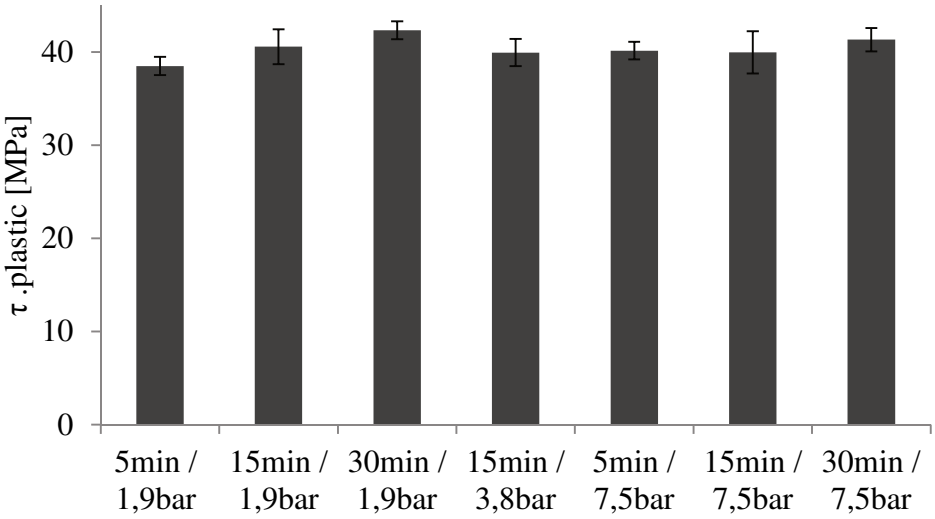

Figure 4.8 Plastic interlaminar shear strength after consolidation and thermoforming

Figure 4.9 split results for $\tau_{plastic}$ according to maximum consolidation pressure during processing. Consolidation levels from both consolidation and thermoforming were considered. First three columns show $\tau_{plastic}$ for different consolidation pressure levels. Last column is a mean value of specimens after consolidation and thermoforming. Thermoforming pressure level was kept constant for all specimens at 50bar (Table 4-2). A clear trend for increase of $\tau_{plastic}$ along with increase in maximum consolidation pressure level was shown. The plastic interlaminar shear rate increased from 24,5MPa at 1,9bar consolidation pressure up to 40,4MPa at 50bar thermoforming process pressure. Along with the increase in consolidation pressure the deviation decreased from 14% down to 4% of the average value. There was only a very small deviation of overall $\tau_{plastic}$ of thermoformed specimens. Impact of prior consolidation process variation could not be seen.

For consolidation of complex organo sheets a consolidation process of 5min at 1,9bar is sufficient. Processing conditions of the thermoforming process were found dominating over con-

solidation conditions. Overall deviation of thermoforming specimens was smaller than each deviation value of consolidated specimens. Consolidation time was reduced by 83% in comparison to press forming process recommendations. Consolidation pressure level during consolidation was reduced by 85%.

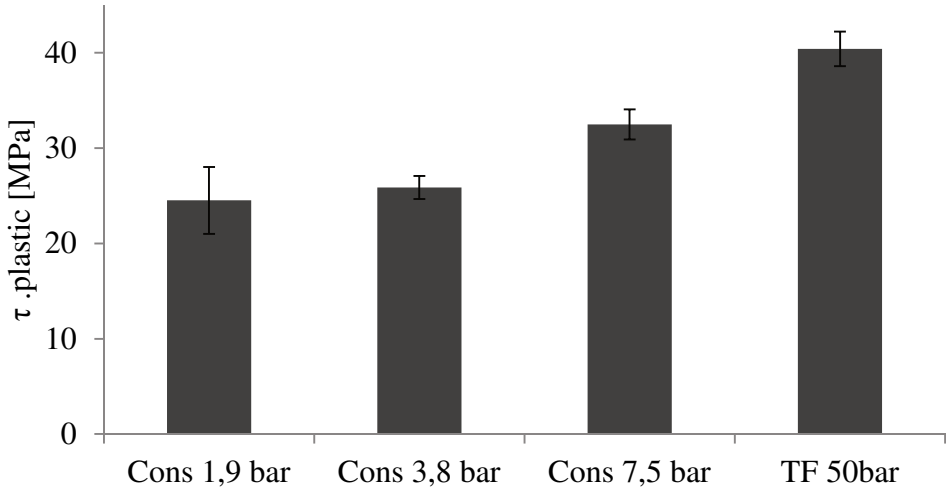

Figure 4.9 Plastic interlaminar shear strength over processing conditions

4.2. Thermoforming

During thermoforming of composite material its matrix material is brought to melt and cooled afterwards. A semi-crystalline polymer like PPS loosens its polymer structure during melting and builds up crystalline and amorphous areas during cooling. Ideal processing conditions are derived from the crystallization kinetics of the polymer used. There are three main mechanisms responsible for building up of the crystalline structure for a polymer like PPS: isothermal crystallization (tool temperature), non-isothermal crystallization (cooling rate) and time and temperature in melt. Formation of crystals and rate of crystallization are dependent on those parameters. The crystalline structure and degree of crystallinity have impact on mechanical performance. In general, higher degree of crystallinity gives the polymer higher stiffness and tensile strength, low degree of crystallinity (high amorphous content) improves impact resistance. For details see 2.4.1.

Processing conditions of a part of wall thickness from 2-10mm differ from recommended processing conditions. This results in different temperature profiles within the material. Heating rate, time above melting temperature, maximum material temperature and cooling rate vary according to local wall thickness and processing conditions.

Panels of thicknesses from 2mm to 10mm were processed and tested to study the impact of temperature during thermoforming. The effect of wall thickness variation for identical process conditions on mechanical behavior was studied as well as impact of non-ideal processing as occurring during complex thermoforming.

During thermoforming above mentioned crystallization effects depend on each other and cannot be seen separately. Their impact under processing conditions was studied. The different crystallization mechanisms were rated and temperature based processing window for complex organo sheets was derived.

4.2.1. Processing

Complex thermoforming implies processing outside of recommended processing windows provided by suppliers. The definition of acceptable maximized processing conditions is necessary to define a processing window for organo sheets of variable wall thickness. A variation in temperature history is studied to see how far ideal processing can be stretched. Recommended thermoforming conditions are introduced in 2.3.

Table 4-3 summarizes the process parameters, that were left constant during this study. Heater distance was at 100mm and sample organo sheet size was 200x400mm. Maximum infrared heater temperature was held constant at 360°C. Thermoforming pressure was set on 50bar (70bar projected area) for 2min. Consolidation time was increased as wall thickness was up to 10mm and cooling time therefore prolonged. Sufficient cooling is important to ensure dimensional stability of the polymer before demolding. Cooling time required varied with a variation in tool temperature and wall thickness.

Impact of temperature history on performance was investigated for determination of a processing window.

Table 4-3 Constant defined thermoforming conditions

Infrared heater distance [mm]	100
Organo sheet size [mm²]	200x400
Max. infrared heater temperature [°C]	360
Thermoforming pressure [bar]	50
Time in mold [min]	2

In 2.4.1 the impact of temperature profile during processing for a semi-crystalline polymer was introduced. Process parameters of melt temperature, time in melt, cooling rate and tool temperature have an impact on the degree of crystallinity of the material.

Regarding time and temperature in melt, mid material temperature during preheating was varied from 300°C, 330°C and 360°C. 330°C was the recommended processing temperature from ideal processing conditions. This did lead to variable heating times and variable material temperatures in melt. Resulting temperature profiles were logged.

Tool temperature was varied from140°C, 170°C and 200°C. Temperature of minimum crystallization half time is at 170°C. Temperature of minimum crystallization half time is the temperature of fasted crystallization building (see 2.4.1).

Cooling rate is a resulting figure from both, temperature in melt and tool temperature. Cooling rates increase with a rising temperature delta between material temperature and tool temperature. A variation in organo sheet wall thickness also impacts the cooling rate.

Wall thickness was varied at 2mm, 4mm, 6mm, 8mm, and 10mm. A detailed overview of combined parameters tested is given in Table 4-4.

Table 4-4 Test matrix – Impact of thermoforming conditions

Mold temperature [°C]	140	170	200
Mid material temperature [°C]	Wall thickness variations [mm]		
300	2,6,10	6	2,6,10
330	6	2,4,6,8,10	6
360	2,6,10	6	2,6,10

Consolidation conditions for all panels were identical. Intermediate conditions of 15min consolidation at 330°C and a pressure level of 3,8bar with subsequent cooling of 15K/min were chosen. Panels all had a symmetric cross ply lay-up, with an uneven number of layers, resulting in 0° layer on both surfaces and mid of preform.

Impact of processing on material was studied via mechanical testing. ASTM D 6415 is chosen (2.6.3) [70]. A special forming tool to ensure a constant inner radius and a wall thickness dependent outer radius according to the standard were designed and used for specimen manufacturing. Displacement rate was 5mm/min. All testing was performed at a universal testing machine Inspekt 100, Hegewald & Peschke GmbH, Nossen, with a 10kN load cell. At least five samples were tested.

4.2.2. Results

Evaluation of impact of the thermoforming process was done via determination of interlaminar strength, which is equivalent to the maximum radial stress (2.6.3). Aspects of investigation were temperature in melt, tool temperature and cooling rate. Time in melt and cooling rate were resulting figures.

Cooling rate is dependent on melt temperature, tool temperature and wall thickness. According to the test matrix, 6mm panel thickness was studied with all test matrix variations. Figure 4.10 shows radial stress performance in dependence of cooling rates for panels of 6mm thickness. Symbols depend on the tool temperature level as shown in the legend. Temperatures shown are all temperature from preform mid-plane. Fastest cooling rate was from 360°C melt temperature to 140°C tool temperature at 1,8K/s. Lowest cooling rate was from 300°C melt temperature to 200°C tool temperature at 0,7K/s. The higher the temperature delta between preheating temperature and tool temperature, the faster the cooling was. No trend was derived from cooling rate towards radial stress performance within the studied range from 0,7K/s to 1,8K/s. For a complex preform, a cooling rate variation throughout the material in this range will not affect radial stress values.

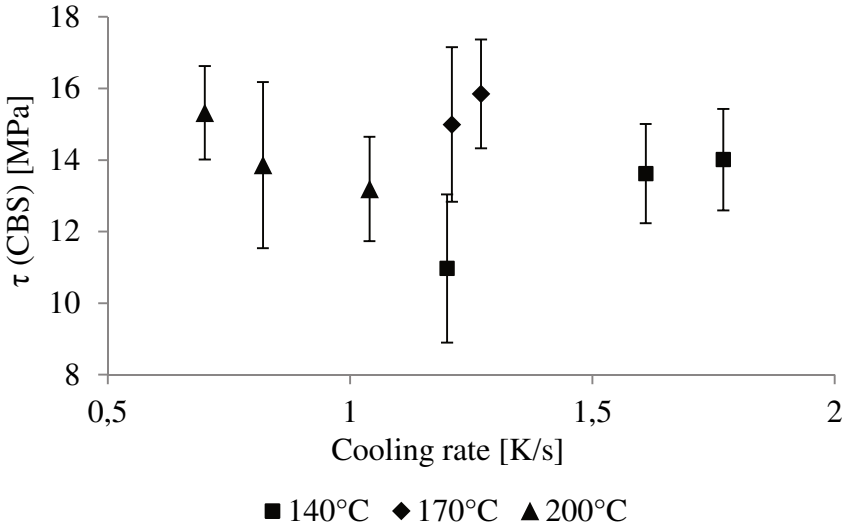

Figure 4.10 Radial stress over cooling rate of 6mm panels

Time in melt depends on the wall thickness and on the temperature of melt. The impact of temperature in melt (mid plane of preform) on radial stress is shown in Figure 4.11. Preform wall thickness of the values shown was 6mm, values each was averaged over the different tool temperature variations. Radial stress values ranged from 13,8MPa to 14,4MPa with deviation of 1,3MPa to 2MPa. A small trend towards improvement for higher melt temperatures by 4% within standard deviation was found. No definite impact of melt temperature was derived from these results.

Time in melt to reach 360°C mid temperature was about 35s longer than time in melt when heated to 300°C. Within this range of time and temperature, time in melt does not impact radial stress performance either. Time and temperature in melt do not impact radial stress performance within the studied range.

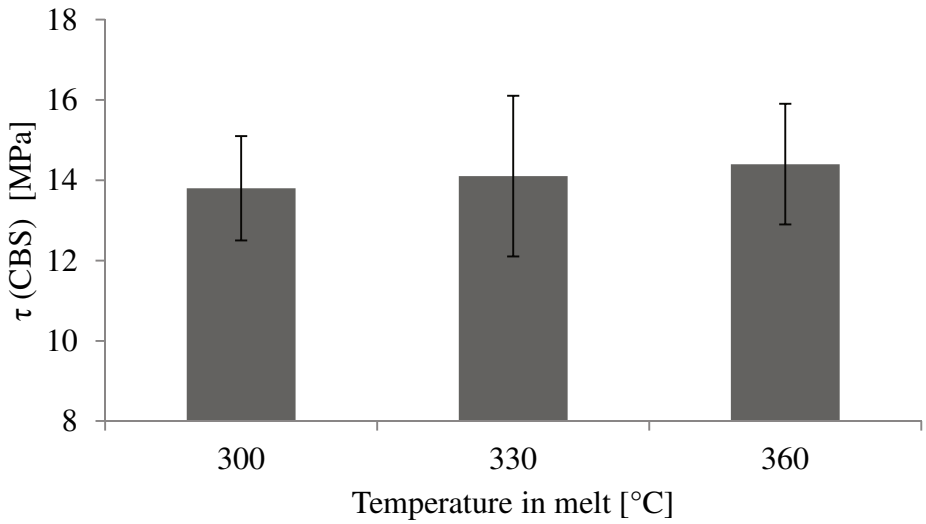

Figure 4.11 Impact of melt temperature on radial stress

Values for degree of crystallization in dependence of melt temperature are summarized in Table 4-5. Degree of crystallization was determined for all variation via thermal analysis using DSC (2.6.4). Determination of degree of crystallization was based on a maximum crystallization enthalpy of 112J/g and an average matrix weight content of 40%. Cold crystallization was negligible due to a heating rate of 20K/min and could not be determined from enthalpy curves. For all degree of crystallinity values for this test series, deviation was at 2% degree crystallization for identical processing conditions.

Looking at results of degree of crystallization for variation of melt temperature (Table 4-5), a trend for slight crystallization increase from 40% to 43% was shown.

Table 4-5 Degree of crystallization according to melt temperature for 6mm panel

Melt temperature [°C]	Degree crystallization [%]
300	40
330	42
360	43

Figure 4.12 shows the radial stress over the variation of wall thickness. Average value of the presented values is shown by the black horizontal line. Radial stress values ranged from 11,3MPa to 15,4MPa, average radial stress was at 13,6MPa. Values were determined from different processing conditions regarding temperature in melt. Impact of temperature in melt was shown insignificant (Figure 4.11). Tool temperature was constant at 170°C. Radial stress performance of panels of 2mm, 4mm, and 6mm was above average; performance of 8mm and 10mm was below average. 10mm thickness panel resulted in the lowest radial stress value at 17% below average.

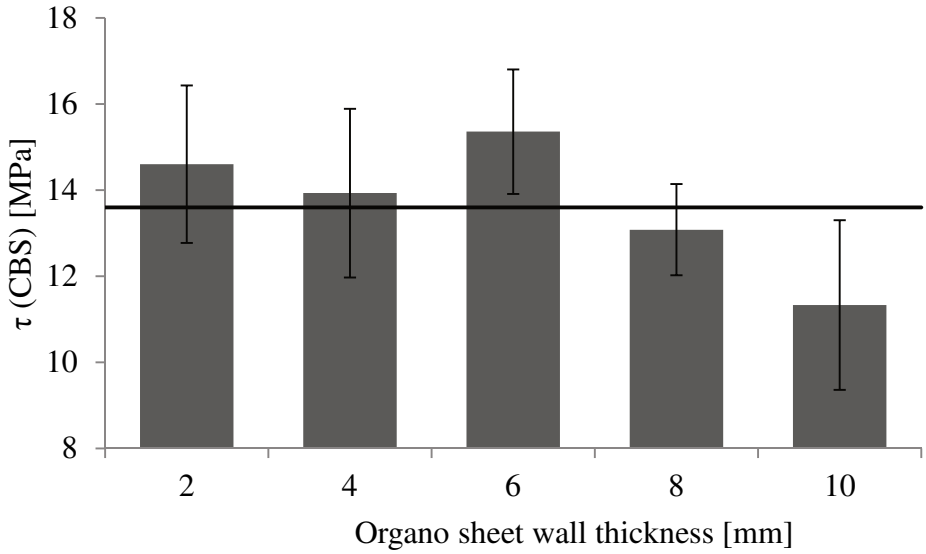

Figure 4.12 Radial stress over organo sheet wall thickness

An organo sheet of increased wall thickness has a lower surface temperature and lower overall heating rate. Table 4-6 gives an overview on thickness dependent average time in melt and maximum surface temperatures reached. The increase of time in melt can be clearly seen rising from 25s to 103s for a wall thickness change from 2mm to 10mm. Maximum surface temperature increased with wall thickness from 360°C to 435°C. The performance decrease went along with the onset of degradation at 410°C-420°C (2.4.1).

Table 4-6 Wall thickness dependent time in melt and maximum surface temperature

Organ sheet wall thickness [mm]	2	4	6	8	10
Average time in melt [s]	25	45	68	83	103
Max. surface temperature [°C]	360	380	400	420	435

A trend for lower degree of crystallization for higher wall thicknesses was found. Values for degree of crystallization in dependence of wall thickness are shown in Table 4-7. Samples of a wall thickness of 2-6mm resulted in an average degree of crystallization of 40%. Samples of wall thickness of 8-10mm had an average degree of crystallinity of 38%.

The impact of degree of crystallinity on mechanical performance like curved beam strength is complex. A reason for increased performance at an increased degree of crystallization might be due to the spherulites formed in the polymer matrix which might restrain the movement of molecular chains [36].

Table 4-7 Degree of crystallization according to wall thickness

Wall thickness [mm]	Degree crystallization [%]
2-6	40
8-10	38

The impact of tool temperature on radial stress is shown in Figure 4.13. Values were taken from constant 6mm wall thickness panels. Values were summarized for temperature levels of 300°C, 330°C and 360°C. Radial stress values ranged from 12,9MPa to 15,4MPa at standard deviation of 1,4MPa to 1,7MPa. A trend for improved radial stress performance at a tool temperature at minimum crystallization half time of 170°C was shown (2.4.1).

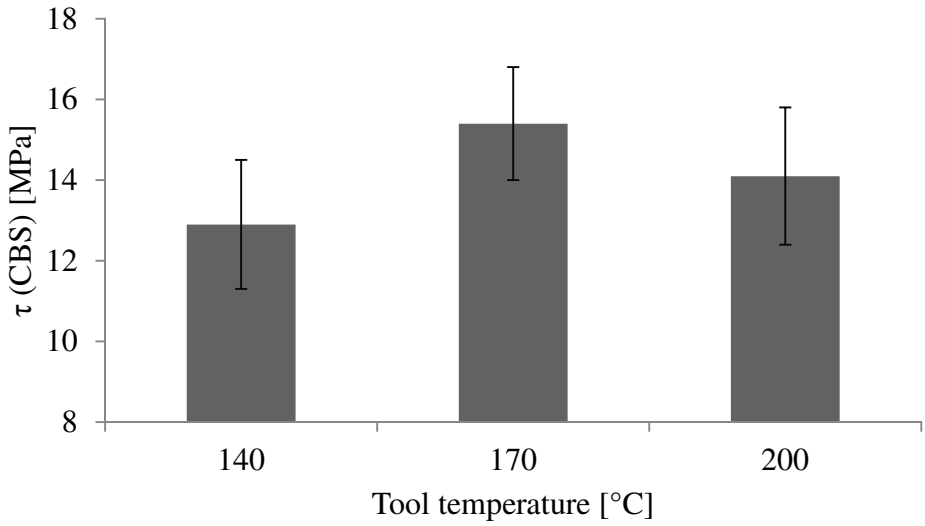

Figure 4.13 Impact of tool temperature on radial stress

At 170°C tool temperature, a tendency for an increased degree of crystallization value of 43% versus 41% and 40% for a 30K decrease or increase in tool temperature was found (Table 4-8).

Table 4-8 Degree of crystallization according to tool temperature for 6mm panel

Tool temperature [°C]	Degree crystallization [%]
140	41
170	43
200	40

Summarizing, an impact of radial stress performance in dependence of processing conditions was shown. The impact of several parameters which will vary during complex thermoforming from recommended processing conditions were studied. An impact on radial stress performance for material temperature in melt and tool temperature was found.

A tool temperature at temperature of minimum crystallization time was found to have a positive impact on radial stress. Temperature of minimum crystallization time of PPS is at 170°C. A tool temperature at 170°C increased radial stress performance by 12% compared to a 30K tool temperature offset. Tool temperature can be set independent from other processing conditions. It is important to radial stress performance of the thermoformed part and independent from other process conditions.

Impact of material temperature in melt on radial stress was found from degradation onset temperature upwards. Degradation onset of PPS is at about 410°C. Average radial stress decrease was 16% for temperatures of 420°C and higher. Further, a trend for decreased degree of crystallinity along with material temperatures above degradation onset was found.

PPS polymer properties are strongly related to the crystallinity structure [30]. The decrease of radial stress performance might be caused by less spherulites formed due to the lower degree of crystallinity. Spherulites restrain molecular chains from movement; hence increase material performance [36]. Crystalline phase further improves polymer stiffness [52] which also improves curves beam strength of the specimen. Upper temperature limit for PPS was therefore set at 410°C.

Minimum temperature limit was set at 310°C. This limit was chosen to ensure material temperature above melting temperature after transport and forming of thin walled materials (2mm). Considering a melt temperature of PPS is at about 282°C and an average material cooling rate of 3K/s [77], a time frame of 8s for transport and forming is acceptable.

Following, temperature processing window could be set from 310°C-410°C for complex thermoforming. An organo sheet of wall thickness from 2mm-10mm can have a minimum

material temperature of 310°C and a maximum material temperature of 410°C during preheating.

4.3. Conclusions

For a polymer, material properties depend on the temperature history (2.4.1). Several factors of temperature history have impact on the crystalline structure and hence the performance of the polymer. In literature, three main effects are described: time and temperature in melt, cooling rate and consolidation temperature [50,55]. During complex thermoforming, these effects occur in dependence of wall thickness. Their impact was studied by variation of process settings. Parameters varied were melt temperature and tool temperature. Depending on these parameters time in melt and cooling rate did change. Experimental evaluation was done on the basis of shear strength from V-shaped specimens of variable wall thickness (2.6.3).

Time in melt and cooling rate were found to have no significant impact on the shear strength or degree of crystallinity (4.2.2). Those variables seem to be insignificant within the occurring preheating process variations. An impact of performance on temperature of melt and tool temperature was determined. The tool temperature was found to be best at the temperature of minimum crystallization time (Figure 4.13). The tool temperature is the temperature towards which the material is cooled down after preheating and forming and which is independent from other process conditions. Minimum crystallization time describes the temperature of fastest crystallization during consolidation. For CF/PPS this was at 170°C. A tool temperature of 170°C increased the shear strength by 12% compared to a 30K temperature offset in either way. A change in cooling rate due to different temperature of melt or local wall thickness seems to be less important than the tool temperature level. Temperature of melt only had an impact on shear strength and crystallization above degradation onset (4.2.2). Degradation onset of CF/PPS is at 410°C. The average shear strength dropped by 16% when maximum melt temperature reached temperatures of 410°C and more. Material damage seems to occur above degradation onset as the shear strength decreases.

The upper temperature limit for processing was set at 410°C to avoid material damage due to degradation. The lower preheating temperature limit was set 30K above material melting temperature. Melting temperature of PPS is at about 282°C. This was to ensure sufficient material temperature during forming for thin walled sections. An average literature value for material cooling rate of 3K/s during forming and transport was applied, allowing at maximum a time period of 8s. Temperature processing window for CF/PPS during thermoforming was set from 310-410°C.

Process parameters were defined basis of the temperature process window defined above. Detailed process definition is only necessary for the preheating phase. The preheating phase describes the infrared heating of the organo sheet before transport and forming (2.3). Cooling rate and tool temperature do not require special attention. The tool temperature is kept con-

stant at minimum crystallization time which resulted in different cooling rates depending on the wall thickness. It was shown that these cooling rates have no impact on the material shear properties within defined process temperature conditions (4.2.2). The preheating phase is dominated by the infrared heating. Relevant heat flows during infrared heating are due to radiation, convection and conduction.

5. Numerical tool development for thermoforming process definition

Temperature control during complex thermoforming is necessary for successful processing of complex organo sheets. Most critical phase during thermoforming is temperature control during preheating phase. In this phase, matrix material is brought to a temperature level above melting temperature to allow further processing. The temperature process window of preheating phase for complex organo sheets made from PPS has been defined in chapter 4.

Objective of this section is the development of a numerical tool to predict material temperature during preheating to ensure material temperatures within the defined window. The temperature window from 310°C-410°C.

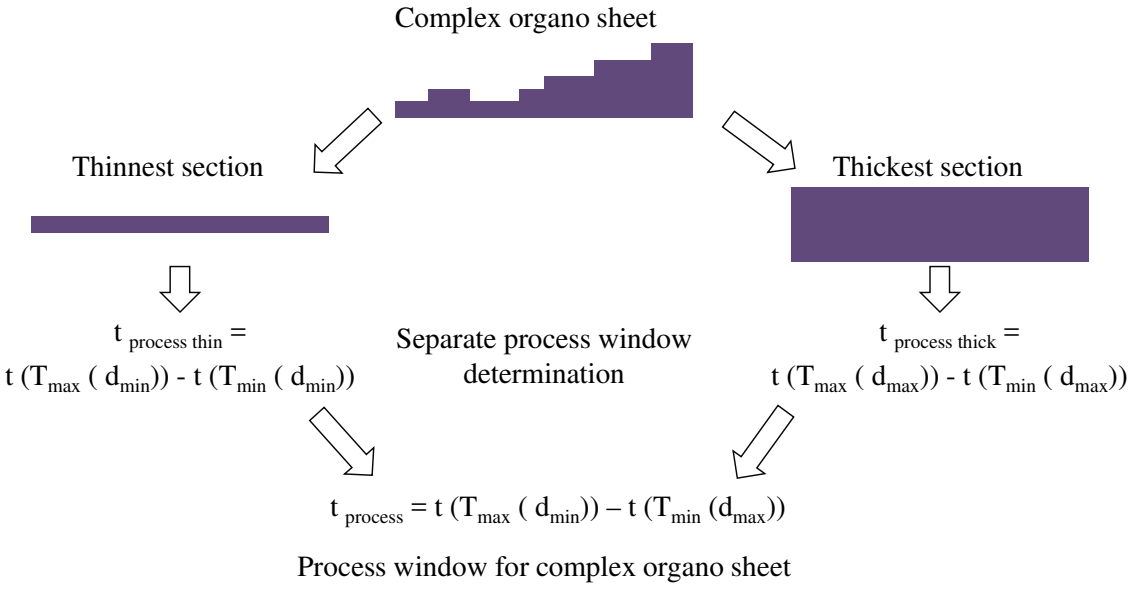

Figure 5.1 Scheme of process window determination for complex organo sheets

Figure 5.1 shows the scheme of the numerical tool for the process window determination. Process conditions for complex organo sheets depend on the thickest and thinnest wall sections. Therefore, process windows regarding time and temperature for thinnest and thickest wall sections are determined separately. Process window for complex organo sheets $t_{process}$ is derived from the overlap over the determined processing windows for thinnest section $t_{process\ thin}$ and thickest section $t_{process\ thick}$. Maximum temperature of the thinnest section

$T_{max}(d_{min})$ and minimum temperature of the thickest section $T_{min}(d_{max})$ limit the process window for complex organo sheets. Regarding PPS, T_{min} and T_{max} equal the defined temperature window from 310°C to 410°C. Wall thickness d_{min} and d_{max} are equal to 2mm and 10mm, respectively.

Organo sheet temperatures are derived from heat flows during infrared heating taking radiation heating, convection heating and conduction heating into account. The numerical tool determines the temperature T of the material in dependence of through thickness position z and heating time t. Process window in dependence of wall thickness is derived from the heating time to reach temperatures minimum and maximum process window temperatures T_{min} and T_{max} .

5.1. Assumptions

Follow heat flow mechanism by a modelling approach requires idealized assumption regarding process conditions. Following general assumptions for the numerical model are introduced. Further, equipment specific assumptions regarding temperature accuracy are explained.

5.1.1. General

The numerical model is an idealized model of the real temperature development during heating. The calculation of heat flows from an infrared heater to an organo sheet during thermoforming requires some simplifications based on assumptions. Following assumptions were made for the numerical approach:

- Organo sheet is a cuboid
- No material sagging during infrared heating
- Constant material values during heating
- Heater temperature set equal to surrounding air temperature
- Symmetric heating process
- One-dimensional heat conduction within the material

Assumptions towards symmetric heating and one-dimensional heat conduction are discussed in detail below.

The organo sheet is heated by an infrared heater from above and below during preheating. Due to their body temperature both heater and laminate (organo sheet) radiate and exchange energy. The radiation energy exchange of the laminate and the heater is a symmetric set up as shown in Figure 5.2.

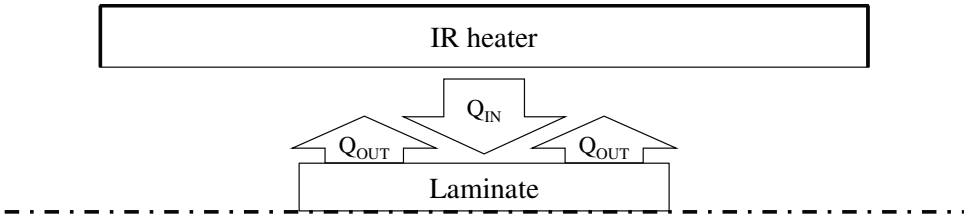

Figure 5.2 Radiation heat flows during IR heating

The temperature of a body depends on the equivalent of incoming and outgoing power (energy over time). The power change of a laminate $\dot{Q}_{Laminate}$ depends on the difference of incoming power $\dot{Q}_{IN}$ and outgoing power $\dot{Q}_{out}$.

$$\dot{Q}_{Laminate} = \dot{Q}_{IN} - \dot{Q}_{OUT} \qquad 5.1.$$

The assumption of a symmetric temperature profile of a body is valid when ambient temperature is homogenous (see Figure 5.3) [79].

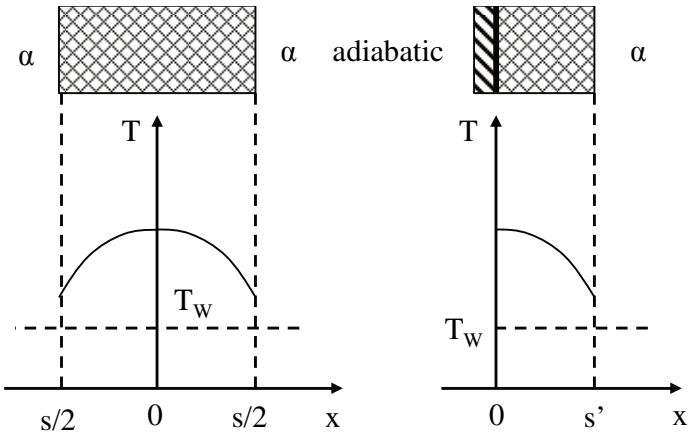

Figure 5.3 Assumption of a symmetric model [79]

Double sided infrared heating with heater distance *a* (100-350mm) << heater size (1300x1500mm²) leaves the organo sheet to an almost homogenous ambient temperature. Organo sheet size is at 4% of the heater's size. Side effects, heating difference from top to bottom side and convection effects are neglected.

The assumption of a one-dimensional temperature profile is very important for the process window determination from separate, constant minimum and maximum wall thickness processing slots. A one-dimensional temperature profile builds up when surface temperature is constant over the surface area. To proof this, the impact of the organo sheet size on surface temperature was studied. Heater distance was chosen as comparative parameter. Results are shown in Figure 5.4. The temperature curves from panels of size *S1* (200x400mm²) and *S2* (600x600mm²) processed at variable heater distance *a100* (100mm) and *a350* (350mm). No impact on temperature profile development due to panel size was found, whereas the impact of heater distance can clearly be seen. Evaluated panel sizes were at 4% (S1) and 18% (S2) of the infrared heater area, located in the heaters center.

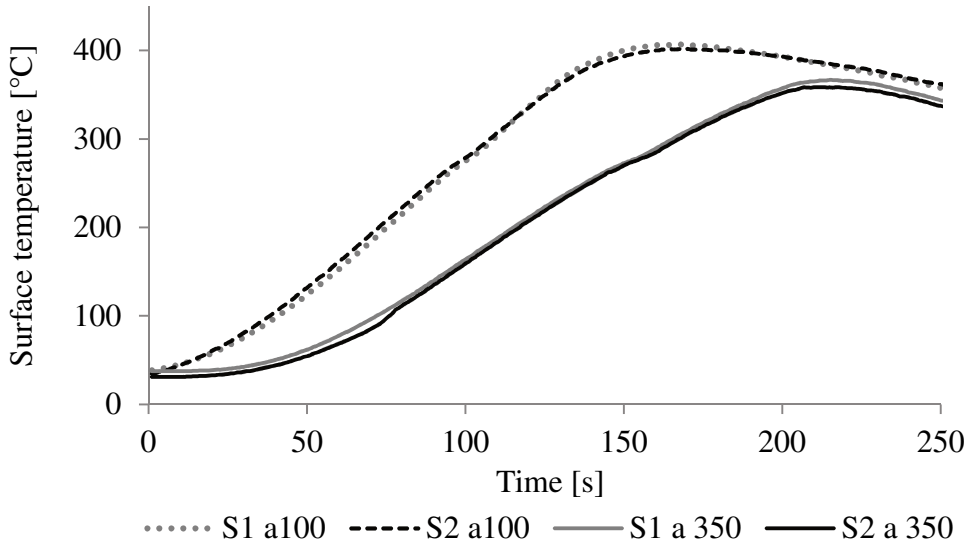

Figure 5.4 Impact of panels size S and heater distance a on surface temperature

In literature, a constant surface temperature is described as long as infrared heater size is significantly bigger than panel size [24].

5.1.2. Heating method specific

The set-up of a numerical temperature model requires consideration of heating method and equipment specific effects. In this work a thermoforming unit Rucks KV 289 was used. Preheating station has doubled sided infrared heaters Raymax 1120 from Watlow [62].

To define general preheating conditions, the parameters heater distance, maximum heater temperature, and temperature overshooting of the heater were studied. Those parameters have direct impact on material temperature development and can be varied for processing. Maximum preheating time is an imprecise value which is dependent on initial temperature of the infrared heater. Emitted power is dependent on heater temperature. Initial heater temperature is dependent on prior usage and cannot be set for processing.

Maximum heater temperature can be set up to a limit of 400°C. At the beginning of the thermoforming process, heaters are switched on and heating starts. At maximum set temperature, heaters are turned off shortly and temperature starts oscillation around the maximum set temperature. Figure 5.5 shows the temperature curve of an infrared heater having a maximum set temperature of 320°C. Oscillation of heater temperature (black line) and organo sheet surface temperature (grey line) around the heater set temperature (dashed line) can be clearly seen.

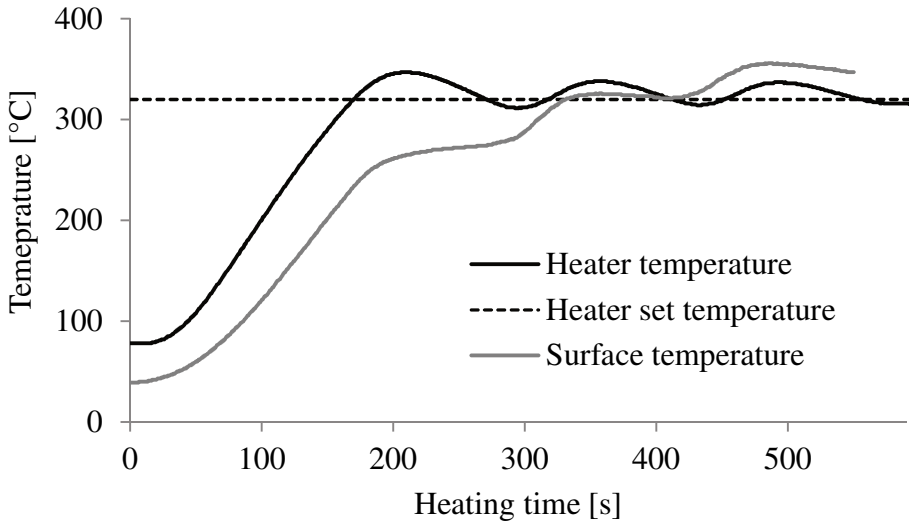

Figure 5.5 Oscillation of infrared heater temperature over time

The maximum occurring temperature was 345°C in the first overshoot. The second and third overshoots had a maximum temperature of 338°C and 337°C. Minimum temperatures during oscillation were 314°C and 316°C. Heater average temperature occurred at a level slightly above set temperature. A set temperature of 320°C resulted in a heater average temperature of 328°C. Panel surface temperature is affected by this heater oscillation, as emitted power varies according the oscillation.

Oscillation range depends on the maximum set temperature. Figure 5.6 shows maximum heater temperature in relation to the heater set temperature. Overshoot range is from 25°C at a maximum heater temperature of 320°C to 5°C at the heater temperature limit of 400°C. The overshooting decreases with an increase in maximum set temperature.

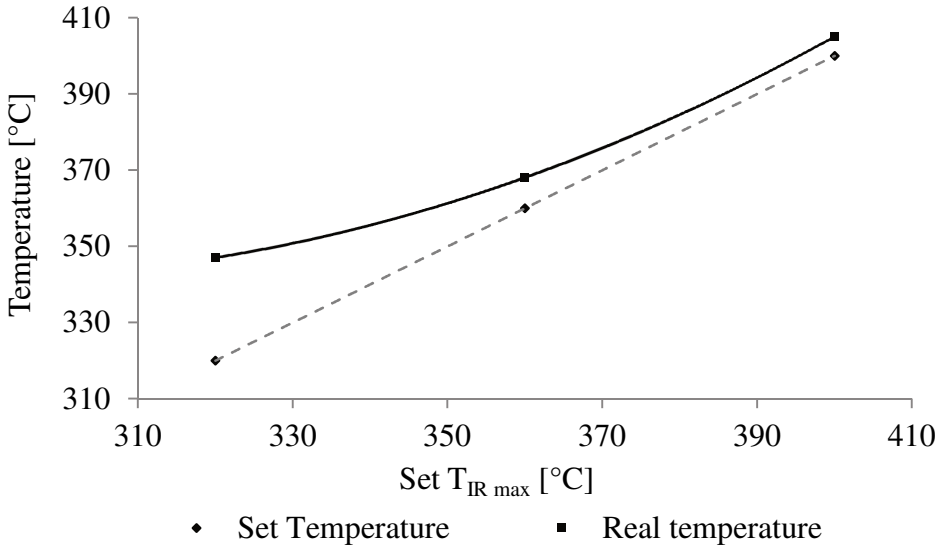

Figure 5.6 Heater maximum set temperature over maximum occurring temperature

A good approximation for the numerical tool during heater temperature oscillation was to assume the heater temperature at a constant level10K above maximum set temperature and reducing the emitted energy to 80% constant energy emission after reaching this temperature limit.

Figure 5.7 shows the impact of maximum heater temperature on surface temperature development. The surface temperature development of two 2mm CF/PPS organo sheets having a different maximum infrared heater temperature is shown. Continuous line represents organo sheet surface temperature for a maximum heater temperature of 400°C. Dashed line represents the organo sheet surface temperature for a maximum heater temperature of 320°C. Vertical lines indicate the time when in mid preform a certain temperature level is reached (minimum heating time) indicating the start for further thermoforming processing.

Heating time for decreased maximum heater temperature was prolonged only at elevated temperatures. At the same time very high surface temperatures (above degradation onset) were avoided. The limitation of the maximum heater temperature is and efficient parameter to limit surface temperatures, therefore chosen as parameter for the numerical tool evaluation, hence process window definition.

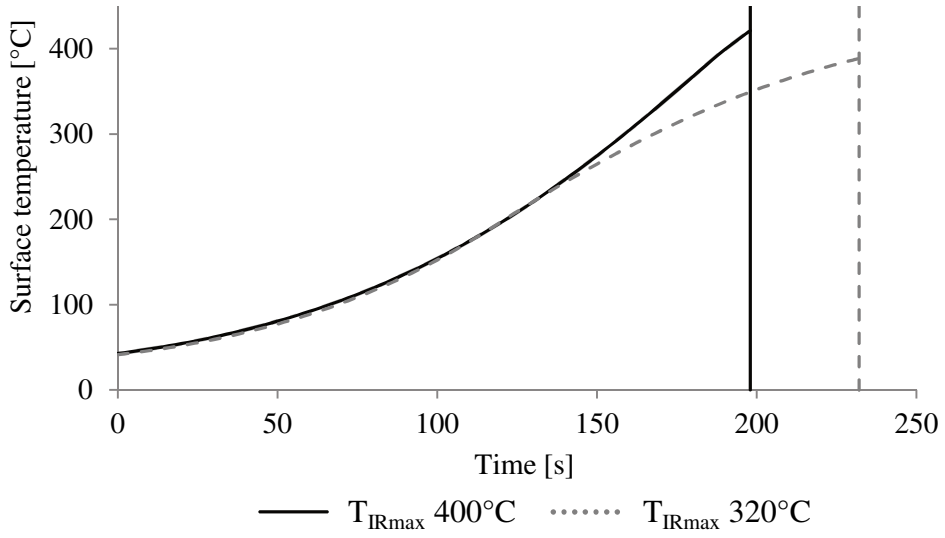

Figure 5.7 Comparison of heating time variation until T_{mid} 330°C is reached - surface temperature development for heater maximum temperature variation [40]

Second parameter to impact surface temperature development is infrared heater distance. A comparison of heater distance on surface temperature of a 2mm CF/PPS organo sheet is shown in Figure 5.8. Dashed line indicates a heater distance *a100* of 100mm; black line indicates a heater distance *a350* of 350mm. Surface temperature heating rate was decreased for an increased heater distance and overall heating time prolonged. These parameters impact the temperature increase over the whole heating time. It is not as efficient for avoidance of very high surface temperature as the limitation of infrared heater temperature.

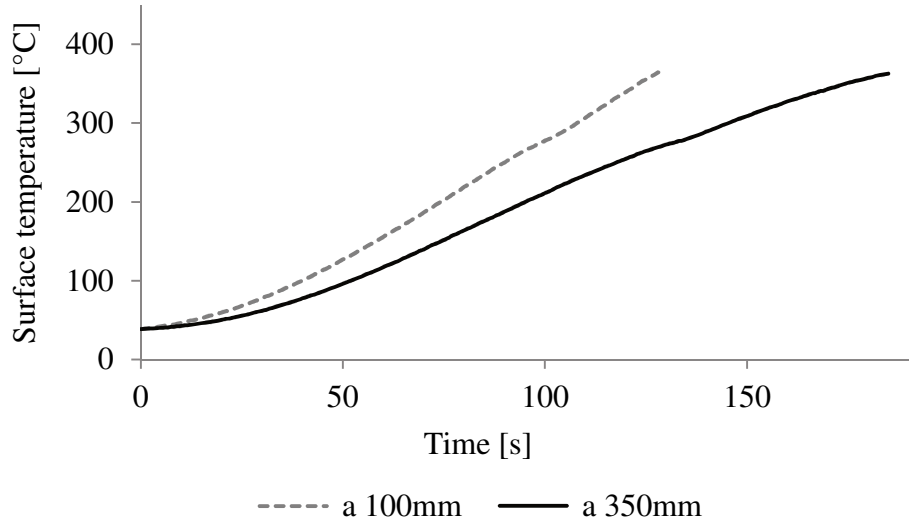

Figure 5.8 Surface temperature development for variation of heater distance *a* [40]

5.2. Numerical approach

The numerical tool is based on thermodynamic heat flows during infrared heating. Energy source is the infrared heater. Infrared radiation from the heater increases the surface temperature of the organo sheet. The organo sheet emits energy in dependence of its own temperature. In case of a temperature delta from the heater towards organo sheet surface free convection occurs. The sum of radiation and convection heat flow heats up the organo sheet surface. The whole organo sheet is heated via heat conduction from the temperature delta from surface towards the inner layers of the organo sheet.

The material temperature throughout the organo sheet is determined in dependence of position and time from radiation, convection, and conduction heat flows. Following the calculation of the heat flows is described in detail.

5.2.1. Radiation heating

The organo sheet is heated via radiation by power from the infrared heater. The power from the heater heating the laminate $\dot{Q}_{IR,H}$ depends on the heater size A_H, size and geometry of the laminate towards the heater (represented by the view factor of the heater towards the laminate $F_{H\rightarrow La}$) and the power density of the heater L_H.

$$\dot{Q}_{IR,H} = F_{H\rightarrow La} * A_H * L_H \qquad 5.2.$$

Organo sheet (panel) top side and bottom side surface areas are heated by a lower and a upper side heater. Vertical surfaces are heated from both lower and upper heater. View factors and heat flows have to be determined in dependence of surface and side areas. A symmetric assumption was used to determine radiation heat flows (5.1.1).

View factors were determined for every surface of the organo sheet. Upper and lower surface view factors were looked at first. Figure 5.9 shows the upper surface S_u seen by the upper infrared heater IR_u and lower surface S_l seen by the lower infrared heater IR_l. View factors F of the upper side and the lower side are equal.

$$F_{IRu-Su} = F_{IRl-Sl} \qquad 5.3.$$

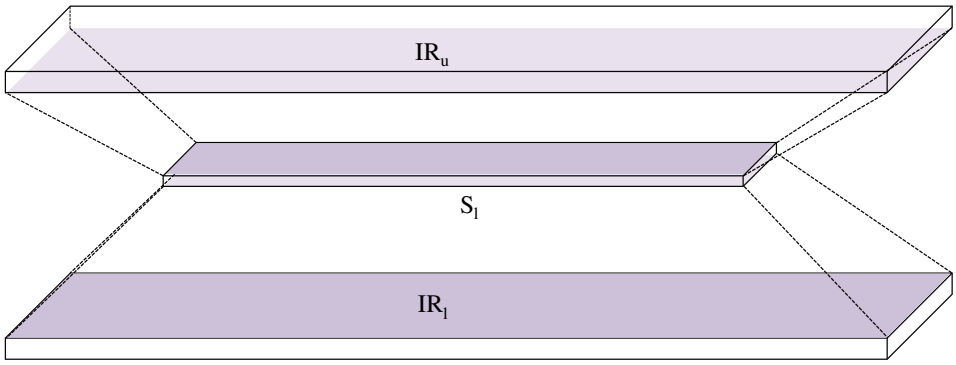

Figure 5.9 Relevant areas for view factors of panel surfaces

The calculation of these surface view factors was done using the approximation for the view factor of unequal coaxial square discs by Howell [80]. The assumption for two square surfaces instead of rectangular surfaces was valid as the panel located in the center of the heater having covering only 4% of the heaters area (5.1.1.). Surface square area values were determined from the equivalent surface rectangle area. The view factor F_{12} [80] is calculated via

$$F_{12} = \frac{1}{\pi * w_1^2} * \left(ln \frac{p}{q} + s - w \right) \qquad 5.4.$$

5.4 is applied for view factors F_{IR-S} and F_{s-IR} . The geometrical details for the determination on surface areas W_1 and W_2 and distance H are shown in Figure 5.10. Using W_1, W_2 and H equation 5.4 can be solved according to 5.5 – 5.11.

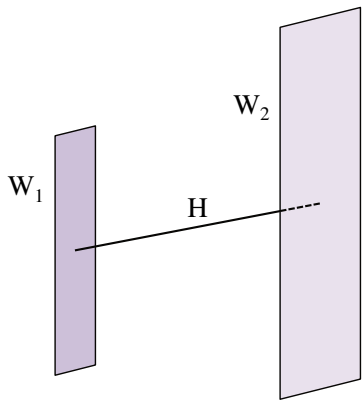

Figure 5.10 Geometrical assumption to determine view factor from heater to surface [80]

$$w_1 = \frac{W_1}{H} \quad w_2 = \frac{W_2}{H} \tag{5.5.}$$

$$x = w_2 - w_1 \quad y = w_2 + w_1 \tag{5.6.}$$

$$p = (w_1^2 + w_2^2 + 2)^2 \tag{5.7.}$$

$$q = (x^2 + 2) * (y^2 + 2) \tag{5.8.}$$

$$s = u * \left(x\, arctan\frac{x}{u} - y\, arctan\frac{y}{v}\right) \tag{5.9.}$$

$$w = v\left(x\, arctan\frac{x}{v} - y\, arctan\frac{y}{v}\right) \tag{5.10.}$$

$$u = \sqrt{x^2 + 4} \quad v = \sqrt{y^2 + 4} \tag{5.11.}$$

Relevant side view factor areas are shown in Figure 5.11. Each side surface of the panel has a correspondent area of seeing from each infrared heater. For example, panel side e_1 is seen by infrared heater areas IR_{2u} and IR_{2l}. View factors $F_{e1IR2-l}$ and $F_{e1IR2-u}$ are equal, as well as the corresponding view factors $F_{e2IR2-l}$ and $F_{e2IR2-u}$.

$$F_{e1IR2-l} = F_{e1IR2-u} = F_{e2IR2-l} = F_{e2IR2-u} \tag{5.12.}$$

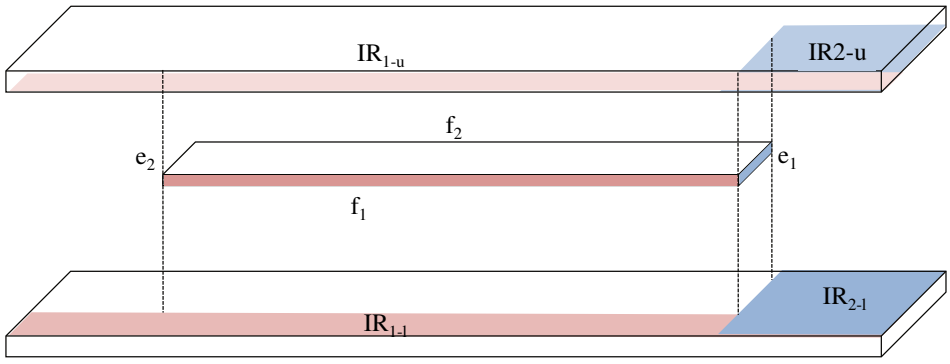

Figure 5.11 Relevant areas for view factor of panel side surfaces

View factors were calculated for each side of the panel towards each infrared heater and from each infrared heater to each side of the panel. View factor for panel sides and infrared heaters were calculated using a solution of [64] for perpendicular plates. Geometrical details are shown in Figure 5.12.

Geometric factors are

$$s^2 = x^2 - (y-\eta)^2 + \xi^2 \tag{5.13.}$$

$$cos\,\theta_1 = \frac{\xi}{s} \quad and \quad cos\,\theta_2 = \frac{x}{s} \tag{5.14.}$$

The view factor of perpendicular surfaces is calculated via

$$F_{1\to 2,\perp} = \frac{1}{A_1}\sum_{l=1}^{2}\sum_{k=1}^{2}\sum_{j=1}^{2}\sum_{i=1}^{2}\left[(-1)^{(i+j+k+l)}G(x_i, y_j, \eta_k, \xi_l)\right] \tag{5.15.}$$

G is calculated via

$$G(x,y,\eta,\xi) = \frac{1}{\pi}\int_{\xi}\int_{\eta}\int_{y}\int_{x}\frac{x\,\xi}{[x^2+\xi^2+(y-\eta)^2]^2}\,dx\,dy\,d\eta d\xi \tag{5.16.}$$

After integration of G follows

$$G = \frac{1}{2\pi}\left\{(y-\eta)(x^2+\xi^2)^{\frac{1}{2}}\,arctan\frac{y-\eta}{(x^2+\xi^2)^{\frac{1}{2}}} - \frac{1}{4}[x^2+\xi^2-(y-\eta)^2]\,ln[x^2+\xi^2+(y-\eta)^2]\right\} \tag{5.17.}$$

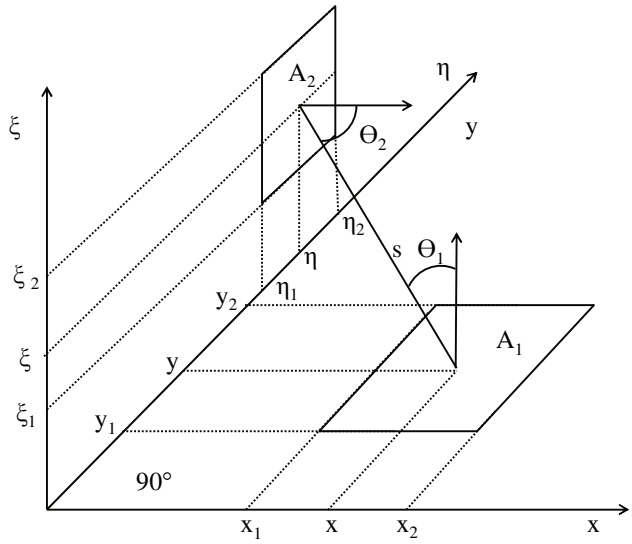

Figure 5.12 Perpendicular view factor determination according to [64]

Power density is the amount of power emitted by a heater. Power density changes with heater temperature and is specific to the heater used.

To determine the temperature of the infrared heater during preheating at a certain time, the heating rate of the heater is needed. The heating rate was derived from experimental data. The heating rate of the heater is independent from the experimental set-up. Table 5-1 summarizes the heating rates of the infrared heater.

Table 5-1 Heating rate of infrared heater

Temperature range	100°C - 150°C	150°C - 300°C
Upper infrared heater [K/s]	$1.51 \pm 11\%$	$1.76 \pm 5\%$
Lower infrared heater [K/s]	$1.41 \pm 18\%$	$1.80 \pm 4\%$

Due to the specific machine set-up heating rates for upper and lower heater differ slightly and were determined separately. Up to 150°C, heating rates of the infrared heater differed very much. Between 100°C and 150°C, heating rates of 1,51°C/s and 1,41°C/s were determined. The deviation of the upper heater was at 11% and of the lower heater was at 18%. From 150°C to 300°C heating rates converged at 1,76°C/s and 1,8°C/s, having a deviation of only 4% (lower heater) and 5% (upper heater). Above 300°C further heating rates were limited and

influenced due to the maximum heater temperature. The assumption of a constant temperature increase until heater set temperature gave a sufficient approximation.

Power density was derived from the infrared heater temperature according to Figure 5.13, which was given by the supplier [62]. The approximate solution for the graph was done via curve fitting and lead to 5.18.

$$L_H(T_H) = c_1 {T_H}^4 + c_2 {T_H}^3 + c_3 {T_H}^2 + c_4 T_H - c_5 \qquad 5.18.$$

Constants for determination of power density in dependence of heater temperature are listed below:

$$c_1 = 4 \cdot 10^{-7} \frac{W}{m^2 \cdot (K)^4}$$

$$c_2 = -3 \cdot 10^{-4} \frac{W}{m^2 \cdot (K)^3}$$

$$c_3 = 1{,}121 \cdot 10^{-2} \frac{W}{m^2 \cdot (K)^2}$$

$$c_4 = 5{,}7423 \frac{W}{m^2 \cdot K}$$

$$c_5 = -167{,}38 \frac{W}{m^2}$$

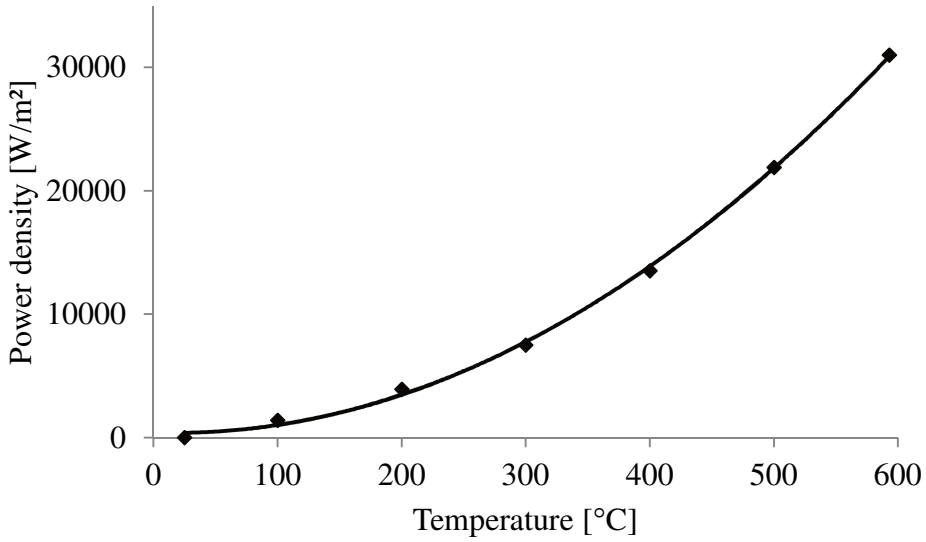

Figure 5.13 Power density curve fitting [62]

As panel temperature was above absolute zero, the panel itself radiated. The emitted power of the panel was equivalent to the outgoing power $\dot{Q}_{out}$ introduced in 5.1.1 . Radiation of the panel is determined using the Stefan-Boltzmann equation (2.5.1) for a black body stating the specific emission is dependent on the temperature to the power of four and the Stefan-Boltzmann constant σ_B [66]. The amount of power emitted from the panel is dependent on the panel surface temperature $T_{La,W}$, panel surface area A_{La}, view factor $F_{La\rightarrow H}$ and material emission coefficient ε_{La}.

$$\dot{Q}_{out} = \dot{Q}_{IR,La} = F_{La\rightarrow H} \cdot A_{La} \cdot \varepsilon_{La} \cdot \sigma_B \cdot T_{La,W}^4 \qquad 5.19.$$

Similar to incoming power, horizontal and vertical surfaces of the panel radiate.

5.2.2. Free convection

Free convection occurs when temperature between heater and panel differs. Free convection power $\dot{Q}_{Con}$ is dependent on the heat transfer coefficient α, the panel surface area A , the temperature difference between panel surface temperature T_W and surrounding temperature T_H which is set equal to heater temperature [61].

$$\dot{Q}_{Con} = \alpha\, A\, (T_W - T_H) \qquad 5.20.$$

On basis of the Nusselt number, heat transfer coefficient can be determined (2.5.2). Material constants needed to determine the heat transfer coefficient were considered constant over the occurring temperature range by taking an average value (Table 5-2).

Table 5-2 Free convection material constants

Material constant	Value
Thermal conductivity $\boldsymbol{\lambda_{air}}$ [W/mK]	0,0375
Density $\boldsymbol{\varrho_{air}}$ [kg/m³]	0,84
Dynamic viscosity $\boldsymbol{\eta_{air}}$ [Pa s]	$24{,}46 \cdot 10^{-6}$
Kinematic viscosity $\boldsymbol{\nu_{air}}$ [m²/s]	$3{,}4 \cdot 10^{-5}$

Free convection was determined for top and bottom side of the panel separately (2.5.2) as conditions, hence dimensionless numbers change. Free convection on panel topside α_{top} is solved according to 5.21.

$$\alpha_{top} = \frac{Nu_{top}\,\lambda_{air}}{L_C} \tag{5.21.}$$

The thermal conductivity λ_{air} is known from Table 5-2. The characteristic length L_C is the quotation of the surface area A over the panel compass C.

$$L_C = \frac{A}{C} \tag{5.22.}$$

The Nusselt number Nu needs to be determined for laminar flow conditions. Rayleigh number Ra and Prandtl number Pr are required to determine Nusslet number

$$Nu = 0{,}766 \cdot [Ra \cdot f_2(\mathrm{Pr})]^{1/5} \tag{5.23.}$$

Rayleigh number is determined from Prandtl and Grashof number Gr.

$$Ra = Gr \cdot Pr \tag{5.24.}$$

The Prandtl number is determined by the kinematic viscosity ν_{air} (Table 5-2) over the thermal conductivity λ_{air} .

$$Pr_{air} = \frac{\nu_{air}}{\lambda_{air}} \tag{5.25.}$$

The Grashof number is determined by:

$$Gr_{top} = \frac{\beta_{top} \cdot g \cdot (T_W - T_{H,top}) \cdot L^3}{{\nu_{air}}^2} \tag{5.26.}$$

T_W is the top surface temperature of the panel and $T_{H,top}$ was set equal to the top infrared heater temperature representing air surrounding temperature. Air was assumed to be an ideal gas; its thermal expansion coefficient is dependent surrounding temperature.

$$\beta_{top} = \frac{1}{T_{H,top}} \qquad 5.27.$$

For the determination of the bottom-side free convection α_{bottom} on the panel downside formulas 5.26-5.27 are solved putting the temperature of the lower infrared heater equivalent to T_H.

The Grashof number Gr_{bottom} depends on the temperatures of panel and heater. When the heater temperature is above panel temperature, the panel is heated.

Nusselt numbers have to be determined according to the heat flow and Rayleigh numbers (5.21 – 5.25).

As side effects from outside the heater area were not considered within this calculation, a small heater – laminate distance gives more precise results as side effects cooling surrounding temperature below heater temperature hardly occur.

5.2.3. Heat conduction

Heat conduction within the laminate occurs when a temperature delta occurs. If surface temperature is increased due to radiation and convection heating; a temperature profile built up along through thickness.

Material constants relevant for heat conduction are summarized in Table 5-3. All values were assumed to be constant over the occurring temperature range. Melt energy released when melting crystalline structure of the polymer was not considered in the numerical model. At higher wall thickness; melting area was not clearly defined anymore and overlap with the power density reduction due to oscillation of heater around maximum temperature occurred.

Table 5-3 Material constants of laminate

Material constant	Value
Density $\boldsymbol{\rho}$ [kg/m³]	1580
Thermal conductivity $\boldsymbol{\lambda_L}$ [W/mK]	9,1
Specific heat capacity $\boldsymbol{c_{p\,L}}$ [J/kgK]	1236
Temperature conductibility $\boldsymbol{a_L} = \frac{\boldsymbol{\lambda}}{\boldsymbol{\rho * c}}$ [m²/s]	$4{,}66*10^{-6}$

Material density ρ was taken from the material data sheet [74]. Thermal conductivity λ_L was determined according to the rule of mixture for a fiber volume content of 53%.

The temperature distribution within the laminate was assumed one-dimensional (5.1.1). Through thickness temperature determination depends on the temperature conduction a and temperature profile in dependence of time and position along z-axis.

$$\frac{\partial \vartheta}{\partial t} = a\left(\frac{\partial^2 \vartheta}{\partial z^2}\right) \qquad 5.28.$$

Heat conduction occurs along z-axis (

Figure 5.14). In order to determine the temperature on certain positions within the laminate the variable z_i was introduced. R is equal to half the panel thickness *d/2*, representing the wall thickness for a symmetric assumption (5.1).

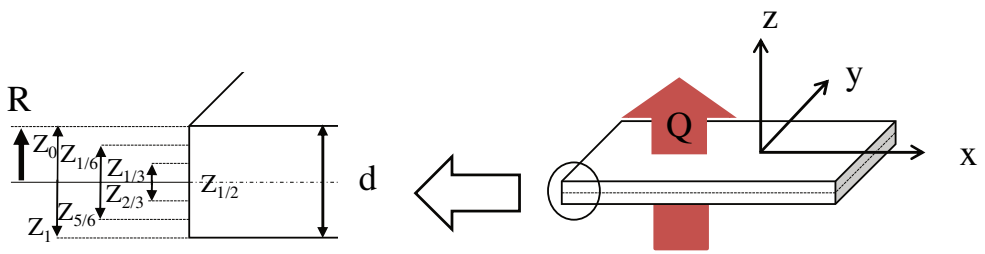

Figure 5.14 One-dimensional heat conduction variable z

Power $\dot{Q}_{IN}$ that heats up laminate surface is summing up from radiation power of laminate and radiation power of heater and convection power.

$$\dot{Q}_{IN} = \dot{Q}_{IR\,total} + \dot{Q}_{Con,La} = \dot{Q}_{IR,H} - \dot{Q}_{IR,La} + \dot{Q}_{Con,La} \qquad 5.29.$$

Using Fourier's law, the incoming power distributes within the material in dependence of thermal conductivity λ, panel surface area A. This results in a time and position dependent temperature change within the material $\frac{\partial \vartheta(z,t)}{\partial z}$. [81]

$$\dot{Q}_{IN} = \dot{Q}(z,t) = -\lambda A \frac{\partial \vartheta(z,t)}{\partial z} \qquad 5.30.$$

As a one dimensional temperature profile is assumed, the heat flow density $\dot{q}_{(z,t)}$ was determined by dividing over the surface area A.

$$\dot{q}(z,t) = \frac{\dot{Q}(z,t)}{A} = -\lambda \frac{\partial \vartheta(z,t)}{\partial z} \qquad 5.31.$$

The temperature field was assumed quasi-stationary. The non-stationary process was time-averaged over short time periods of two seconds. The surface temperature of the laminate was determined after each time sequence and the heat conduction calculation followed. The surrounding temperature of the heater T_∞ follows the quasi-stationary assumptions with a constant average heating rate HR_∞ over each time period step Δt.

$$T_\infty(t + \Delta t) = HR_\infty \cdot \Delta t + T_\infty(t) \qquad 5.32.$$

The system was assumed symmetrically and calculations were done for top and bottom side separately. Due to the quasi stationary calculation the long term assumption (heat conduction happens and has changed the temperature level) of $Fo > 0{,}3$ for a panel needed to be fulfilled.

The Fourier term Fo describes the temperature conduction a by the time t over the half laminate wall thickness squared R^2. The Fourier number is used to determine which kind of boundary condition assumption can be chosen.

$$Fo = \frac{at}{R^2} \qquad 5.33.$$

The surface temperature of the laminate is dependent on heat flow density $\dot{q}$ and the rate of heat conduction. This was assumed by an approximate solution for boundary condition type 2.

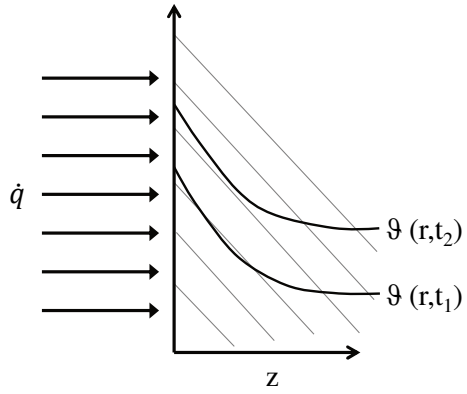

Figure 5.15 Resulting temperature profile for boundary condition approximation type 2

A boundary condition type 2 approximate solution assumes that the heat flow density $\dot{q}$ is known in dependence of time t and position r. The resulting temperature profile $\vartheta(r,t)$ is shown in Figure 5.15. A constant heat flow density level keeps the temperature distribution curve constant; an increase lifts the temperature level.

The approximate solution defines a dimensionless temperature Θ as the temperature chance according to start temperature T_0 over a reference temperature T_{ref}.

$$\Theta = \frac{T - T_0}{T_{ref}} \qquad 5.34.$$

The reference temperature was calculated from the heat flow density $\dot{q}$ by the half laminate wall thickness R over the thermal conductivity.

$$T_{ref} = -\frac{\dot{q} \cdot R}{\lambda} \qquad 5.35.$$

The dimensionless position ξ was defined as

$$\xi = \frac{z}{R} \tag{5.36.}$$

For surface temperature $z = R$ followed $\xi = 1$. Further values of z and ξ are summarized in Table 5-4.

Table 5-4 Dimensionless coordinates

z	ξ
$z_{1/3}$; $z_{2/3}$	$^1/_3 = 0{,}3333$
$z_{1/6}$; $z_{5/6}$	$^1/_6 = 0{,}1667$
$z_{0;}$; z_1 ;	0

The approximate solution for long periods is introduced in 5.37. [81]

$$\Theta = \frac{1}{2}\xi^2 + A_1 \cdot Fo - B_1 \tag{5.37.}$$

For a panel $A_1 = 1$ and $B_1 = \frac{1}{6}$ can be assumed.

The dimensionless temperature Θ is only dependent on the Fourier number Fo, which itself only changes with variation of time periods and laminate thickness and the position within the laminate ξ.

$$\Theta = \frac{1}{2}\xi^2 + 1 \cdot Fo - \frac{1}{6} \tag{5.38.}$$

Solving 5.35 using 5.31, 5.33, 5.36, and 5.38 allowed material temperature determination in dependence of position, time, part geometry and incoming surface power.

$$T(z,t) = \left(\frac{1}{2}\left(\frac{z}{R}\right)^2 + 1 \cdot \frac{at}{R^2} - \frac{1}{6}\right) \cdot \left(-\frac{\frac{\dot{Q}_{IN}(z,t)}{A} \cdot R}{\lambda}\right) + T(z, t - \Delta t) \tag{5.39.}$$

Equation 5.39 allows the determination of the material temperature in dependence of through thickness position and heating time. Process window $t_{process}$ for a specific material can now be determined in dependence of minimum and maximum process window temperatures T_{min} and T_{max} . 5.39 is the basis for determination of the process window $t_{process}$ for a complex organo sheet.

5.3. Validation

The numerical tool was set up using Microsoft Excel. Figure 5.16 gives an overview on the calculation pattern. General input data regarding material values are set in “Material constants”. In “Process parameter definition” process conditions are set including minimum and maximum wall thickness. Heat flow calculations in dependence of wall thickness are automatically done in “Process window determination”. In time steps of two seconds the development of the surface temperature in dependence of radiation power and convection power is determined. In parallel, temperature increase of inner material is determined from the arising temperature delta via power conduction.

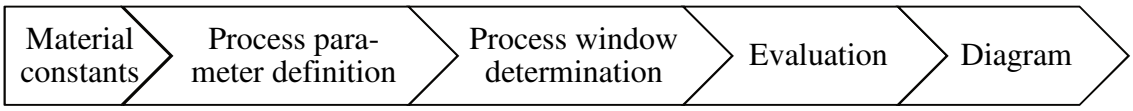

Figure 5.16 Calculation pattern for numerical process definition

Temperature curves and hence processing windows are determined for minimum and maximum wall thickness in separate spreadsheets.

“Evaluation” summarizes the temperature curves of top, mid and bottom of the heated organo sheet in dependence of wall thickness. Potential overlap of processing windows of minimum and maximum wall thickness is determined (Figure 5.17). Top surface temperature of the thin walled section and mid material temperature of the thick walled section are critical temperatures. For visual evaluation the temperature curves are shown in “Diagram” (see also Figure 5.18).

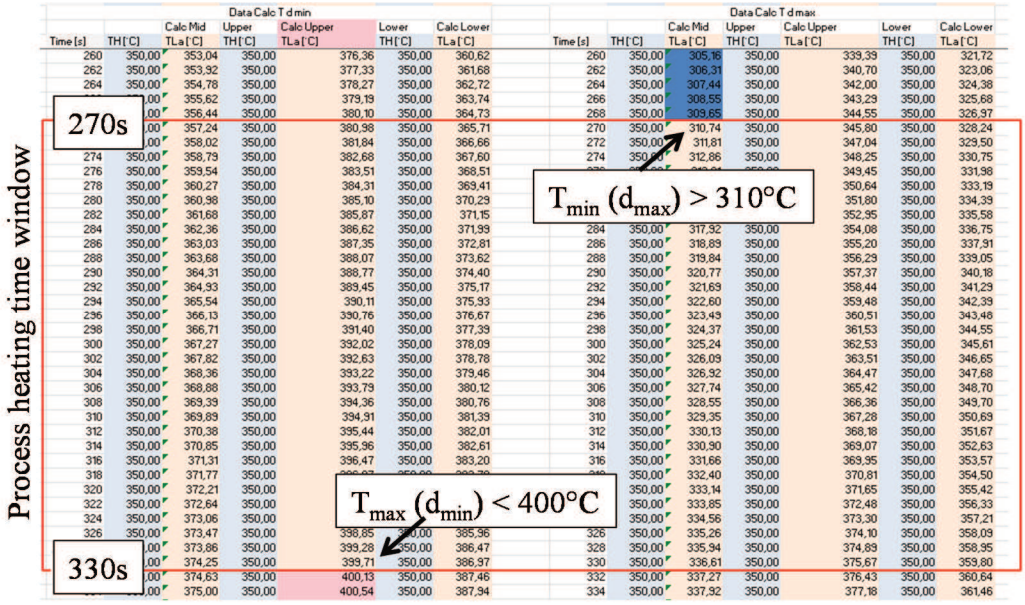

Figure 5.17 Evaluation of numerical process definition tool

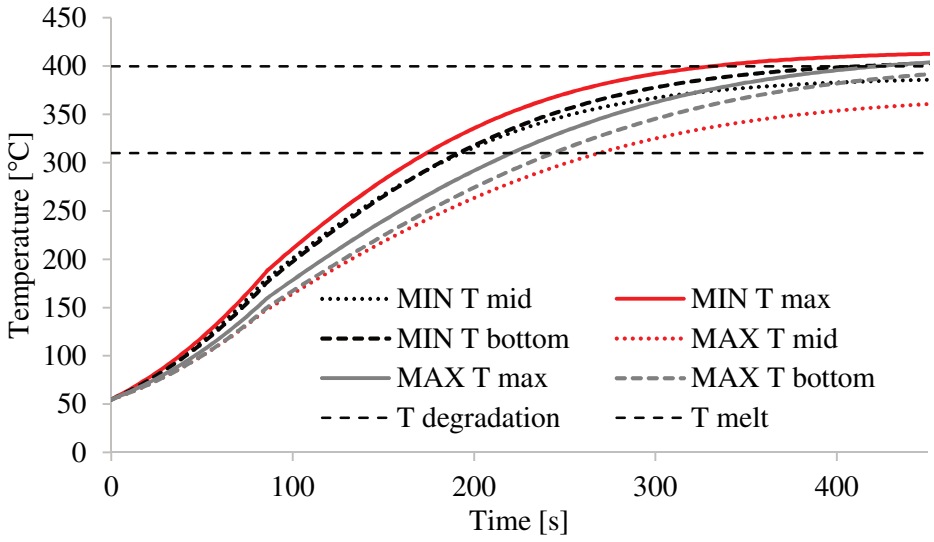

Figure 5.18 Diagram output of numerical process definition tool

Temperature based processing window is marked with horizontal dashed lines. Lower line represents minimum temperature limit, upper line represents degradation onset temperature. Surface temperatures and mid temperature of thin and thick section are further shown according to legend. Red lines mark minimum and maximum occurring temperatures represented by surface temperature of thin section and mid temperature in thick section. Existence of a time based processing window can be derived from the crossing of red lines (minimum and maximum material temperature) and dashed horizontal lines (temperature process window).

Model validation was done on basis of experimental data. Accuracy of the model regarding heating time and temperature were determined in an error calculation. Validation focus was on heating time and material temperature. Figure 5.19 shows the heating time results of experiment and numerical model for several set-up variations of, heater distance a, maximum infrared temperature T_{IR} and wall thickness d. Column names are to be read: heater distance [mm] / maximum infrared heater temperature [°C]/ wall thickness [mm]. Calculated heating times vary from 1% up to 29% from the experimental data. General variation of heating times was caused by variation in initial heater and material temperatures. Large off-set of model results towards experimental results was caused be increased initial heater temperature. An increased initial heater temperature caused radiation and convection heating of panel before process start which resulted in a temperature profile development within material before experiment start. In the model constant through-thickness material temperature before process start was assumed and could not compensate this. This effect occurs in dependence of detailed process set-up and can be treated like a constant delta if occurring during high volume manufacturing.

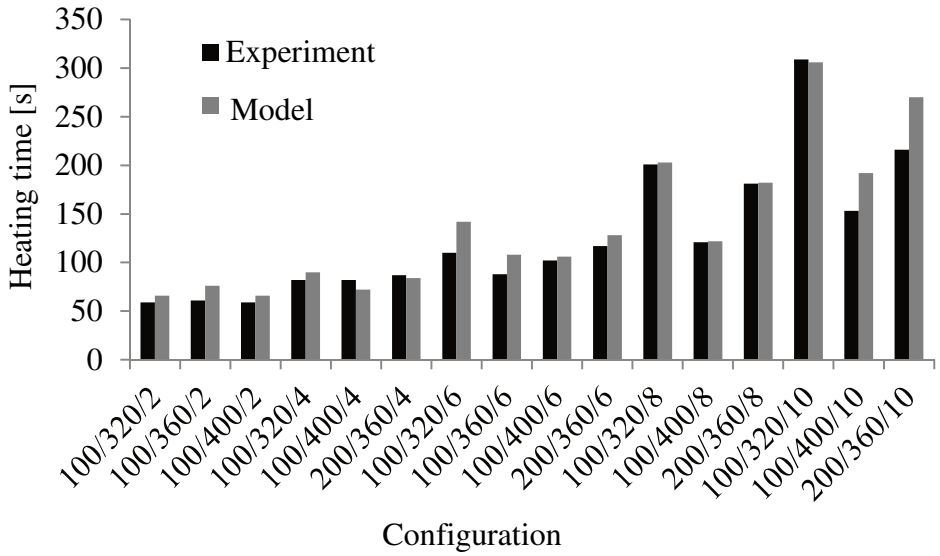

Figure 5.19 Heating time comparison for evaluated configurations (a, T_{IRmax}, d) [40]

Heating time accuracy was defined as the difference in heating times of model and experiment over the model heating time.

$$Heating\ time\ accuracy = \frac{t_{\ heating\ model} - t_{heating\ experiment}}{t_{heating\ model}} \quad 5.40.$$

Heating time accuracy mean value was at 10%, this means average predicted heating time was 10% longer than real heating time. Heating time accuracy is important for absolute heating time comparison. Overall heating time is very sensitive towards initial temperatures. Process window determination is dependent on heating time overlap, not on absolute heating times determined.

Temperature accuracy is more important for process window determination. Temperature accuracy describes difference in surface temperature from model to experiment on basis of model surface temperature. Panel surface temperatures were compared at mid preform temperature of 310°C.

$$Suface\ temperature\ accuracy\ = \frac{T_{\ surface\ model} - T_{surface\ experiment}}{T_{surface\ model}} \quad 5.41.$$

Figure 5.20 shows the comparison of results from calculation and experiment for an organo sheet of thickness *d* 2mm at maximum heater temperature T_{IRmax} 320°C and heater distance *a* 200mm. Horizontal lines indicate temperature processing window for calculation. Full temperature lines are results from the experiment; dashed temperature lines are results from the numerical model.

Temperature accuracy mean value was at -2.7%, hence average predicted surface temperatures were 2,7% (11K) below real surface temperatures. The error induced by temperature accuracy is important for the model evaluation. The upper material temperature before degradation start was at 410°C – 420C° (4.2.2). For compensation of the temperature accuracy, the maximum surface temperature in the numerical model was limited to 400°C taking the calculation error into account.

Maximum infrared heater temperature was detected as relevant parameter for studying the processing windows (5.1.2). It ensures efficient heating at maximum power transmission at low temperature and only a slowing down at higher temperatures due to a limitation of maximum power emitted. Maximum infrared heater temperature was set at 400°C as this was the maximum temperature limit. Minimum infrared heater temperature was set at 320°C. This was the minimum temperature required to ensure sufficient through thickness heating for thick laminates. A maximum infrared heater temperature below 320°C did not heat thick laminates to a mid-preform temperature of 310°C. Processing conditions during evaluation were kept constant except for maximum heater temperature.

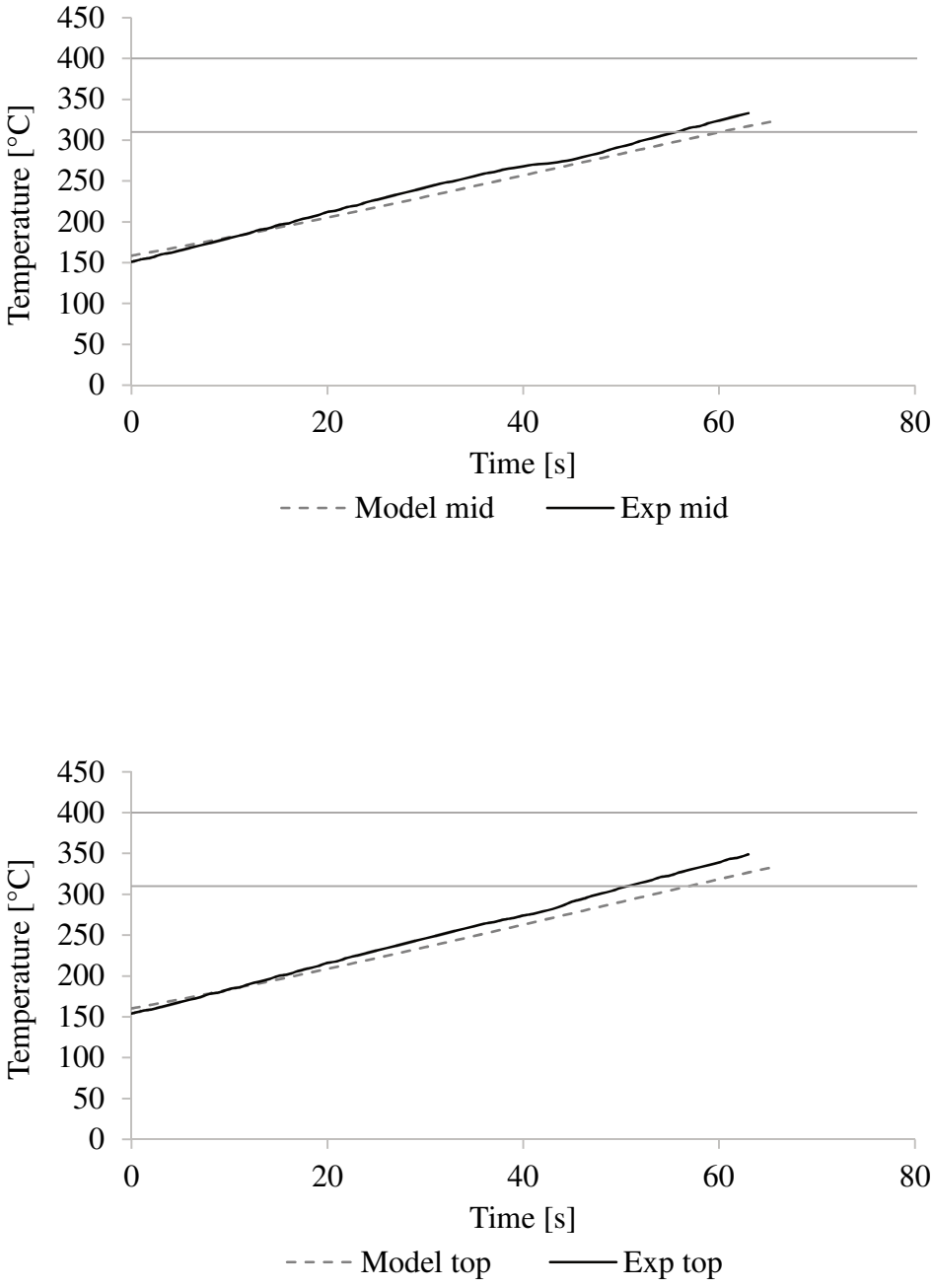

Figure 5.20 Comparison of temperature accuracy on Basis of model results (dashed) and experimental results (full) shwoing surface temperature (upper) and mid temperature (lower) (a=200mm, T_{IRmax} 320°C, d=2mm) [40]

5.4. Evaluation

Thermoforming processing conditions for complex organo sheets were evaluated on basis of the numerical model. Wall thickness dependent processing windows were determined for a set of defined infrared heating conditions including initial heater temperature and heater distance. Heater temperature limit variation was studied from 320°C to 400°C. Wall thickness was varied from 2mm to 10mm.

Figure 5.21 shows the process time slots of 2mm, 6mm and 10mm for organo sheets of constant wall thickness. Process time was limited to 500s (>8min) in the figure. After this time no significant temperature change did occur any more. Figure 5.21 shows, that organo sheets of a constant wall thickness up to 10mm can be processed having a maximum infrared heater temperature range from 320°C to 400°C. Increasing heater temperature leads to decreased heating times and smaller processing windows especially for thick walled parts. For thin walled organo sheets (~2mm) no change in processing time is achieved from 360°C heater temperature upwards. Due small organo sheet mass, organo sheets heat up faster than the infrared heater itself. Hence, maximum material surface temperature is reached, while the heater has not reached its maximum temperature. In general, an increase in heater temperature results in a reduction of processing slot and a reduction of maximum heating time.

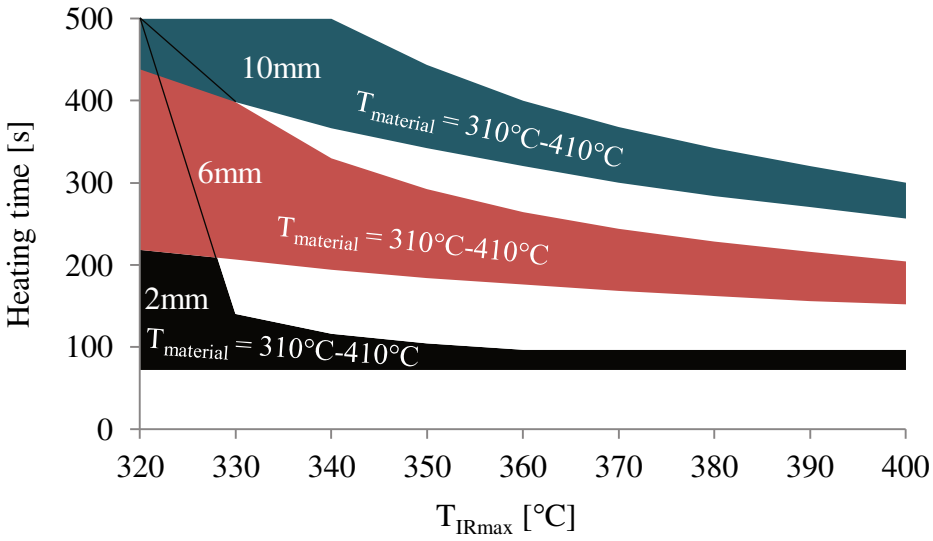

Figure 5.21 Process time window for organo sheets of constant wall thickness in dependence of T_{IRmax} (according to 40)

The processing time $t_{process}$ of complex organo sheets with wall thickness variations is determined from the processing time of the maximum temperature of the thin section $t\left(T_{max}(d_{min})\right)$ and the processing time of the minimum temperature of the thick section $t\left(T_{min}(d_{max})\right)$ (see also Figure 5.1).

$$t_{process} = t\left(T_{max}(d_{min})\right) - t\left(T_{min}(d_{max})\right) \quad 5.42.$$

In other words, the overlap areas shown in Figure 5.21 represent potential processing windows. Processing time is derived from the equivalent y-axis section.

Processing possibilities for 2mm wall thickness variable organo sheets is shown in Figure 5.22 . Column names represent the minimum and maximum wall thickness. Heating of complex panels of a wall thickness variation of 2mm are dependent on maximum infrared heater temperature. A thin complex organo sheet of 2mm wall thickness variation requires a lower maximum infrared heater temperature level compared to a thicker 2mm variable wall thickness organo sheet.

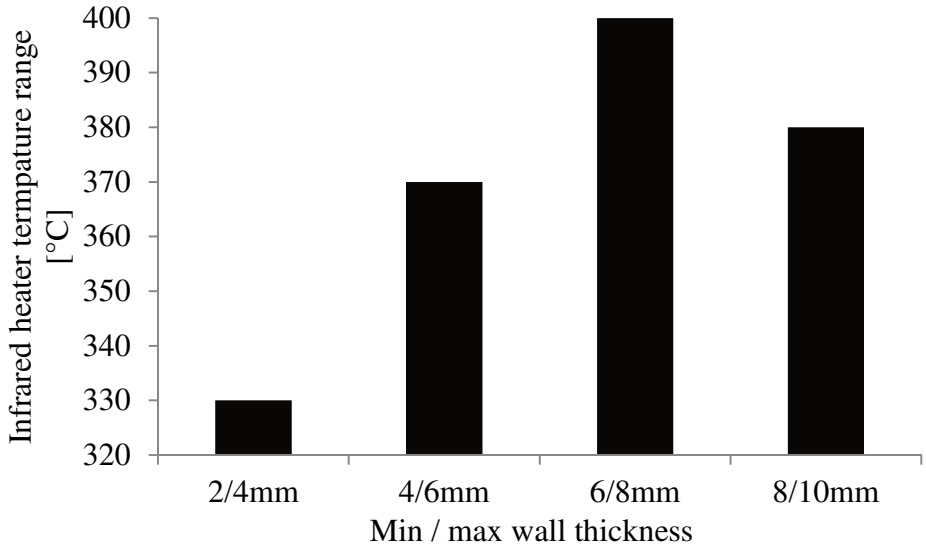

Figure 5.22 Maximum heater temperature over 2mm wall thickness variation [40]

Suitable maximum infrared heater temperature range increases from 2/4mm (320°C-330°C) towards 6/8mm (320°C-400°C) and then decreases again from 6/8mm towards 8/10mm (320°C-380°C). For a 6/8mm panel, mid plane temperature of 8mm section reaches 310°C before surface temperature of 6mm section exceeds 400°C for a maximum heater temperature range above 380°C. At the same time, surface temperature of an 8/10mm panel within the 8mm sections exceeds 400°C before mid-plane temperature of the 10mm section reaches 310°C.

If a variation of maximum infrared heater temperature is possible, processing becomes more efficient for higher maximum infrared heater temperatures. Figure 5.23 shows the processing time slots for an organo sheet of 6/8mm wall thickness. Processing window becomes narrower with an increase in maximum heater temperature. In consequence, through thickness tem-

perature profile becomes tighter towards a through thickness temperature delta of 90K. Maximum process time reduction by increasing maximum heater temperature level is in the range of two minutes. Potential process time reduction is dependent on the individual organo sheet set up and time savings might be lower as possible processing conditions depend on wall thickness variation. Figure 5.24 shows the heating time for a complex organo sheet of a minimum wall thickness of 2mm and variable maximum wall thickness at a maximum infrared heater temperature of 320°C.

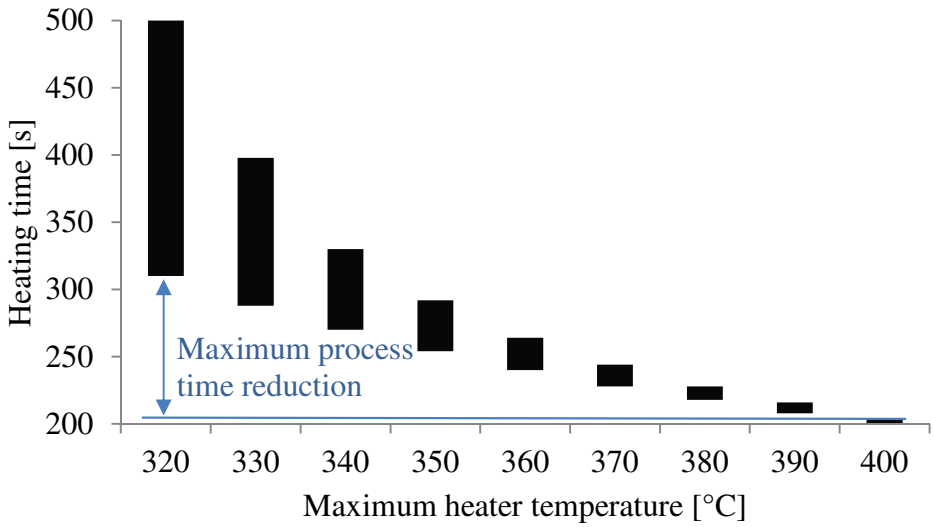

Figure 5.23 Processing time slot in dependence of heating time and $T_{IR\ max}$ for 6/8mm organo sheet [40]

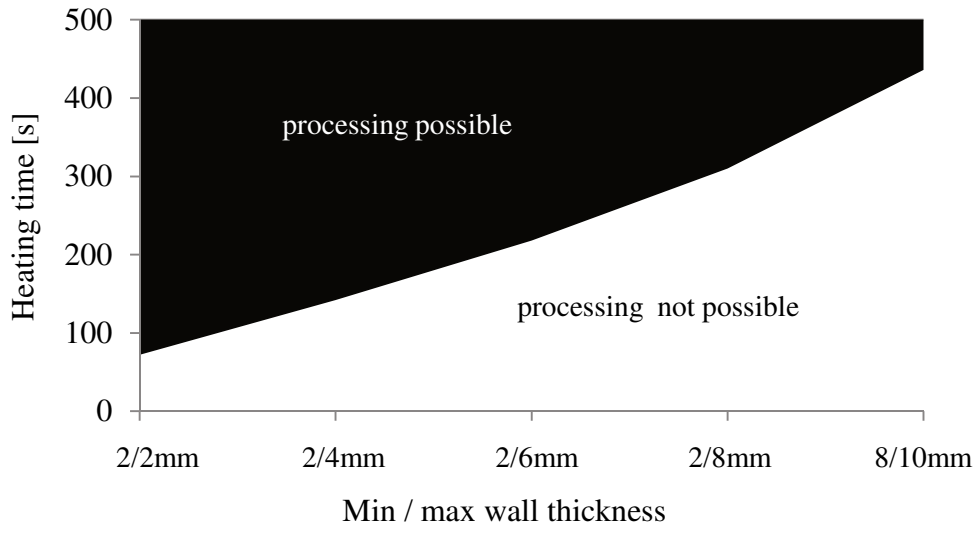

Figure 5.24 Heating time according to wall thickness variation at $T_{IR\ max}$ 320°C [40]

Organo sheets having a wall thickness variation of 2mm within the total wall thickness range of 2mm to 10mm are processable for variable but limited heater temperature ranges. Infrared heater temperature has to be chosen according to minimum and maximum wall thickness. A summary of possible preheating conditions for organo sheets of variable wall thickness is shown in Figure 5.25.

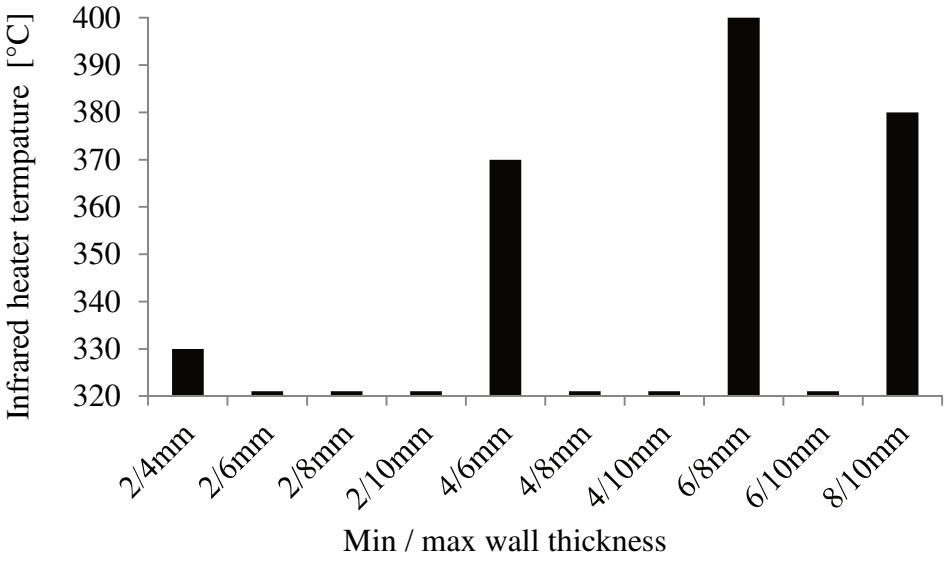

Figure 5.25 Possible infrared processing temperature over wall thickness variation [40]

In general, processing of complex organo sheets having a variable material thickness from 2mm to 10mm is possible. A wall thickness variation of maximum 2mm allows a process optimization by increasing maximum infrared heater temperature. An increase in maximum heater temperature results in a reduction of process time, as shown in Figure 5.23. Maximum process time reduction by increasing maximum heater temperature level is in the range of one minute. Time reduction is dependent on the individual organo sheet set up and time savings might be lower as possible processing conditions depend on material thickness. Wall thickness variations of more than 2mm are advised to be processed only at maximum heater temperature of 320C°. 320°C was found to be a good compromise for not heating surface temperature above 400°C during long term heating and still reach a mid-preform temperature of 310°C. This resulted in prolonged heating times ranging from 1min to 7min depending on maximum wall thickness.

5.5. Conclusions

A numerical tool to define process parameters for complex thermoforming in dependence of wall thickness was set up. The general approach of the tool is shown in Figure 5.26. A temperature processing window was defined in 4.2.2. The process windows are wall thickness related.

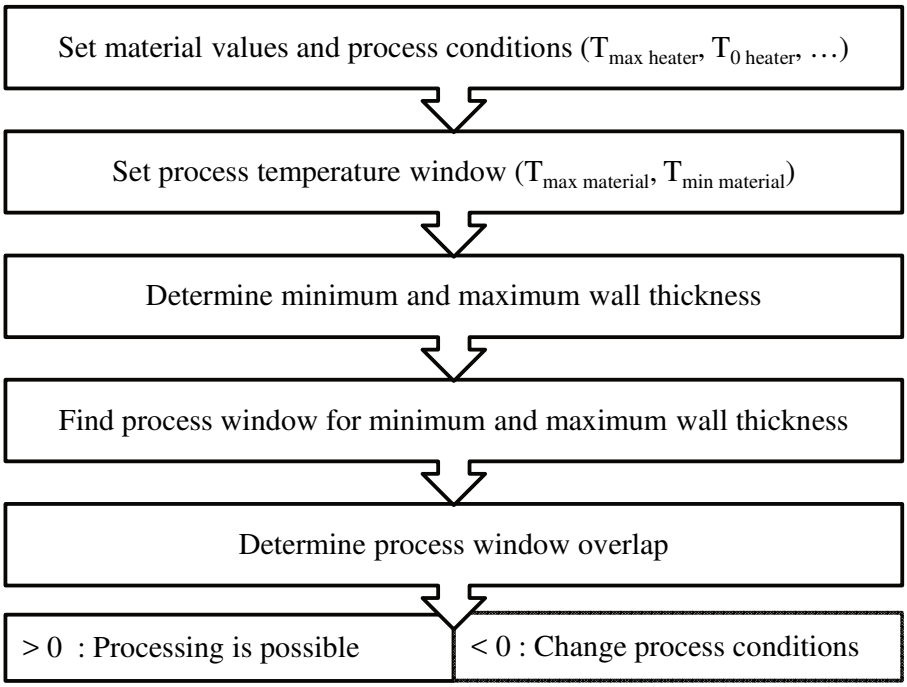

Figure 5.26 Guideline for determination of process window using numerical model

Processing is possible when the inner material of a thick walled section is heated above minimum temperature before surface temperature of thin walled section reaches maximum temperature (5.3). Hence, process windows need to be determined for minimum and maximum wall thickness. According to literature a symmetric system for double sided heating was assumed (5.1). Temperature gradient is only dependent on wall thickness [24]. Experimental investigations did show that in-plane geometry and panel size (x-y-plane) are not relevant regarding surface temperature development. In consequence, the through thickness temperature profile is only dependent on wall thickness (Figure 5.4). The numerical tool needs the input of material values (e.g. temperature conductivity, heat capacity), wall thicknesses and process conditions (e.g. initial and maximum heater temperature, heater distance). Output is a heating time process window. The material heating curve is determined on basis of heat flows. Radiation and convection heating increase the material surface temperature, which in turn is responsible for further material through thickness conduction heating in dependence of the resulting temperature delta. The temperature change is calculated in time periods of two

seconds. Emitted heat flows are integrated over this time period and resulting temperatures determined for the next time step. Process windows are determined separately in dependence of minimum and maximum wall thickness. In case of process window overlap, processing of the complex organo sheet is possible; otherwise process parameters need to be changed. The most relevant parameter to increase the process window overlap was found to be the maximum infrared heater temperature.

Temperature increase during preheating was determined from thermodynamic equations for radiation power, convection power and conduction power. Radiation of both heater and panel was considered as both radiate electromagnetic waves. Energy emission of the heater is determined in dependence of time on basis of the initial heater temperature, heating rate and heating time. The amount of energy over time absorbed depends on the view factor from heater and panel towards each other. Panel radiation is determined on basis of the Stefan-Boltzmann equation (5.2.1). Free convection occurs as heater and panel temperatures differ during heating. On basis of dimensionless numbers the power exchange is determined in dependence of the temperature difference (5.2.2).

The panel temperature increase is determined from radiation power and convection power. The through thickness temperature profile is determined from the conduction power caused by the temperature delta arising from increased surface temperature and unheated mid-temperature in dependence of wall thickness and through thickness position (5.2.3).

In general, the maximum infrared heater temperature was found to be the most important process parameter to impact heating conditions (5.1.2). By limiting infrared heater temperature maximum, overall heating process was prolonged only at elevated temperatures avoiding fast surface temperature increase and allowing mid surface temperatures to rise above minimum temperature limit (Figure 5.7). A distance increase from panel towards infrared heater was another process parameter used to prolong heating time, hence allowing more time for mid temperature rise. The increase in heater distance lowed heating rates over the whole temperature range and was not as efficient as maximizing infrared heater temperature regarding processing flexibility towards heating time (Figure 5.8).

Evaluation of the numerical tool was done for carbon fiber reinforced PPS material having a wall thickness between 2mm and 10mm. An infrared heater temperature limit of 320°C allowed heating of wall thickness variations from 2mm to 10mm within one processing window. The surface temperature of thin sections did not exceed upper the temperature limit of 400°C. At the same time, minimum mid temperature of 310°C was still reached in thick walled sections. A maximum infrared heater temperature of 330°C - 400°C resulted in shorter and wall thickness dependent processing windows and reduced overall heating times. The surface temperature did exceed upper temperature limit. Only certain wall thickness variations were processable. (0)

6. Economic tool development for cost efficiency evaluation

Cost efficient manufacturing is very important for a new technology like complex thermoforming. Therefore an economic tool for a cost based comparison of complex thermoforming with other, standard composite manufacturing techniques was developed. The tool compares manufacturing chains for building a joined, sub-structure demonstrator based on the investigated demonstrator geometry.

Base of comparison was the cost arising for a joined sub-section part. Manufacturing techniques for RTM, prepreg and thermoforming were compared. For all processes manual and automated manufacturing chains were compared.

The evaluation shall identify potentials of the thermoforming process using thermoplastic composites. Thermoset matrix composites are mainly used in composites. They require time intense curing, have limited storage times and require cooling. Thermoplastic composites, as processed during thermoforming, are not as widely used but show great potential regarding rapid processing (no curing necessary) and storage conditions (unlimited at room temperature). RTM (resin transfer mold) is a thermoset infusion process. Preforming is done using dry fiber only. Dry preform is infused and cured in a closed mold at high pressure and temperature. Prepreg process uses also thermoset resins. Pre-impregnated plies are laid up into a mold and are press cured applying temperature and pressure.

This tool does not include a full cost accounting calculation, but a cost based technology evaluation. Only direct manufacturing costs were considered. This included equipment and labor cost, tool cost and material cost. Engineering, development, general workshop costs and energy consumption were not considered. Manufacturing costs were determined in dependence of manufacturing numbers and level of automation. Manufacturing chain started from rolled-goods and ended with quality control after joining.

6.1. Assumptions

Composite manufacture techniques RTM, prepreg and thermoforming were compared. Base for this comparison was a generic airfoil doublet which was assumed to be a structural part located in the bypass of an aircraft engine.

The assembled part (doublet) consists of four separate parts. A sketch of the doublet is shown in Figure 6.1. The doublet consists of two identical airfoils that are connected by two connect-

ing parts called bridges of different radius. All four parts manufacturing was assumed separately and subsequently joined and quality controlled.

Separate, non-integral manufacturing for all processes was assumed to keep a high level of comparison. Integral manufacturing reduces the number of process steps but implies more complex tooling hence higher risk of large number of scrap parts. Joining was regarded very important for any process, and was therefore included in all processes.

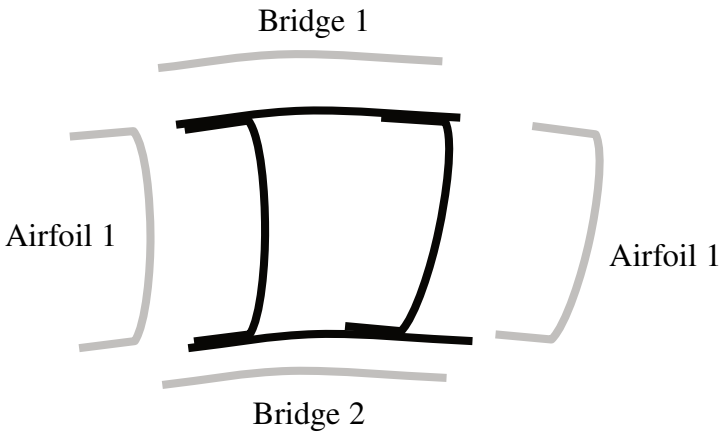

Figure 6.1 Airfoil doublet

An airfoil blank was assumed at 180mm x 500mm and a bridge blank 180mm x 300mm. Final airfoil size is at approximately 180mm x 400mm x 40mm, bridge about 180mm x 250mm x 20mm.

Manufacturing requirements regarding part complexity were derived from the generic demonstrator geometry defined in Chapter 3. Preform geometry of bridges and airfoil varied in ply geometry. A pick and place technology for preforming was chosen for all processes to ensure possibility for variation of single ply geometries as shown in Figure 6.2.

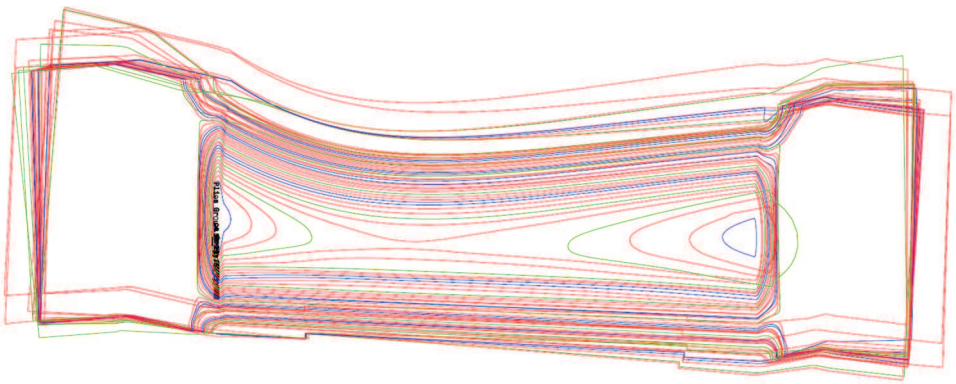

Figure 6.2 Single ply variation of demonstrator

The possibility for complex ply shape design was considered as an important and relevant feature for design of high performance complex structural parts. Regarding preforming, only technologies that have the ability for such ply shaping were taken into account.

Automated thermoplastic preform lay-up processes like fiber placement were not considered suitable for such geometries. The variable geometry in each ply would require a very narrow tape to ensure an accurate geometry. Potential use of very narrow tape or fiber placement, lay-down rate becomes low, hence inefficient. Instead a pick and place process was chosen.

Manufacturing numbers of 1.000, 10.000 and 20.000 doublets per year were assumed. The variation in manufacturing number was chosen to represent the application from a small series up to a high volume application. Depreciation time was set on five years, resulting in total part manufacturing numbers of 10.000 to 200.000. All machines were assumed to be exclusively used for the set-up process. Equipment share with other processes was not considered. Depreciation time was set as time span for machine usage. Machine and tooling were assumed to last for this time span, a sum for maintenance was assumed on annual basis. Per year an average of 250 workdays was assumed as well as a 2-shift 7,5h working hours for staff less 10min administration time per shift and 30 days for holiday and sickness resulting in 774min of daily labor and 880min machine runtime. An overview of basic assumptions is given in Table 6–1.

Table 6-1 Manufacturing assumptions

Depreciation time [year]	5
Workdays per year [-]	250 machine / 220 labor
Daily labor time [min]	774 (2 shift)
Annual part number (doublet) [-]	1.000 / 10.000 / 20.000
Doublets / day [-]	4 / 40 / 80
Manufacturing time /doublet [min]	194 / 19 / 10

6.1.1. Processing

Following, all process chains are described on basis of manufacturing steps and process times assumed.

Process chains all imply a custom made preform manufacturing followed by the actual part manufacturing process. Base material is a single ply, rolled fiber material suitable for the specific process. Single plies are cut from a cutter and a ply stack is built. The ply stack is consolidated during or after lay-up using vacuum or temperature and pressure. Afterwards the actual part building process follows including infusion, curing or forming. In all processes, four separate parts are made, separately finished via milling and NDT control. Erosion protection is put on before joining. Finally the assembled doublet is controlled again. Table 6-2 gives an overview on the general manufacturing process chain.

Table 6-2 General process chain

Process step	Equipment used
Cut plies from base material	Cutter
Build preform stack	Manual / Pick and Place
Consolidate preform stack	Hotpress / Vacuum
Built single part	Infusion / Curing / Forming
Finish single part	Milling / NDT / Erosion protection
Joining	Adhesive joining or welding
Finish	Joined control

For each process variation manual and automated process chains are developed. For automated manufacturing all transport in between two process stations is done using a robot, no labor is needed. A single robot can be used in between identical process stations for identical work. At least one robot after each processing station is needed. For manual preforming, lay-up will be supported via laser projection to ensure rapid and accurate ply positioning.

Process time for equivalent manufacturing steps is identical throughout different processes. Within the different processes, cutting time only varies according to the number of plies needed in dependence of ply thickness. Finishing (Milling, NDT, erosion protection) as well as final control (C-Scan) are identical for all process chains including manual and automated variations. Equipment costs for automated processes are higher as more equipment is needed and used instead of labor. The need for communication with transport systems and additional features like the recognition of misplaced parts further increase invest cost.

Base material for the RTM process is a dry fabric material. Single plies are cut using a cutter. Preform stack is built up and plies are locally fixed using binder activation. Energy input for binder activation comes from an ultrasonic welding unit. Accurate positioning is ensured using laser projection for manual processes and pick and place for automated processing. During manual manufacturing, preforming is done in a three-dimensional preform tool to ensure preform fitting into the injection tool. For automated manufacturing preforming is done flat and subsequently thermoformed to fit in three dimensional tools. Dimensional stability is ensured by the binder. After tool preparation (cleaning) the preform is put into the injection tool. Injection is done using a pressure vessel (manual process) or an injection unit (2K / automated process) in a heated press. After curing single parts are milled and NDT (C-Scan) tested. Erosion protection is put on. Joining is done via adhesive and riveting to fulfil aviation requirements. Joints on the final doublet are checked (A-Scan).

Prepreg process chain starts with ply cutting on cutter. Preform lay-up requires compaction cycles for good material quality. Preform lay-up during manual manufacturing is on a three-dimensional tool generating a near-net shape preform. Automated processing involves a pick and place for process including backing paper removal on a plane surface and subsequent thermoforming to a three-dimensional preform. Preforms are assembled in separate tools and cured in a hot press. Quality control including erosion protection and joining is equivalent to the RTM process.

Thermoforming starts similar to the other process chains with cutting preform plies. Preforming is done via ultrasonic welding and subsequent press consolidation. Accurate ply positioning is ensured similar to former processes. Short term consolidation of 5min at 1-2bar above melting temperature is sufficient when thermoforming is applied in a latter process (4.1.2). During manual processing, the consolidation tool has to be put in and taken out of press. Reduced temperatures are necessary. For automated consolidation, press temperature is kept at a high level. Tool is locked in press under pressure and locks hold mold part in position after pressure release. Mold is taken out of press automatically and preform cooled within closed mold. Thermoforming is done in a separate thermoforming unit. Finishing, erosion protection and quality control are again similar to former processes. Joining is done via resistance welding. No riveting is required due to material bonded joining.

All processes are assumed to be free of scrap parts. Additional material considered is a 30% material waste after ply cutting, which is included in all material cost calculations. An overview on set-up process chains including the equipment needed is given in Table 6-3. An overview on assumed process times is given in Appendix b.

Table 6-3 Overview on manufacturing process chains and equipment

Process step	**RTM equipment**	**Prepreg equipment**	**Thermoforming equipment**
Preforming	Cutter Table + US welding unit/ Laser positioning / P&P unit - / Thermoforming unit	Cutter Table + vacuum table Laser positioning / P&P unit - / Thermoforming unit	Cutter Table + US welding unit Tool + hot press
Main process	Tool Hot press Infusion equipment	Tool Hot press	Tool Thermoforming Unit
Joining	Tool Adhesive / curing oven Riveting equipment	Tool Adhesive / curing oven Riveting equipment	Tool Resistance welding unit
Finishing	Milling machine NDT Erosion protection	Milling machine NDT Erosion protection	Milling machine NDT Erosion protection

Preforming times depended on cutter speed and total cutting length of single plies. Lay-up times depended on the number of plies and material used. Prepreg lay-up was considered slower than dry fabric or thermoplastic tape lay-up. Main processes like thermoforming, injection and curing were broken down into separate, single manufacturing steps. Joining and riveting dependent on the number of joints and joint length. Single process chains were set up. If manufacturing numbers exceeded 100% machine runtime, local parallel manufacturing was introduced.

6.1.2. Cost determination

Total part costs were summed up from machine, labor, tool, and material cost. According to set up process chains, the necessary equipment was determined. Equipment (machine and tools) was assumed in whole numbers; every equipment was used only by the specific process. Both, equipment cost and tool cost were estimated. An overview on assumed cost is given in Appendix b.

In order to estimate machine cost, general assumptions for the calculation are made. Time based machine cost is determined from the total machine cost (invest and maintenance) and the total time used. It was assumed that all machinery is amortized over depreciation time. Machine cost is determined for each equipment separately.

$$Machine\ cost\ [€/h] = \frac{Total\ machine\ cost\ [€]}{t(use\ in\ depreciation\ time)\ [h]} \qquad 6.1.$$

Manufacturing relevant machine costs were derived from hour dependent machine cost and the actual time used.

$$Machine\ cost\ [€/part] = Machine\ cost\ [€/h] \times\ Machine\ time[h/part] \qquad 6.2.$$

The machine cost depended on the initial invest, annual maintenance cost, and the number of identical machines needed. Machine cost and tool cost were considered to be constant. This means no discount for high number purchase was taken into account.

$$\begin{aligned} Total\ machine\ cost\ [€] \\ = Initial\ invest + Maintenance\ cost\ [€] \\ \times No.of\ identical\ machines\ needed \end{aligned} \tag{6.3.}$$

High manufacturing numbers needed a number of identical machines to realize manufacturing numbers. The number of identical machines needed was dependent on the daily machine use over the daily available time of the machine. Machine availability was determined from the daily manufacturing time by the overall equipment effectiveness, which was set to 85% for dynamic moving or electric devices and 100% for static equipment like cutting tables.

$$\begin{aligned} No.of\ identical\ machines\ needed\ [-] \\ = round\ up\left[\frac{Daily\ machine\ time\ needed\ [h]}{Daily\ \ time\ available\ [h]}\right] \end{aligned} \tag{6.4.}$$

Daily runtime of a machine depends on part manufacturing numbers. It was determined from the machine time per part by the required number of parts per day.

$$\begin{aligned} Daily\ machine\ runtime\ [h] \\ = Machine\ time\ per\ part\ [h] \\ \times No.of\ parts\ per\ day\ [-] \end{aligned} \tag{6.5.}$$

Machine time needed per part depends on the process definition. Operating grade rated the efficiency of a machine workload. The operating grade was derived from the machine time over the maximum machine time. It was assumed that all equipment is only used for the process shown (no share machine use with potential other manufacturing). Maximum operating grade is 100% otherwise the number of identical machines had to be increased to rise maximum machine time.

$$Operating\ grade[\%] = \frac{Machine\ time\ used\ [h]}{Maximum\ machine\ time\ [h]} \tag{6.6.}$$

Maximum machine time depends on the equipment effectiveness. Equipment effectiveness represents the time availably as percentage of the total machine time (see above). Maximum machine time was determined by multiplying total machine time by equipment effectiveness.

$$Maximum\ machine\ time\ [h] = Total\ machine\ time\ [h] \times Equipment\ effectiness[\%] \quad 6.7.$$

Process time calculation was based on the processes defined in 6.1.1. Each process consists out of a sum of sub-processes.

Identical process steps in different processes were assumed identical regarding time consumption. Identical processes occur during ply cutting, finishing, joining and final control. In automated processes all transport was assumed identical. During manual manufacturing transport was considered within the time of the process step. Process and labor times were presumed independent from manufacturing numbers.

Automated production caused additional cost for robot, gripper and linear axis in between every two manufacturing steps. Parallel manufacturing was done when part manufacturing times exceed capacities for a single line manufacturing. Automated transport in between more than one parallel manufacturing step was assumed to be done by a single transport system.

Labor cost was assumed as an average value, starting in 2014 with 36€/h with an annual increase of 3% over the 5-year time span resulting in an average labor cost of 38,2€/h.

$$Average\ labor\ cost = 38{,}2€/h \quad 6.8.$$

Demonstrator doublet was assumed to be manufactured in four separate parts and assembled in a following process step. Hence separate tooling was needed for all preforming and part manufacturing. Milling tools were needed according to three different part geometries and one assembly tool was needed. General trend for tool cost increase for automated processing in comparison to manual processing was assumed. Tools endurance was over the whole depreciation time, annual maintenance cost of 10% of tool price were assumed. Total tool number depended on the number of parallel machines needed. In case a tool was needed in more than one process step, the number of necessary tool sets was determined in dependence of the operating grade of the machines. Maximum tool operating grade is 100%. All processes required four different tool sets according to processing steps: preforming (either for 3-D preform layup or 3-D preform shaping), part manufacturing (curing, injection, and thermoforming), finishing, and joining.

Tool costs were determined by adding tool invest cost and maintenance cost. It was assumed that a tool, including maintenance, lasts over the depreciation time of five years.

$$\begin{aligned} &Overall\ tool\ cost\ \ [€] \\ &\quad = Tool\ invest\ cost\ [€] + (Tool\ maintencance\ cost\ [€/yr] \\ &\quad \times Depreciationtime\ [yr]) \end{aligned} \tag{6.9.}$$

Tool cost per part needed to be divided over the total part number in depreciation time.

$$Tool\ cost\ per\ part\ [€] = \frac{Overall\ tool\ cost\ [€]}{Total\ part\ number\ [-]} \tag{6.10.}$$

Tools for curing and infusion were assumed to last only a limited number of parts of 6.000 parts before being replaced. Thermoforming tools (preforming and part forming) were considered to last over depreciation time. Thermoplastic consolidation tools needed replacement every 10.000 parts.

Material cost was assumed according to standard aviation material with focus on toughened systems. Preform material used is based on a high performance, intermediate modulus, PAN based carbon fiber like Hecxel HexTow IM7 [82]. Matrix material assumed is either a toughened epoxy for RTM (e.g. Cytec Cycom PR 520[83) and prepreg (e.g. Hexcel Hexply 8551-7 84) processing or PEEK for thermoplastic processing (e.g. Tencate Cetex TC 1200 85). As all material combinations are high end performance, similar costs for all materials of ~160€/kg were assumed.

Material costs per doublet depended on the amount of material needed for a doublet and the amount of scrap material produced.

$$Doublet\ material\ cost = Material\ cost * \left(weight_{Doublet} + weight_{Scrap}\right) \tag{6.11.}$$

Material needed by weight depended on the amount of material needed per volume and specific material weight (density). Material calculation is volume-based on the assumption for an average constant wall thickness of 6mm for an airfoil and 3mm for a bridge. There was no part design regarding specific loads done. Basis for comparison was an identical geometry.

Material scrap was set at 30%, assuming an optimized ply arrangement for complex geometry shapes plies during cutting. As shown in Table 6-4 material needed is 30% above doublet weight (composite weight only, no additional joining weight considered). Material prices shown are calculated from the assumed material cost of 160€/kg. Material costs using thermoforming were increased due to the higher specific weight of the material.

Table 6-4 Doublet weight and respective material cost

Material according to process	RTM	Prepreg	Thermoforming
Doublet weight [kg]	1,96	1,91	2,20
Weight material needed [kg]	2,54	2,48	2,86
Doublet material cost [€]	407	396	458

6.2. Evaluation

Technology comparison has been evaluated on basis of the assumptions introduced in the former sections. All numbers from this evaluation cannot be seen as absolute manufacturing cost and time, even though numbers will be given in € and time. All numbers must be seen for relative comparison only and in relation with process, usage, and depreciation assumptions made above.

Calculations were done using MS Excel. Calculations are designed in the same pattern for all processes and are shown in Figure 6.3.

Figure 6.3 Calculation pattern for economic efficiency determination

“General assumptions” summarizes general manufacturing details (depreciation time, annual part numbers, daily working hours), labor cost, part geometry details and data for general machine and process assumptions equivalent in at least two process chains. “Invest cost and process definition” defines process equipment, its cost and process chain details. “Machine cost” involves the determination of operating grade and machine cost per hour in dependence of number of identical equipment needed. “Material cost” includes a volumetric based calculation of material needed and the resulting cost including cut-offs. “Cost” summarizes and adds up all separate cost in dependence of manufacturing number and processing type (automated/manual). Overall evaluation is done in separate evaluation sheets.

Following evaluation focus will be set on overall invest, invest per part, part manufacturing time, times shares, cost shares, part cost, part cost shares, and cost per weight.

Invest cost development is shown in Figure 6.4. Invest cost are summed up from initial cost for machining, maintenance over depreciation time and tooling cost. In general, invest cost for automated processing was higher than for manual processing. RTM had highest invest costs. Thermoforming had least invest costs. For small numbers (2.000 parts per year and below), prepreg invest cost were the least and automated thermoforming invest cost were highest. High manufacturing numbers (5.000 parts per year and above) lead to lowest invest cost for thermoforming process.

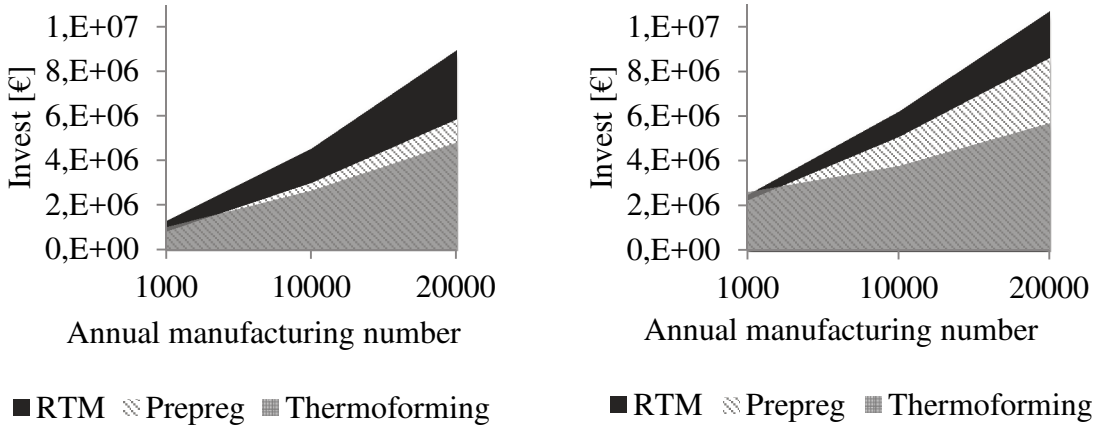

Figure 6.4 Invest costs in dependence of annual manufacturing number for manual (left) and automated (right) process chains

Highest invest for each process was found in the main process. Main processing step describes the part making process step (e.g. curing). Looking at single machine prices, thermoforming unit is the most expensive single equipment required. Action period per part during thermoforming is short compared to curing processes of RTM and prepreg. This makes the thermoforming unit a very efficient equipment for high volume manufacturing. For RTM and prepreg, high manufacturing numbers required a large amount of parallel machining resulting in high invest cost. As RTM requires injections times at increased temperature levels, higher machine times result and more parallel machining for high volume production were required. Tooling invest cost for all process set-ups ranged from 3% - 4% of the total invest cost for all process variations.

Invest costs per part for manual and automated manufacturing are shown in Figure 6.5. Automated manufacturing at low manufacturing numbers had highest invest cost per part of 450€ - 525€, in other words 95% - 160% above invest costs for manual part manufacturing which ranged from 163€ - 256€. For both manual and automated manufacturing, significant decrease of invest costs per part came with increased annual manufacturing numbers. Invest cost per part for automated manufacturing was about 20% (thermoforming, RTM) to 50%

(prepreg) above invest cost per part for manual manufacturing at an annual manufacturing number of 20.000.

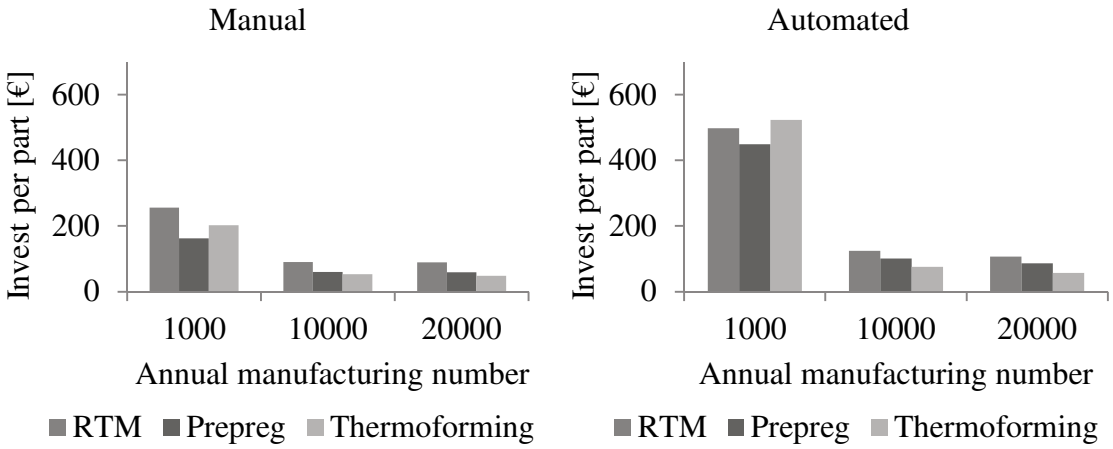

Figure 6.5 Invest cost per part according to annual manufacturing number

Manufacturing time per part is dependent on process way (automated / manual) and type (Figure 6.6). It is not dependent on manufacturing numbers as no learning curve was assumed. In general, prepreg was most time intense manufacturing technique per part; thermoforming the most efficient. Relative manual single part manufacturing times varied from 60% (thermoforming) and 85% (RTM) to 100% (prepreg). Manufacturing time for automated manufacturing was shorter than for manual manufacturing, labor times were reduced. Relative automated single part manufacturing times varied from 45% (thermoforming) and 92% (RTM) to 100% (prepreg).

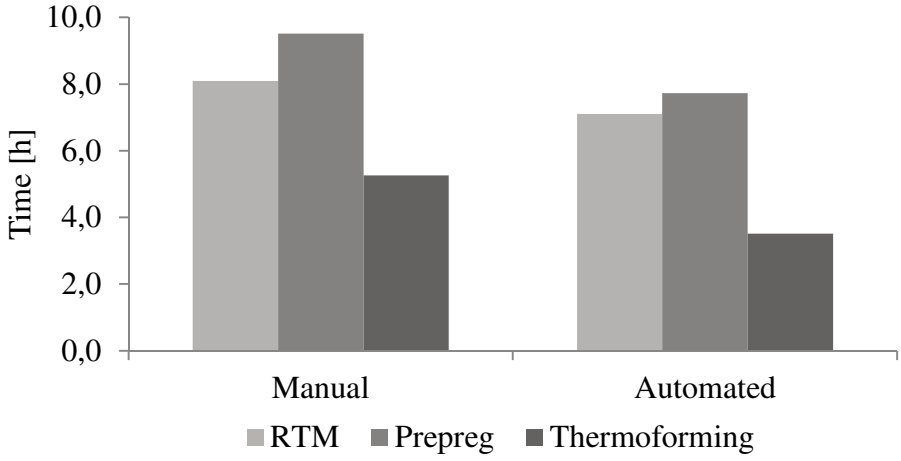

Figure 6.6 Process dependent manufacturing time per part

Time shares for manual and automated manufacturing are shown in Figure 6.7. Both, total manufacturing time (machine time) and labor time per doublet are given. The term “main process” describes thermoforming, injection and curing (RTM), or curing only (prepreg). “Preforming” includes potential preform consolidation or compaction times.

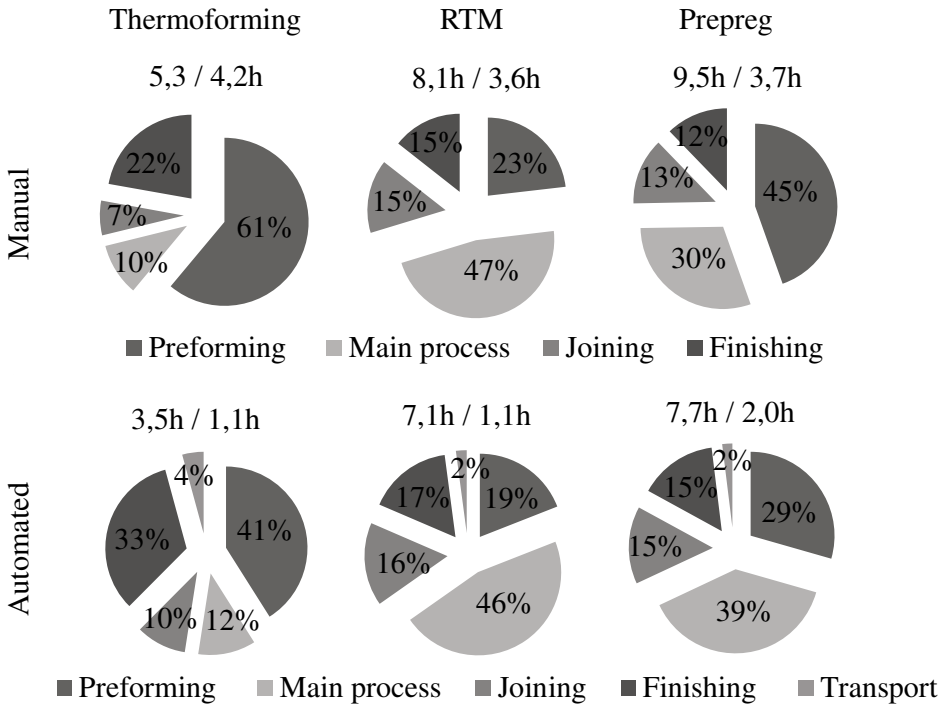

Figure 6.7 Time shares for part manufacturing: total time / labor time

Most intense processing step during thermoforming was the preforming (cut, lay-up, consolidate), due to the press consolidation requiring 61% of the total manufacturing time for manual manufacturing. Automation had high potential for preforming optimization reducing the preforming time down to 41%. Actual thermoforming of four single parts for the demonstrator only required 10-12% of manufacturing time. Labor time was reduced by 70% from manual to automated production.

Optimization of the consolidation process regarding process time (4.1) was considered in this evaluation. The reduction in consolidation time resulted in an overall process time reduction of 10% for automated thermoforming. A reduction of heating time via optimization (4.2) by 50% would decrease the overall demonstrator manufacturing time by 3% (5,5min /3,5h). Machine time of the thermoforming unit and equivalent tooling would be reduced by 24% (5,5min/23min).

RTM had a time intense main process step (injection and curing) requiring close to 50% of the overall manufacturing time. Automation did not give significant time reduction as hardly any manual work could be replaced. General time shares for RTM manufacturing were independent from manual and automated manufacturing meaning all process steps were optimized

in a similar way. Labor time was reduced by 70% and manufacturing time by 12% from manual to automated processing.

Prepreg manufacturing was the most time consuming manufacturing technique. For manual manufacturing, preforming (cut, lay-up, and compaction) and curing required 75% of the overall manufacturing time. Using automation, preforming time share was reduced from 45% down to 29%. Overall manufacturing time share using automation was reduced by 45%.

Overall comparison identified prepreg processing as most time intense manufacturing step. Automated processing involved nearly twice as much labor as RTM or thermoforming processes. Thermoforming had shortest manufacturing times of 35-45% below other manufacturing times. Manual thermoforming was most labor intense due to time intense preforming (lay-up and US-welding, consolidation).

Process cost during manufacturing summed up from machine and labor cost. An overview on process cost is given in Figure 6.8. Both, cost shares for automated and manual processing in dependence of annual manufacturing numbers (machine cost) and labor cost are shown. Labor costs are independent from manufacturing numbers.

All processes required a number of identical machining for material cutting, preform lay-up, finishing, and control. Automated processing had transport (robots, gripper, linear axis) as additional cost. Transport costs did depend on the number of stations per process. Special process dependent equipment was needed for preforming (preform stabilization), joining (curing or welding), and the main process step. Thermoforming required a thermoforming unit. RTM and prepreg both required curing machining, RTM additional injection equipment.

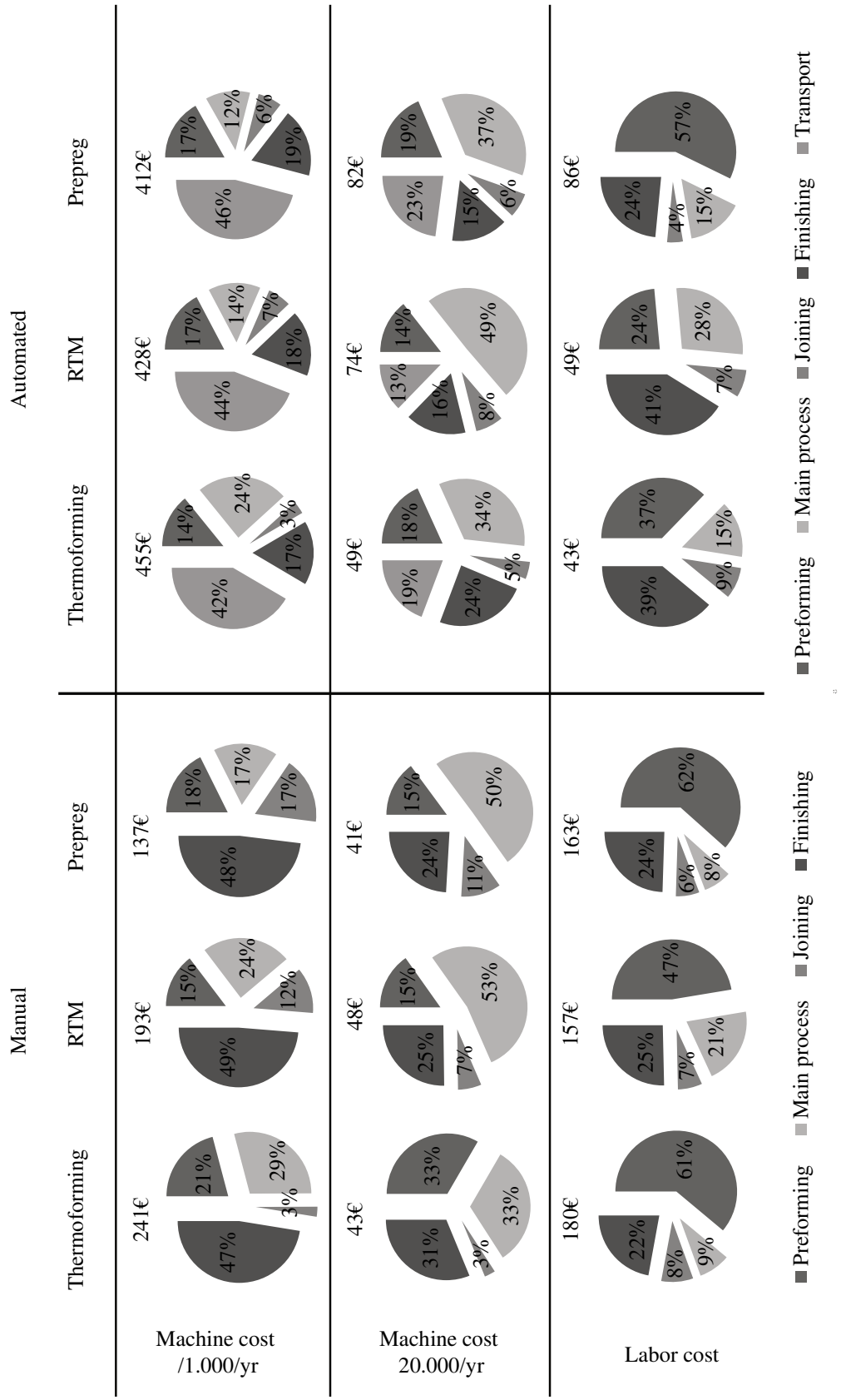

Figure 6.8 Overview on process cost shares and part cost for manual and automated manufacturing

During manual processing at low manufacturing numbers, finishing (milling, control, joining) caused close to 50% of machine cost as expensive equipment was needed at low operating grades. For high manufacturing numbers, dominating cost factor for RTM and prepreg processing became the main process step (curing + injection and curing) at about 50% cost share. Due to high machine times per part, operating grades of the machining could not be optimized much with increasing manufacturing numbers.

For manual thermoforming, a nearly balanced cost share at high manufacturing numbers of preforming, main process and joining was found.

Transport costs for automated processing at low manufacturing numbers (1.000 per year) were dominating cost shares of 42% - 46%. Increase in manufacturing numbers decreased the transport cost share down to 19% - 23%. Main cost driver was dependent on the manufacturing way chosen. Thermoforming and prepreg curing had 34% - 37% cost share on the main processing step, whereas during RTM 50% of machine cost were generated during injection and curing. Throughout all processing scenarios, finishing cost ranged from 15% - 19%, except for high volume thermoforming. Finishing cost share increased to 24%. This indicated a very efficient overall processing, as actual finishing costs were assumed independent from manufacturing number and processing way. With the increase in manufacturing number, total machine cost were reduced down to 10% - 20% of the machine cost at low number. Highest potential for cost reduction within machine cost had the thermoforming process.

Process costs were reduced for increased manufacturing numbers due to the rising machine operating grade, hence optimized machine use.

Labor cost shares are independent from manufacturing numbers, as no process optimization factor for high volume manufacturing was assumed. For all manual processes, labor cost were dominating, having a cost share of 47% (RTM) to more than 60% (prepreg, thermoforming). Overall costs were determined at 157€ - 180€. At automated processing, thermoforming and RTM had similar finishing cost shares of about 40% and below 10% for joining. Main cost driver for thermoforming was the preforming process, whereas during RTM injection and curing (molding / demolding) was the main cost driver. Overall costs were assumed at 43€ - 49€. Labor costs for prepreg processing were roughly twice as much. Main cost driver was the preforming process. Preform lay-up was more time consuming than for other technologies due to the additional backing paper removal and more difficult layup still requiring labor.

Figure 6.9 shows an overview of machine operating grade and part cost according to annual manufacturing numbers.

Machine operating grades are mainly depended on the annual manufacturing number. Annual manufacturing numbers of 1.000 parts had highest variation of machine operating grade of 11% (automated thermoforming) up to 25% (manual prepreg). Rising manufacturing numbers of 10.000 parts per year had machine operating grades of 70% - 72% for manual processing and 67% - 75% for automated processing. A further increase in manufacturing numbers to 20.000 parts per year only slightly increased machine operating grade to 77% - 80% (manual) and 76% - 82% (automated). Highest operating grade was reached by RTM process. Operating grades for transport during automated processing were not considered in this summary, as

transport systems operating grades were at 10% maximum. This would distort average machine operating, due to the high number of transport systems.

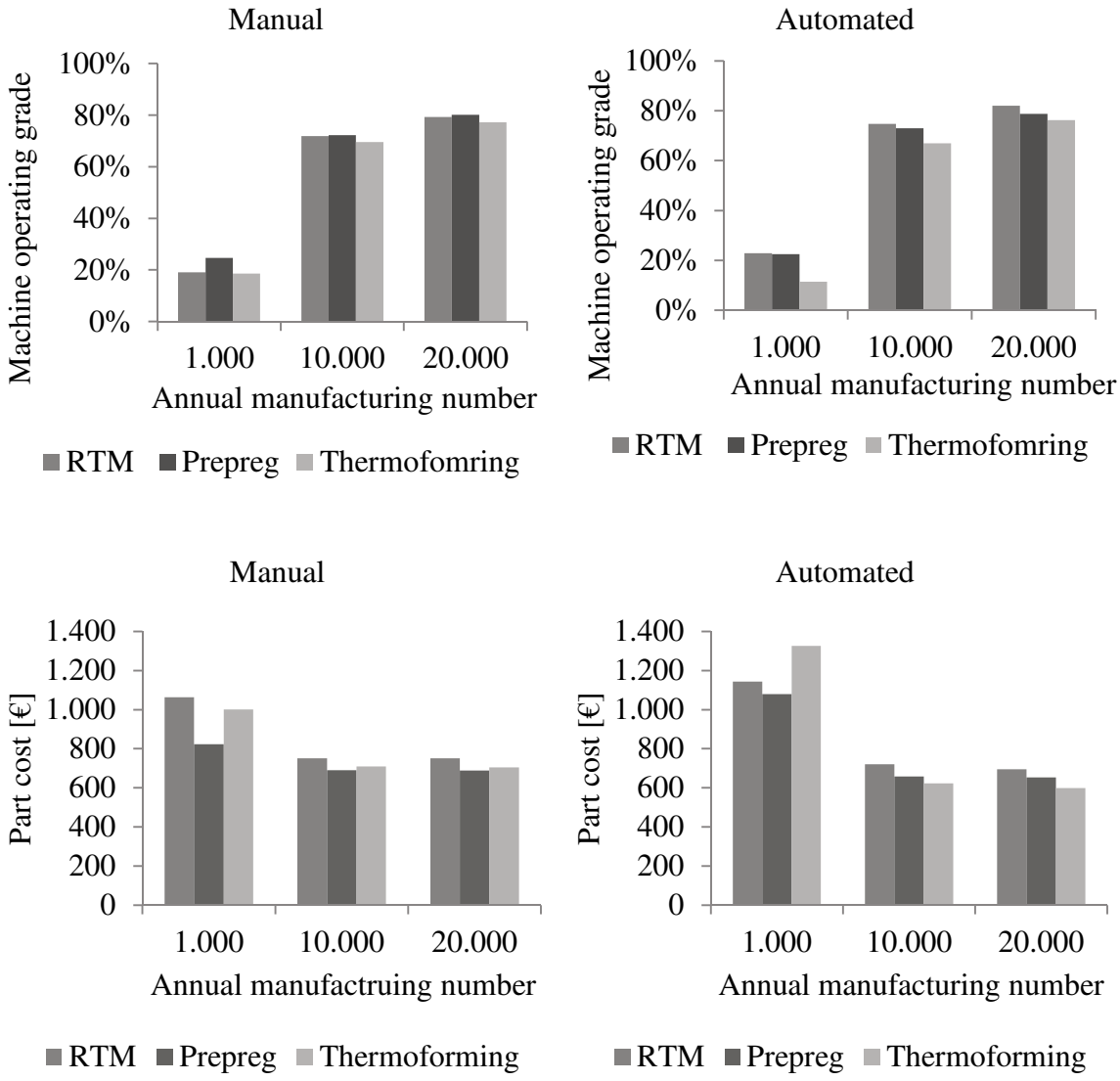

Figure 6.9 Machine operating grade and part cost according to annual manufacturing number

Part cost is a value summed up from machine cost, labor cost, tool cost and material cost depending on manufacturing numbers. Highest part costs were seen for manufacturing number of 1.000 parts per year. Here, thermoforming was the most expensive at1.300€ per part. Most efficient manufacturing technique at this number was manual prepreg processing resulting in 824€ per part. High annual manufacturing numbers reduced part cost. A significant cost reduction was seen at an increase of annual manufacturing number from 1.000 to 10.000 of 17% - 30% (manual processing) and 36% - 54% (automated processing). A further increase in annual manufacturing number from 10.000 to 20.000 resulted in a cost per part decrease of

1% (manual processing) and 1-4% (automated processing). Most cost efficient manufacturing method for manufacturing of 20.000 parts per year was thermoforming, resulting in 600€ per part.

For low manufacturing numbers (1.000 demonstrators per year) manual Prepreg process was found to be most cost efficient being 18% - 38% below other process variation costs. For increased annual manufacturing numbers of 20.000 parts per year thermoforming was found to be most efficient resulting in 8% - 14% less cost per part compared to RTM and Prepreg for similar conditions.

Thermoforming is most cost efficient for high volume manufacturing. Material costs are dominating the part manufacturing cost. Cost share comparison for automated high volume manufacturing shows a dominating impact of material cost. For RTM and Prepreg processing material cost sum up to 60% at 20.000 parts per year, for Thermoforming this is increased to 77%. Comparing pure process cost (machine, labor, and tool cost) at this manufacturing level; thermoforming process costs are at about 50% of RTM and Prepreg process costs.

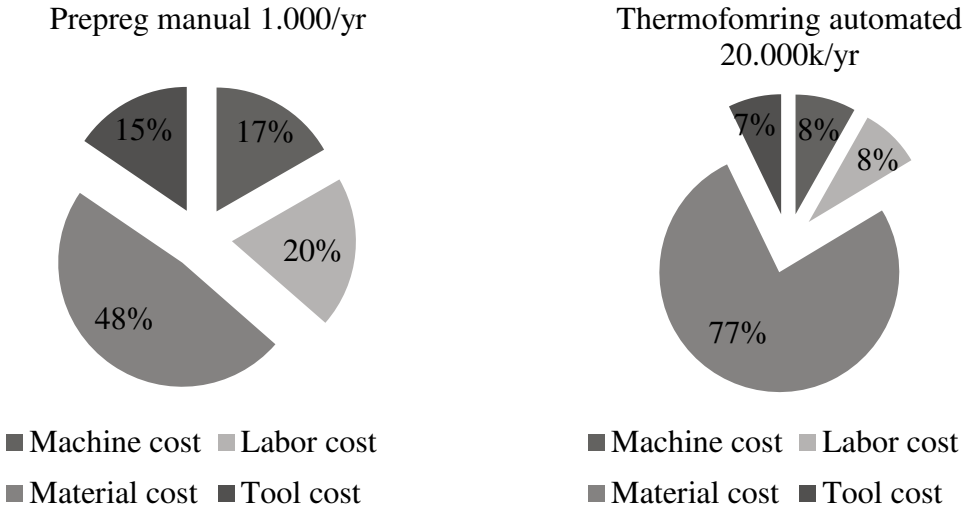

Figure 6.10 Part cost shares

Part cost shares (Figure 6.10) are given for the most efficient process variation at 1.000 and 20.000 parts per year. For 1.000 parts per year manual Prepreg was most efficient. Material cost required close to 50% of total part cost. Machine, labor and tool cost varied from 15% - 20%. At 20.000 parts per year thermoforming was most efficient. Material costs became dominating requiring 77% of the total part cost. Machine, labor, and tool cost varied from 7% - 8%. Automated prepreg and RTM processes had a 60% material cost share for high manufacturing numbers.

Process optimization of the thermoforming process regarding consolidation and heating time did result in minor cost saving. Consolidation optimization resulted in a cost reduction of 2%,

potential heating time optimization will result in a maximum cost reduction of 1,3% (5,5min). The latter is equivalent to a material cost reduction of 2% or 3€/kg.

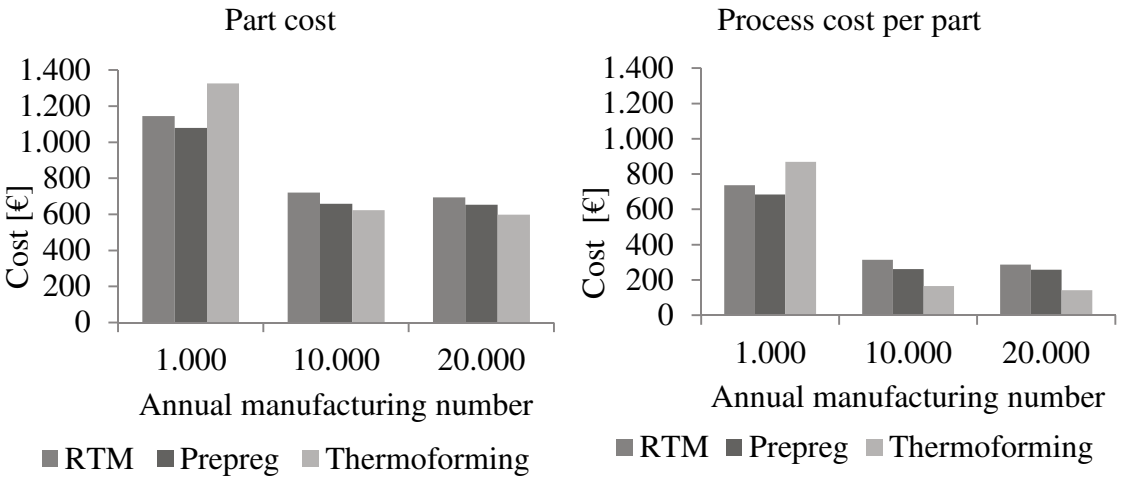

Figure 6.11 Part cost and process cost per part (no material cost considered) in dependence of annual manufacturing number for automated processing

Material costs are not discussed in detail, as material prices were assumed independent from amount needed and material type; hence assumed constant. Material cost share regarding optimization of process cost has very high potential, as these cost were dominating over all processes. Cost saving potential during thermoforming was highest, as the biggest cost share of material cost was found.

Figure 6.11 compared part cost and process cost per part for automated manufacturing. Process parts cost were summed up from machine cost, labor cost and tool cost. Material costs are not considered. As material costs did dominate part cost, a pure process comparison is done comparing process part cost. Thermoforming process part costs for high volume manufacturing was at 55% of RTM process part cost and 49% of Prepreg process part cost.

A common comparative number is cost-per-weight, which is shown in Figure 6.12. The cost per weight for manual manufacturing ranged from 320€/kg - 544€/kg depending on manufacturing number and process. Automated manufacturing resulted in 272€/kg - 603€/kg. The variation of cost depended on the annual manufacturing number assumed, resulting in a reduction of machine and tool cost at higher numbers due to higher operating grades. Automated manufacturing was found profitable at high manufacturing number and thermoforming most efficient.

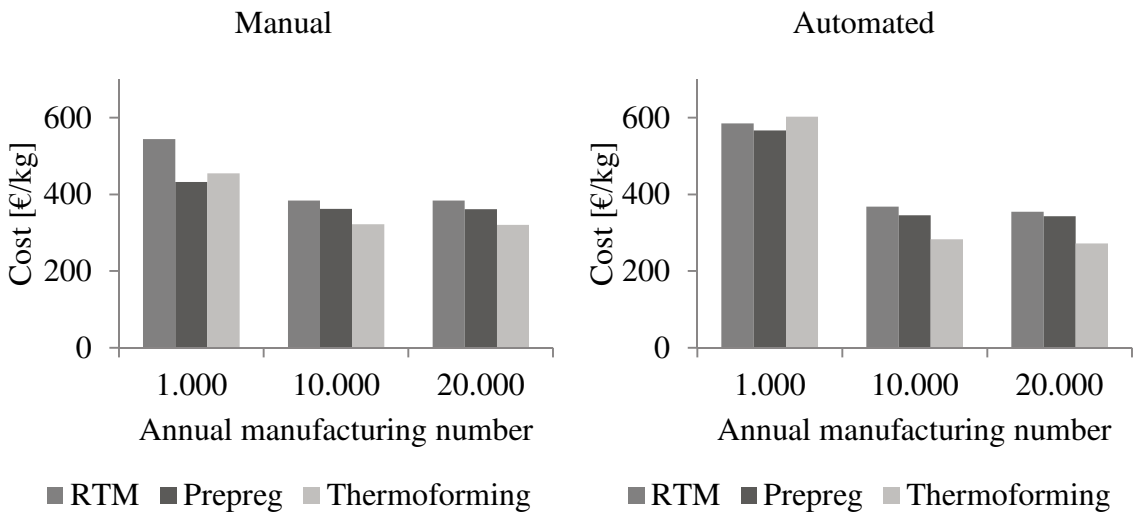

Figure 6.12 Cost per weight according to annual manufacturing number and process

6.3. Conclusions

To evaluate potential for complex thermoforming, the whole manufacturing chain from rolled-goods to final part has to be taken into account. Material used in the thermoforming process requires consolidation besides custom made cutting and preform lay-up. Standard organo sheets cannot be used due to the geometrical flexibility required. Press consolidation process recommendations for organo sheet preparation exist [39,77]. These consolidation processes require high pressure and long cycle times to ensure good material quality. Investigations regarding consolidation process optimization towards shorter consolidation times and lower pressure levels were made to reduce overall manufacturing time (4.1.1). A set of 13 cross-ply / 2mm constant wall thickness organo sheets was manufactured. An upper consolidation limit was chosen close to recommended consolidation times found in literature. The lower limit was orientated on a short time and low pressure press consolidation process. Subsequent thermoforming was conducted under standard thermoforming process conditions for state of the art parts. Evaluation was done on basis of interlaminar shear strength (2.6.2). Plane specimens were chosen for level of comparison as the shear performance was evaluated before and after thermoforming. A repeating plastic interlaminar shear failure behavior was found. Specimens were cut from plane panels after consolidation and from flanges of V-shape thermoformed panels. Shear performance of consolidated panels ranges from 20MPa - 34MPa showed clear dependency on consolidation conditions. After thermoforming, the shear strength was elevated up to a constant level above 40MPa (deviation 4%) for all specimens independent from prior consolidation processing. No significant impact of prior consolidation

time was found. The organo sheet manufacturing time was reduced by 83% (4.1.2). Pressure level during consolidation can be reduced by 85%. Consolidation time and pressure for complex thermoforming organo sheet manufacturing were significantly reduced from recommended processing conditions. The pressure level of last processing step seemed to be most important for shear strength level achieved. Last processing step including pressure during complex thermoforming is during forming and cooling. During the preheating phase in the thermoforming process material is heated without external pressure. This decreases material compaction. Former high level compaction due to high pressure and time consolidation cannot be preserved.

Market potential for complex thermoforming process was determined by a process efficiency evaluation. A tool for economic efficiency evaluation was developed to compare complex thermoforming with standard composite manufacturing technologies as RTM and prepreg (6.1). Base of comparison was the manufacturing chain for a sub-component having four separate parts to be built and subsequently joined. Technologies were compared by their manufacturing cost consisting of equipment, labor, material and tool cost. Process chains were aligned whenever possible. Identical processes and equipment were assumed identical in cost and durance. Factors regarding improvement of cost due to learning curve or quantity increase for material, machining and tools were disregarded.

Compared to other technologies complex thermoforming implies high initial invest and very time efficient manufacturing (6.2). Initial minimum investment for set-up of a thermoforming based manufacturing chain is high due to equipment cost of a thermoforming unit. In comparison to thermoset composites, the main reason for rapid processing time is the elimination of curing during single part manufacturing and joining. At high annual manufacturing number above 10.000 parts per year complex thermoforming is the most cost efficient process. Material cost become dominating, resulting in close to 75% part cost share (6.2). Process cost optimization regarding further manufacturing time reduction only results in very little cost reduction. Consolidation process optimization resulted in a 10% overall time reduction and only in 2% cost reduction. Potential heating process optimization depends on the wall thickness variation and can make up to 1,3% cost reduction at best conditions. A material cost reduction of 2% would be equivalent to the reduction achieved by heating time optimization. Hence, material cost reduction has the highest cost saving potential during complex thermoforming.

7. Summary

Technology development for manufacturing processes is driven by the factors weight and cost. Fiber reinforced thermoplastic composites offer great potential for lightweight parts manufacturing at short cycle times. The material is established in a range of primary aircraft applications. The thermoforming process is suitable for automated, high volume manufacturing of thermoplastic composite parts. State of the art thermoformed parts have a limited 1mm to 4mm constant wall thickness.

In this thesis, complex thermoplastic thermoforming was investigated with respect to process efficiency and process design. Complex thermoplastic thermoforming describes the manufacturing of thermoformed parts with wall thickness variations from 2-10mm. Constant wall thickness organo sheets cannot be used for complex thermoforming due to their thickness variable geometries. Therefore, complex thermoforming requires the consideration of the process manufacturing chain from organo sheet manufacturing to thermoforming and finishing. In this thesis, the consolidation process of the organo sheet manufacturing was optimized in comparison to standard thermoplastic consolidation recommendations. Further, process constraints to enable complex thermoforming process design were identified. Existing thermoforming process recommendations are only suitable for constant wall thickness of 1-4mm thermoforming. These recommendations cannot be applied complex parts. Due to local wall thickness differences up to 8mm and a maximum wall thickness of 10mm, a through thickness temperature gradient and wall thickness dependent surface temperatures develop during processing. Process design guidelines have to ensure material temperature within a defined temperature window to avoid material damage. Using CF/PPS, a temperature based processing window was determined by experimental investigations. A numerical tool was developed to determine suitable process conditions within set temperature limitations. Further, a technology evaluation tool to determine suitability of the process for a certain part on basis of required machining, labor and tooling was set up.

Complex thermoforming requires a custom made pre-consolidated organo sheet. Consolidation ensures material intraply bonding for rapid heat conduction during infrared heating phase of latter thermoforming. Taking the full process chain for manufacturing complex thermoplastic thermoformed parts, consolidation is the most time intense processing step offering highest potential for process time reduction. Consolidation conditions were optimized over recommended press processing conditions for standard organo sheet manufacturing. The impact of consolidation on mechanical performance was studied before and after thermoforming. Before thermoforming, variation in consolidation time and pressure impacted shear performance. After thermoforming, no difference in shear performance could be determined. In

consequence, the consolidation time was reduced by 83% in comparison to standard press forming process recommendations. Consolidation pressure level was reduced by 85%.

A temperature based processing window for complex thermoforming was determined. For semi-crystalline polymers, material properties depend on the temperature history. Several factors of temperature history such as time in melt have impact on the crystalline structure and hence the performance of the polymer. The processing of a complex organo sheet results in a variation of material temperature in dependence of local wall thickness.

Impact of occurring temperature history variations was studied by variation of process temperatures. Cooling rate as well as time and temperature in melt were found to have no impact on shear strength performance as long as temperatures are below degradation onset. Tool temperature was found relevant during processing with best results at temperature of minimum crystallization time. Temperature processing window could be set from melt temperature +30K to degradation onset temperature without impacting material regarding degree of crystallization or shear strength.

A numerical tool for determination of process conditions in dependence of complex organo sheet's wall thickness variation was developed on basis of the defined temperature window. Focus of the numerical tool was the prediction of thermoforming process temperatures during infrared heating. The organo sheets are heated by radiation of the infrared heater. Additional convection heat flow is caused by the developing temperature delta between heater and organo sheet. Both radiation power and convection power heat the organo sheet's surface. Inner material of the organo sheet is heated via conduction from the surface. Material temperature increase during infrared heating is only dependent on wall thickness and not dependent on panel. Hence, the process windows are thickness related and need to be determined for minimum and maximum wall thickness.

The numerical tool is adaptable to specific process conditions to define best overlap conditions, hence best processing conditions for a complex organo sheet. Material values, heater specific power density curve, heater distance and initial and maximum heater temperature can be defined and separately varied. The numerical tool was evaluated on basis on CF/PPS. For a maximum infrared heater temperature of 320°C processing was found to be possible for wall thickness variation from 2-10mm. Maximum infrared heater temperatures above 320°C result in a reduced processing time window and reduction possible wall thickness variations.

A tool for cost efficiency evaluation was developed. The tool is based on the determination of cost shares for a complex structure consisting of four sub-components. Costs are determined in dependence of part numbers, part geometry, material cost, and manufacturing technique. Manufacturing techniques for automated and manual processing of thermoforming, prepreg, and RTM were implemented. The consolidation time optimization as described above resulted in 10% manufacturing process time reduction and only 2% overall cost share reduction. Impact of potential infrared heating process optimization was below 1,5%. Thermoplastic material cost share is dominating (~75%) at high manufacturing numbers and most promising for further process cost reduction. Including those high material cost, complex thermoforming was found to be the most cost efficient process for high volume applications.

This thesis draws the baseline for complex shape thermoforming. Process constraints were found and a process design tool was developed. For future process development, both process reliability and process efficiency have to be improved. For process reliability, investigations regarding forming limitations (draping) and preform handling (clamping frame) for complex preforms are required. Software tools to simulate draping behavior from current research need further development towards the specifics of complex thermoforming. One specific topic is the positioning of single plies within a stack without fixation in a clamping frame during three dimensional forming. Automated and optimized handling of complex preforms is required for further process automation.

A flexible and automated process to manufacture customized blacks would help to increase complex thermoforming attractiveness. As material costs are the main cost driver in high volume production, the reduction of cut-off material is important and new approaches are required. Regarding process efficiency, the consolidation process is still very time-consuming. Out-of-autoclave technologies with increased heating and cooling rates show potential for further process optimization. Consolidation using the microwave process or induction process [86] represent attractive alternatives worth investigating for complex organo sheets as only low pressure levels are required.

Impact on material regarding residual stresses during rapid cooling may require special consideration. The transferability of the results towards crystallization behavior for a different semi-crystalline polymer or composite needs verification.

Additional benefit to the process would be added by the implementation of the joining process into the thermoforming unit. Manufacturing time could significantly be reduced and machine usage times optimized.

After all, further research towards cost and time efficient manufacturing of complex thermoformed parts will strengthen confidence and interest in this high potential material and process.

A. Supervised student thesis

Type	Index	Name	Title
Master	2012-0003	Meike Müller	Untersuchung zum Aufheizverhalten von komplexen Preforms im Thermoformprozess
Bachelor	2013-009	Boyu Yang	Experimentelle und numerische Untersuchungen zum Aufheizverhalten komplexer Preforms im Thermoformprozess
Bachelor	2012-0011	Florian Schlather	Weiterentwicklung der Herstellung eines OGVs mittels Thermoformen
Diplom	2013-0020	Gidon Zeh	Prozessentwicklung zum Handling komplexer Preforms für das Thermoformverfahren
Bachelor	2013-008	Christoph Heinz	Untersuchung zu dickenabhängigen Off-Plane Spannungen im Thermoformprozess

B. Technology evaluation

Cost based assumptions

1. **Machine Cost**

Manual Manufacturing: General equipment

	Single price [€]	Annual maintenance [€/y]
Cutter - no additional automation	100.000 €	1.000 €
Lay-Up table	1.000 €	0 €
Laser positioning	25.000 €	500 €
US-Welding Unit	5.000 €	500 €
Milling Machine	100.000 €	2.000 €
NDT (flat C-Scan)	140.000 €	1.000 €
Erosion protection	15.000 €	5.000 €
Welding line control (A-Scan)	10.000 €	5.000 €
Rivet positioning equipment	15.000 €	1.000 €
Sand blasting machine	30.000 €	2.000 €
Washing machine	10.000 €	2.000 €
Adhesive curing oven	30.000 €	2.000 €

Equipment RTM manual

	Single price [€]	Annual maintenance [€/y]
Press (200°C / 100t)	100.000,00 €	3.000,00 €
Pressure vessel	60.000,00 €	3.000,00 €

Equipment Prepreg manual

	Single price [€]	Annual maintenance [€/y]
Vacuum table (compaction)	10.000 €	1.000 €
Lay-Up table	1.000,00 €	0,00 €
Heating press	100.000 €	3.000 €

Equipment Thermoforming manual

	Single price [€]	Annual maintenance [€/y]
Consolidation press (350°C, 2bar)	100.000 €	2.000 €
Thermoforming unit	300.000 €	5.000 €
US Welding Unit for joining	20.000 €	1.000 €

Automated manufacturing: General equipment

	Single price [€]	Annual maintenance [€/y]
Cutter - automated material collection	120.000 €	5.000 €
Lay Up Table	1.500 €	0 €
Pick and Place Unit	20.000 €	1.000 €
US fixation for P&P-Unit	20.000 €	1.000 €
US fixation / Binder activation RTM	20.000 €	1.000 €
Automated transport (robot, gripper, linear axis)	100.000 €	1.000 €
Milling Machine	100.000 €	2.000 €
NDT (flat C-Scan)	180.000 €	2.000 €
Erosion protection	20.000 €	5.000 €
Joining control/ Final control (A-Scan)	15.000 €	5.000 €
Rivet positioning equipment	20.000 €	2.000 €
Sand blasting machine	30.000 €	2.000 €
Washing machine	15.000 €	2.000 €
Adhesive curing oven	30.000 €	2.000 €

Equipment RTM automated

	Single price [€]	Annual maintenance [€/y]
Thermoforming unit (100°C, 70t)	150.000 €	5.000 €
Robot + gripper for preform assembly + table	100.000 €	1.000 €
Press (200°C / 100t)	120.000 €	5.000 €
2K Injection machine	120.000 €	5.000 €

Equipment Prepreg automated

	Single price [€]	Annual maintenance [€/y]
Thermoforming for 3-Preform /Double diaphragm (2 Airfoil or 2 Bridge preforms formed at once)	150.000 €	5.000 €
Automated transport (robot, gripper, linear axis)	100.000,00 €	1.000 €
Automated placement - Preform in tool	100.000 €	1.000 €
Automated transport (robot, gripper, linear axis)	100.000,00 €	1.000 €
Heating press / curing	120.000 €	5.000 €

Equipment Thermoforming automated

	Single price [€]	Annual maintenance [€/y]
Consolidation press (400°C, 4bar)	100.000,00 €	5.000 €
Thermoforming unit	500.000,00 €	5.000 €
Automated Resistance welding	40.000,00 €	2.000 €

2. Material cost

Material cost	160 €/kg

Identical cost for all material assumed.

3. Labor cost

Average labor cost	43,44 €/h

Basis is 36€/h in 2014 and an average annual labor increase of 3%.

4. Tool cost

Tools RTM manual

Preform Draping tool (price for set of 4)	30.000,00 €	3.000,00 €
RTM Injection Tools (price for set of 4)	80.000,00 €	8.000,00 €
Milling Tool (price for set of 3)	5.000,00 €	500,00 €
Assembly Tool Adhesive	10.000,00 €	1.000,00 €

Tools Prepreg manual

Draping tools (price for set of 4)	25.000 €	2.500 €
Curing tools (price for set of 4)	45.000 €	4.500 €
Milling Tool (price for set of 3)	5.000 €	500 €
Assembly Tool Adhesive	10.000 €	1.000 €

Tools Thermoforming manual

Consolidation Tool (2-sided / 3D) (price for set of 4)	40.000 €	4.000 €
Thermoforming tools (price for set of 3 (1A +2B))	50.000 €	5.000 €
Milling Tool (price for set of 3)	5.000 €	500 €
Assembly Tool Resistance Welding	10.000 €	1.000 €

Tools RTM automated

Preforming-TF tool (price for set of 3)	50.000 €	5.000 €
RTM Injection Tool (price for set of 4)	120.000 €	6.000 €
Milling Tool	8.000 €	800 €
Assembly Tool Adhesive	15.000 €	1.500 €

Tools Prepreg automated

Preforming-TF tool (price for set of 3)	50.000 €	5.000 €
Curing tool (price for set of 4)	60.000 €	3.000 €
Milling Tool	8.000 €	800 €
Assembly Tool Adhesive	15.000 €	1.500 €

Tools Thermoforming automated

Consolidation tool (2-sided) (price for set of 4)	70.000,00 €	7.000 €
TF tool (price for set of 3)	80.000,00 €	8.000 €
Milling tool	8.000,00 €	800 €
Pick and Place Tool Assembly	15.000,00 €	1.500 €

Process time assumptions

RTM manual

	Process time [min]	Labour time [min]
Cut Material Airfoil 1 (2 U-shaped preforms)	29,7	20,0
T:Lay-up + Binder act A1, P1+2	82,7	82,7
T: RTM preparation	10,0	10,0
T: Assembly in RTM mold A1	10,0	10,0
T: Assembly in RTM mold A2	10,0	10,0
RTM injection + curing process	199,0	15,0
Mechanical treatment	10	10
NDT	30	15
Erosion protection	20	20
Assembly /Rivet + Adhesive	74,2	14,2
Control joining (A-Scan)	10	10

Prepreg manual

	Process time [min]	Labour time [min]
Cut Material A1, A2 (2 U-shaped preforms) B1, B2	35,8	20,0
T:Lay-up of all parts	98,4	98,4
Compaction during lay-up for all parts	120,0	20,0
T: Tool assembly	10,0	10,0
Press curing	162,1	7,0
Mechanical treatment	10	10
NDT	30	15
Erosion protection	20	20
Assembly /Rivet + Adhesive	74,2	14,2
Control joining (A-Scan)	10	10

Thermoforming manual

	Process time [min]	Labour time [min]
Cut Preforms (A1,A2,B1,B2)	47,9	40,0
Lay-up + US welding (A1, A2, B1, B2)	64,74	62,0
Consolidation preparation (A1, A2, B1, B2) (no bagging)	40,0	40,0
Press consolidation	40,0	10,0
Preparation TFU Tool	2,3	3,0
Thermoform A1, A2, B1, B2	29,6	18,0
Mechanical treatment	10	10
NDT	30	15
Erosion protection	20	20
Assembly / Resistance Welding	21,0	21,0
Control joining (A-Scan)	10	10

RTM automated

	Process time [min]	Labour time [min]
Cut Preforms A1 A2 B1 B2	17,7	8,0
Automated transport	1,00	0,00
Lay-up + Binder act A1, A2, B1, B2	43,4	8,0
Automated transport	1,00	0,00
Thermoforming in 3D preforms	20,13	
Automated transport	1,00	0,00
Automated Assembly in RTM molds	20,0	4,0
Automated transport	1,00	0
RTM injection + curing process	177,0	15,0
Automated transport	1,00	0,00
Mechanical treatment / Milling	10	8
Automated transport	1,00	0,00
NDT	30	5
Automated transport	1,00	0,00
Erosion protection	20	5
Automated transport	1,00	0,00
Assembly /Rivet + Adhesive	69,1	5,0
Automated transport	1,00	0,00
Control joining (A-Scan)	10	10

Prepreg automated

	Process time [min]	Labour time [min]
Cut preforms A1, A2, B1, B2	23,77	8
Automated transport	1,00	0,00
Preform lay-up 2D (A1, A2, B1, B2)	92,21	52,21
Automated transport	1,00	0,00
Thermoforming in 3D preform (A1, A2, B1, B2)	20,13	8
Automated transport	1,00	0,00
Automated preform assembly molds	20	4
Automated transport	1,00	0,00
Heating press / curing	159,1	14
Automated transport	1,00	0,00
Mechanical treatment / Milling	10	8
Automated transport	1,00	0,00
NDT	30	5
Automated transport	1,00	0,00
Erosion protection	20	5
Automated transport	1,00	0,00
Joining process (rivet + adhesive)	69,1	5
Automated transport	1,00	0,00
Control joining (A-Scan)	10	10

Thermoforming automated

	Process time [min]	Labour time [min]
Cut preforms (A1, A2, B1, B2)	23,9	8,0
Automated transport	1,00	0,0
Pick and Place +US welding A1, A2, B1, B2	32,4	8,0
Automated transport	1,00	0,0
Press consolidation (4 at once)	10,0	5,0
Automated transport	1,00	0,0
Cooling of preform	20,00	0,0
Automated transport	1,00	0,0
Preparation TFU / Tool	1,0	1,0
Thermoform A1, A2, B1, B2	23,1	8,0
Automated transport	1,00	0,0
Mechanical treatment / Milling	10	8,0
Automated transport	1,00	0,0
NDT	30	5,0
Automated transport	1,00	0,0
Erosion protection	20	5,0
Automated transport	1,00	0,0
Assembly / Resistance welding	21,0	5,0
Automated transport	1,00	0,0
Control joining (A-Scan)	10	10,0

Calculation example

Example data for calculation of 20.000 parts per year via automated thermoforming

Machine operation

Part / day	80		Parts per deprecation	100.000							
Depreciation [years]	5		Workdays per year	250							
Machine time per day [min]	880										
	t (use per part) [min]	t(use per day) [min]	No. Of similar machines needed	Total machine cost / process setp [€] incl. Maitenance	t (use in depresiation time) [h]	Overall equipment effectivness [%]	Depreciation time [h]	Operating grade	Machine cost (acc. to operating grade) [€/h]	Machine cost (100% operation grade) [€/h]
Cutter - automated material collection	23,9	1910	3	435.000 €	39804	85%	46750	85,14%	10,9	9,3
Automated transport (robot, gripper, linear axis)	1,0	80	1	105.000 €	1667	85%	15583	10,70%	63,0	6,7
Pick and Place Unit	32,4	2589	4	100.000 €	53949	85%	62333	86,55%	1,9	1,6
Lay Up Table	32,4	2589	3	4.500 €	53949	100%	55000	98,09%	0,1	0,1
US fixation for P&P-Unit	32,4	2589	4	100.000€	53949	85%	62333	86,55%	1,9	1,6
Automated transport (robot, gripper, linear axis)	1,0	80	1	105.000 €	1667	85%	15583	10,70%	63,0	6,7
Consolidation press (400°C, 4bar)/4tools in parallel	10,0	800	2	250.000 €	16667	85%	31167	53,48%	15,0	8,0
Automated transport (robot, gripper, linear axis)	1,0	80	1	105.000 €	1667	85%	15583	10,70%	63,0	6,7
Table for cooling	20,0	1600	2	3.000 €	33333	100%	36667	90,91%	0,1	0,1
Automated transport (robot, gripper, linear axis)	1,0	80	1	105.000 €	1667	85%	15583	10,70%	63,0	6,7
Thermoforming unit (4 preforms formed at once, side by side)	23,1	1850	3	1.575.000 €	38556	85%	46750	82,47%	40,9	33,7
Automated transport (robot, gripper, linear axis)	1,0	80	1	105.000 €	1667	85%	15583	10,70%	63,0	6,7
Milling Machine	10,0	800	2	220.000 €	16667	85%	31167	53,48%	13,2	7,1
Automated transport (robot, gripper, linear axis)	1,0	80	1	105.000 €	1667	85%	15583	10,70%	63,0	6,7
NDT (flat C-Scan)	30,0	2400	4	760.000 €	50000	85%	62333	80,21%	15,2	12,2
Automated transport (robot, gripper, linear axis)	1,0	80	1	105.000 €	1667	85%	15583	10,70%	63,0	6,7
Erosion protection	20,0	1600	3	135.000 €	33333	85%	46750	71,30%	4,1	2,9
Automated transport (robot, gripper, linear axis)	1,0	80	1	105.000 €	1667	85%	15583	10,70%	63,0	6,7
Automated Resistance welding	21,0	1680	3	150.000 €	35000	85%	46750	74,87%	4,3	3,2
Pick and Place Unit	21,0	1680	3	75.000 €	35000	85%	46750	74,87%	2,1	1,6
Automated transport (robot, gripper, linear axis)	1,0	80	1	105.000 €	1667	85%	15583	10,70%	63,0	6,7
Joint control/ Final control (A-Scan)	10,0	800	2	80.000 €	16667	85%	31167	53,48%	4,8	2,6

Cost summary of calculation example

Process step	Machine cost [€]	Labor cost [€]	Material cost [€]	Tool cost [€]
Cut Material (A1, A2, B1, B2)	4,35 €	5,79 €		
Automated transport	1,05 €	0,00 €		
Pick and Place +US welding A1, A2, B1, B2	2,05 €	5,79 €		
Automated transport	1,05 €	0,00 €		
Press consolidation (4 at once)	2,50 €	3,62 €		21,00 €
Automated transport	1,05 €	0,00 €		
Cooling of preform (4 table + 1 tool set required)	0,03 €	0,72 €		
Automated transport	1,05 €	5,79 €		
Preparation TFU / Tool	0,68 €	0,00 €		
Thermoform A1, A2, B1, B2	15,75 €	5,79 €	457,94 €	18,00 €
Automated transport	1,05 €	0,00 €		
Mechanical treatment / Milling	2,20 €	3,62 €		1,80 €
Automated transport	1,05 €	0,00 €		
NDT	7,60 €	3,62 €		
Automated transport	1,05 €	0,00 €		
Erosion protection	1,35 €	3,62 €		
Automated transport	1,05 €	0,00 €		
Assembly / Resistance welding	2,25 €	3,62 €		2,25 €
Automated transport	1,05 €	0,00 €		
Control joining (A-Scan)	0,80 €	7,24 €		
	49,01 €	49,23 €	457,94 €	43,05 €
Total cost per part				599,22 €

C. Index of Symbols

Latin symbols

Symbol	Unit	Specification
A	m²	Area
a	m	Heater distance
a_{Fl}		Thermal diffusion rate of a fluid
a_P		Thermal diffusion rate of panel
b	m	Width
C	m	Compass (convection)
c_1, c_2, c_3, c_4, c_5	-	Curve fitting constants (power density determination)
D	m	Diameter of cylindrical loading bars (radial stress)
d	m	Wall thickness
d_{max}	m	Maximum organo sheet wall thickness
d_{min}	m	Minimum organo sheet wall thickness
d_x	m	Horizontal distance between two adjacent loading bars (radial stress)
d_y	m	Vertical distance between two adjacent loading bars (radial stress)
$\dot{E}$	J/s	Emitted power
E_r	N/m²	Module in radial direction
E_θ	N/m²	Module in tangential direction
F	N	Force
F_{i-j}	-	View factor of surface i to surface j
Gr	-	Grashof number
g		Parameter used in strength calculation (radial stress)

H	m	Distance between coaxial plate (view factor coaxial plates)
ΔH_{melt}	J/g	Melt enthalpy
ΔH_{CC}	J/g	Cold crystallization enthalpy
ΔH_{max}	J/g	Maximum enthalpy
IR_l	m²	Lower infrared heater area
IR_u	m²	Upper infrared heater area
L	W/m²	Power density
L_H	W/m²	Power density of infrared heater
L_C	-	Characteristic length (convection)
l	m	Bearing distance
Nu	-	Nusselt number
Nu_{top}	-	Nusselt number from top heater and surface area
Pr	-	Prandtl number
Pr_{Fl}	-	Prandtl number of a fluid
p, q, s, u, v, w	-	Geometric factors (view factor)
$\dot{q}$	W/s m²	Power per area
$\dot{Q}$	W/s	Emitted power
$\dot{Q}_{IN}$	W/s	Incoming power
$\dot{Q}_{IR,H}$	W/s	Radiation power from heater
$\dot{Q}_{IR,La}$	W/s	Radiation power of laminate
$\dot{Q}_{OUT}$	W/s	Outgoing power
$\dot{Q}_{Laminate}$	W/s	Laminate power difference
$\dot{Q}_{Con}$	W/s	Convection power
R	m	Half panel wall thickness (power conduction)
Ra	-	Rayleigh number
r_i	m	Inner radius
r_o	m	Outer radius
r_m	m	Intermediate radius
S	m²	Panel surface area
S_u	m²	Upper panel surface area

S_l	m²	Lower panel surface area
T	K	Temperature
T_G	K	Glass transition temperature
T_{max}	K	Maximum temperature (of process window)
T_{min}	K	Minimum temperature (of process window)
T_0	K	Start temperature
T_{ref}	K	Reference temperature (power conduction)
T_H	K	Temperature of heater
T_W	K	Temperature of wall
T_∞	K	Temperature of fluid / surrounding temperature
t	s	Time
Δt	s	Time span
$t_{process}$	s	Process window
$t_{process\,max}$	s	Process window of maximum organo sheet thickness
$t_{process\,min}$	s	Process window of minimum organo sheet thickness
W_1, W_2	m²	Surface of coaxial plate 1 and 2 (view factor coaxial plates)
w_1, w_2	m	Dimensionless surface of coaxial plate 1 and 2
X_C	-	Degree of crystallinity
$X_{normalized}$		Normalized experimental value
$X_{measured}$		Measured experimental value
x	-	Cartesian coordinate
y	-	Cartesian coordinate
z	-	Cartesian coordinate
z_i	m	Through thickness position in panel (power conduction)

Greek symbols

Symbol	Unit	Specification
α		Heat transfer coefficient
Δ		Relative displacement between the top and bottom halves of four point bending fixture (radial stress)
δ_{air}		Density of air
δ_M		Matrix material weight share
ε		Emission coefficient
η_{air}		Dynamic viscosity of air
θ		Dimensionless temperature
ϑ		Body temperature
$\vartheta(r,t)$		Temperature profile in dependence of position and time
κ		Root fraction of module in radial and tangential direction
λ		Thermal conductivity
λ_{air}		Thermal conductivity of air
λ_{Fl}		Viscous diffusion rate of a fluid
ν_{air}		Kinematic viscosity air
ξ		Dimensionless through thickness position (power conduction)
ρ		Fraction of inner over outer radius (curved beam strength)
σ		Flexural strength
σ_B		Stefan-Boltzmann constant
σ_r		Radial stress
τ		Interlaminar shear strength
$\tau_{plastic}$		Plastic interlaminar shear strength
Φ		Angle from horizontal of the specimen legs in degree (radial stress)
ψ		Angle

D. List of Abbreviations

CBS	Curved beam strength
DSC	Differential scanning calorimetry
Fo	Fourier number (power conduction)
FVC	Fiber volume content
HR	Heating rate
$ILSS$	Interlaminar shear strength
$ILSS_{plastic}$	Plastic interlaminar shear strength
IR	Infrared
LCC	Institute for Carbon Composites
PEEK	Polyetheretherketone
PEI	Polyetherimide
PEKK	Polyetherketoneketone
PPS	Polyphenylenesulphide
RTM	Resin Transfer Molding

E. List of Figures

Figure 1.1 Material breakdown of A350-900 XWB, numbers from [8] 1

Figure 1.2 Cost advantage of thermoplastic composites [15] 2

Figure 1.3 Primary thermoplastic composite structures in Gulfstream [22] 3

Figure 1.4 Process chart of the complex thermoforming process 4

Figure 2.1 Synthesis of Polyphenylene Sulfide [30] 9

Figure 2.2 Manufacturing chains for continuous carbon fiber reinforced thermoplastic material [33] 10

Figure 2.3 Thermoforming process [41] 12

Figure 2.4 Typical thermoforming process 13

Figure 2.5 Donier flap rib (1989), A380 rib, A350XWB clip [24–26] 14

Figure 2.6 Temperature dependent behavior of semi-crystalline and amorphous polymers [53] 15

Figure 2.7 Impact of time and temperature in melt on crystallization half time [55] 16

Figure 2.8 Crystallization half time over isothermal crystallization temperature [54] .. 17

Figure 2.9 Impact of degree of crystallization on flexural strength in dependence of tool temperature [36] 18

Figure 2.10 Dependence of degree of crystallinity on cooling rate [38,50] 18

Figure 2.11 Impact of temperature on weight loss of PPS [59] 19

Figure 2.12 Impact of heating rate [°C/min] on onset of material weight loss (degradation) [59] 20

Figure 2.13 Infrared radiation within the electromagnetic wave spectra [63] 21

Figure 2.14 View factor relations 22

Figure 2.15 Free convection of surface (left) and bottom (right) heated panel 24

Figure 2.16 Curved Beam in Four-Point Bending [70] 29

Figure 3.1 Airfoil demonstrator geometry 32

Figure 3.2 Complex geometry challenges 33

Figure 3.3 Side view over demonstrator geometry 33

Figure 3.4 Axis A-A and B-B of wall thickness variation across demonstrator 34

Figure 3.5 Complex preform wall thickness variation over width (A-A) 34
Figure 3.6 Preform maximum wall thickness over length of main section (B-B) 35
Figure 3.7 Process chain of complex thermoforming 35
Figure 3.8 Preform - without cover layer (left) / with cover layer (right) 36
Figure 3.9 Demonstrator before (left) and after (right) consolidation 37
Figure 3.10 Organo sheet in press before thermoforming 39
Figure 3.11 Part in press after thermoforming 39
Figure 3.12 Final demonstrator part 40
Figure 3.13 DSC plot of demonstrator sample – degraded material 40
Figure 3.14 DSC plot of demonstrator sample - standard material 41
Figure 3.15 Demonstrator bottom-side comparison 41
Figure 3.16 Impact of panel thickness d on surface temperature 42
Figure 3.17 Variation of heating rate due to variable wall thickness 42
Figure 3.18 Impact of heater distance a on surface temperature 43
Figure 4.1 Preform stack before (left) and after (right) consolidation 46
Figure 4.2 Consolidation tool 47
Figure 4.3 Panel thickness according to consolidation conditions after consolidation and after consolidation and thermoforming 49
Figure 4.4 Comparison of Flexural Strength Results 50
Figure 4.5 Maximum bending stress after consolidation and subsequent thermoforming 51
Figure 4.6 Applied force over bending distance during ILSS testing 52
Figure 4.7 Plastic interlaminar shear strength after consolidation only 52
Figure 4.8 Plastic interlaminar shear strength after consolidation and thermoforming . 53
Figure 4.9 Plastic interlaminar shear strength over processing conditions 54
Figure 4.10 Radial stress over cooling rate of 6mm panels 57
Figure 4.11 Impact of melt temperature on radial stress 58
Figure 4.12 Radial stress over organo sheet wall thickness 59
Figure 4.13 Impact of tool temperature on radial stress 60
Figure 5.1 Scheme of process window determination for complex organo sheets 65
Figure 5.2 Radiation heat flows during IR heating 67
Figure 5.3 Assumption of a symmetric model [79] 67
Figure 5.4 Impact of panels size S and heater distance a on surface temperature 68

Figure 5.5 Oscillation of infrared heater temperature over time 69

Figure 5.6 Heater maximum set temperature over maximum occurring temperature ... 70

Figure 5.7 Comparison of heating time variation until T_{mid} 330°C is reached - surface temperature development for heater maximum temperature variation 71

Figure 5.8 Surface temperature development for heater distance variation 71

Figure 5.9 Relevant areas for view factors of panel surfaces 73

Figure 5.10 Geometrical assumption to determine view factor from heater to surface [80] 73

Figure 5.11 Relevant areas for view factor of panel side surfaces 74

Figure 5.12 Perpendicular view factor determination according to [64] 76

Figure 5.13 Power density curve fitting [62] 77

Figure 5.14 One-dimensional heat conduction variable z 81

Figure 5.15 Resulting temperature profile for boundary condition approximation type 283

Figure 5.16 Calculation pattern for numerical process definition 85

Figure 5.17 Evaluation of numerical process definition tool 86

Figure 5.18 Diagram output of numerical process definition tool 86

Figure 5.19 Heating time comparison for evaluated configurations [a, T_{IRmax}, d] 87

Figure 5.20 Material temperature curves of numerical model (dashed) and experiment (full) for d = 6mm, T_{IRmax} 400°C, a 100mm 89

Figure 5.21 Process time window for organo sheets of constant wall thickness in dependence of T_{IRmax} 90

Figure 5.22 Maximum heater temperature over 2mm wall thickness variation 91

Figure 5.23 Processing time slot in dependence of $T_{IR\ max}$ for 6/8mm organo sheet 92

Figure 5.24 Heating time according to wall thickness variation at $T_{IR\ max}$ 320°C 92

Figure 5.25 Possible infrared processing temperature over wall thickness variation 93

Figure 5.26 Guideline for determination of process window using numerical model ... 94

Figure 6.1 Airfoil doublet 98

Figure 6.2 Single ply variation of demonstrator 98

Figure 6.3 Calculation pattern for economic efficiency determination 107

Figure 6.4 Invest costs in dependence of annual manufacturing number for manual (right) and automated (left) process chains 108

Figure 6.5 Invest cost per part according to annual manufacturing number 109

Figure 6.6 Process dependent manufacturing time per part 109

Figure 6.7 Time shares for part manufacturing: total time / labor time 110

Figure 6.8 Overview on process cost shares and part cost for manual and automated manufacturing.....112

Figure 6.9 Machine operating grade and part cost according to annual manufacturing number 114

Figure 6.10 Part cost shares.....115

Figure 6.11 Part cost and process cost per part (no material cost considered) in dependence of annual manufacturing number for automated processing 116

Figure 6.12 Cost per weight according to annual manufacturing number and process117

F. List of Tables

Table 2-1 Overview of high performance thermoplastic matrices [28] 8
Table 2-2 Consolidation recommendation for CF/PPS tape by TenCate [39] 11
Table 2-3 Thermoforming parameters for CF/PPS by Tencate [39] 13
Table 2-4 Impact factors for crystallization during thermoforming 16
Table 3-1 Comparison of standard and complex thermoforming 31
Table 3-2 Demonstrator autoclave consolidation parameters 37
Table 3-3 Demonstrator vacuum consolidation parameters 37
Table 3-4 Thermoforming parameters for CF/PPS by Tencate [39] 38
Table 4-1 Consolidation parameters 47
Table 4-2 Thermoforming parameters 48
Table 4-3 Constant defined thermoforming conditions 55
Table 4-4 Test matrix – Impact of thermoforming conditions 56
Table 4-5 Degree of crystallization according to melt temperature for 6mm panel 58
Table 4-6 Wall thickness dependent time in melt and maximum surface temperature .59
Table 4-7 Degree of crystallization according to wall thickness 60
Table 4-8 Degree of crystallization according to tool temperature for 6mm panel 61
Table 5-1 Heating rate of infrared heater 76
Table 5-2 Free convection material constants 78
Table 5-3 Material constants of laminate 81
Table 5-4 Dimensionless coordinates 84
Table 6-1 Manufacturing assumptions 99
Table 6-2 General process chain 100
Table 6-3 Overview on manufacturing process chains and equipment 102
Table 6-4 Doublet weight and respective material cost 107

G. References

[1] Wiedmann T, Minx J. A definition of 'carbon footprint'. In: Ecological Economics Research trends, p. 1–11.

[2] Bishop S, Grayling T. The sky is the limit: Policies for sustainable aviation: Emphasis; 2003.

[3] Upham P, Maughan J, Raper D, Thomas C. Towards sustainable aviation: Earthscan Publications Ldt; 2003.

[4] Red C. Aviation Outlook: Fuel pricing ignites demand for composites in commercial transports: A confluence of aircraft OEM technical innovation and economic pressures on their airline customers creates increasingly favorable market conditions for aerospace composites; 2008.

[5] Smith F. The use of composites in aerospace: past, present and future challenges; 2012.

[6] Wood K. High-performance composites for aircraft interiors conference review: Colocated with Aircraft Interiors Expo Americas, CompositesWorld's HPC4ACI event focused on new material and processing trends that could drive more composites inside the aircraft; 2014.

[7] Herbeck L. Von der Manufaktur zur Produktion - Herausforderungen für die Faserkunststoffverbunde. In: CCeV Automotive Forum.

[8] Airbus Group. Taking the lead: the A350 XWB; 2006.

[9] Boeing. Boeing 787 from the ground up; 2006.

[10] Worthoff F. Composite fan structures design & development. In: GE symposium; 2009.

[11] Rolls-Royce outlines composites use in next-generation engine: The Rolls-Royce Advance and UltraFan engines will feature carbon fiber/titanium fan blades and use ceramic matrix composites in high-heat components; 2014.

[12] Olsson E. Closing the gap between research and industrialization - the pick & place case. In: SiComp Conference.

[13] Kocian F. Strukturelles Leitgitter mit thermoplastischen Leitschaufeln für Triebwerke: Bauweisen Kolloquium. Stuttgart; 2009.

[14] Michaeli W, Greif H, Wolters L, Vossebürger F. Technologie der Kunststoffe: Lern- und Arbeitsbuch. München: Hanser; 1998.

[15] Offringa AR. Thermoplastic composites - rapid processing applications. Composites Part A: Applied Science and Manufacturing 1996;27(4):329–36.

[16] Gardiner G. Thermoplastic composites: Primary structure? Cincinnati, OH 45244-3029; 2011.

[17] Experteninterview Flugzeugbau: Großer Durchbruch für PPS-Composites. In: inform Das Ticona Magazin; 2009, p. 15–8.

[18] Third Gulfstream G650 joins test fleet in quest of type certification in 2011: Aircraft incorporates first-ever carbon/PPS rudder and elevators; 2010.

[19] Meyer D., Bersee HE, Beukers A. Temperature effect on reinforced thermoplastic composite properties for primary aircraft structure applications. In: 49th AIAA Structures, Structural dynamics, and materials conference, Schaumburg, IL.

[20] Airbus. Airbus continues its TAPAS partnership with the dutch thermoplastic composite sector. [March 13, 2014]; Available from: http://www.airbus.com/newsevents/news-events-single/detail/airbus-continues-its-tapas-partnership-with-the-dutch-thermoplastic-composite-sector/.

[21] Offringa AR. Integrally stiffened thermoplastic skin panels. In: Borgmann H, editor. Conference proceedings: WFB Wirtschaftsförderung Bremen GmbH, p. 56–9.

[22] Fokker Technologies. Picture Gulfstream rudder torsion box and elevator.

[23] Vieille B, Albouy W, Chevalier L, Taleb L. About the influence of stamping on thermoplastic-based composites for aeronautical applications. Composites Part B: Engineering 2013;45(1):821–34.

[24] Bartz WJ (ed.). Faserverbundwerkstoffe mit thermoplastischer Matrix: Hochleistungswerkstoffe für rationelle Verarbeitung. Renningen- Malmsheim: expert Verlag.

[25] Fokker Technologies. Picture A380 thermoformed rib. In: High performance composites.

[26] Sloan J. Inside a thermoplastic composites hotbed: As production of the A350 XWB ramps up, so does manufacture of the thermoplastic fuselage clips the plane requires. HPC sees how it's done; 2014.

[27] International Association of Plastics Distribution. Thermoplastic composites for aerospace; 2010.

[28] Leach D. Thermoplastic Composite Materials - Coming of Age! In: ThermoformNet Meeting; 2003.

[29] Edmonds JamesT., Hill HW. Production of polymers from aromatic compounds. 15(US Pat. 3354129).

[30] Brady D. The crystallinity of poly(phenylene sulfide) and its effect on polymer properties. Journal of Applied Polymer Science 1976;20:2541–51.

[31] Vieille B, Aucher J, Taleb L. Carbon fiber fabric reinforced PPS laminates: Influence of temperature on mechanical properties and behavior. Adv. Polym. Technol. 2011;30(2):80–95.

[32] Ehrenstein GW. Faserverbund-Kunststoffe - Werkstoffe - Verarbeitung - Eigenschaften. 2nd ed. München Wien: Carl Hanser Verlag; 2006.

[33] Mitschang P, Blinzler M, Wöginger A. Processing technologies for continuous fibre reinforced thermoplastics with novel polymer blends. Composites Science and Technology 2003;63(14):2099–110.

[34] TenCate Advanced Composites. Tencate material that make a difference: Current applications and new developments in Cetex thermoplastic composites; 2009.

[35] Ulaga T, Meier U. Kohlenstofffaserverstärkte thermoplastische Lamellen für die Verstärkung von Betontragwerken. Rapperswil; 2003.

[36] McCool R, Murphy A, Wilson R, Jiang Z, Price M. Thermoforming of Continuous Fibre Reinforced Thermoplastic Composites. In: The 14th international Esaform conference on material forming: Esaform 2011, Belfast, (United Kingdom), 27–29 April 2011.

[37] Ye L, Lu M, Mai Y. Thermal de-consolidation of thermoplastic matrix composites—I. Growth of voids. Composites Science and Technology 2002;62(16):2121–30.

[38] Kenny JM, Maffezzoli A. Crystallization kinetics of poly(phenylene sulfide) (PPS) and PPS/carbon fiber composites. Polymer Engineering and Science 1991;31:607–14.

[39] TenCate Advanced Composites. Processing guidelines for Cetex thermolite PPS unitape thermoplastic composite materials.

[40] Fröhlich P, Zaremba S, Ladstätter E, Drechsler K. Untersuchungen zum Temperieren dickenvariabler Organobleche durch IR-Strahlung für den Thermoformprozess. Zeitschrift Kunststofftechnik. eingereicht 27.07.2015

[41] Lahr R. Partielles Thermoformen endlosfaserverstärkter Thermoplaste. Dissertation. Kaiserslautern; 2007.

[42] Abbassi F, Elfaleh I, Mistou S, Zghal A, Fazzini M, Djilali T. Experimental and numerical investigations of a thermoplastic composite (carbon/PPS) thermoforming. Struct. Control Health Monit. 2011;18(7):769–80.

[43] Han P, Butterfield J, Price M, Murphy A, Mullan M. Part form prediction methods for carbon fibre reinforced thermoplastic composite materials_Belfast2010. In: 18th International Conference on Composite Materials.

[44] Thermoplastic composite gain leading edge on the A380; 2006.

[45] Deters A, Miaris A, Soehner G. Serial production of thermoplastic CFRP parts for Airbus A350 XWB. In: Borgmann H, editor. Conference proceedings: WFB Wirtschaftsförderung Bremen GmbH, p. 60–3.

[46] Gohl W. Ein Betrag zum Verständis des mechanischen Verhaltens von Thermoplast-Teilen. Dissertation. Stuttgart; 1968.

[47] Cebe P. Review of recent developments on Poly(phenylene sulphide). Polymers & Polymer Composites 1995;3.

[48] Huo P, Cebe P. Effects of thermal history on the rigid amorphous phase in poly(phenylene sulfide). Colloid Polymer Science 1992(270):840–52.

[49] Groß H. Untersuchungen zum Thermoformen teilkristalliner Thermoplaste. Dissertation. Aachen; 1983.

[50] Deporter J, Braird DG. The effects of thermal history on the structure/property relationship in polyphenylenesulfide/carbon fiber composites. Polymer Composites 1993;14:201–13.

[51] Hou M. Zum Thermoformen und Widerstandsschweißen von Hochleistungsverbundwerkstoffen mit thermoplastischer Matrix. Dissertation. Kaiserslautern; 1993.

[52] Spruiell JE, Janke CJ. A review of the measurement and development if crystallinity and its relation properties in neat poly(phenylene sulfide) and its composites.

[53] Biron M. Thermoplastics and Thermopalstic Composites: Technical information for plastics users: Elsevier Science & Technology; 2007.

[54] Jog JP, Nadkarni VM. Crystallization kinetics of polyphenylene sulfide. Journal of Applied Polymer Science 1985;30:997–1009.

[55] Auer C, Kalinka G, Krause T, Hinrichsen G. Crystallization kinetics of pure and fiber-reinforced poly(phenylene sulfide). Journal of Applied Polymer Science 1994(51):407–13.

[56] Long Y, Shanks RA, Stachurski ZH. Kinetics of polymer crystallization. Progress in Polymer Science 1995;20(4):651–701.

[57] Parlevliet PP, Bersee HE, Beukers A. Residual stresses in thermoplastic composites—A study of the literature—Part I: Formation of residual stresses. Composites Part A: Applied Science and Manufacturing 2006;37(11):1847–57.

[58] TenCate Advanced Composites. CETEX - PPS Guide Lines.

[59] Day M, Budgell DR. Kinetics of the thermal degradation of poly(phenylene sulfide). Thermochimica Acta 1992(203):465–74.

[60] Ning H, Vaidya U, Janowski GM, Husman G. Design, manufacture and analysis of a thermoplastic composite frame structure for mass transit. Composite Structures 2007;80(1):105–16.

[61] Langeheinecke K (ed.). Thermodynamik für Ingenieure: Ein Lehr- und Arbeitsbuch für das Studium. 6th ed.: Vieweg Fachbücher der Technik.

[62] Watlow Electric Manufacturing Company. Radiant heating with infrared: A technical user guide to understanding and applying infrared heaters; 1997.

[63] Baehr HD, Stephan K. Wärme- und Stoffübertragung. Berlin, Heidelberg: Springer Berlin Heidelberg; 2010.

[64] Ehlert JR, Smith TF. View factors for perpendicular and parallel rectangular plates. Journal of Thermophysics and Heat Transfer 1993;7(1):173–5.

[65] Weigand B, Wolfersdorf J von. Wärmeübertragung: Manuskript zur Vorlesung. Stuttgart; 2002.

[66] Herwig H, Moschallski A. Wärmeübertragung: Physikalische Grundlagen - Illustrierende Beispiele - Übungsaufgaben mit Musterlösungen. 2nd ed. Wiesbaden: Vieweg + Teubner; 2009.

[67] Deutsches Institut für Normung e.V. Faserverstärkte Kunststoffe, Bestimmung der Biegeeigenschaften(14125); 1998.

[68] Department of defense handbook - Composite Materials Handbook: Volume 1. Polymer matrix composites guidelines for characterization of structural materials; 2002.

[69] Deutsches Institut für Normung e.V. Luft- und Raumfahrt, Kohlenstoffaserverstärkte Kunststoffe, Unidirektional Laminate, Bestimmung der scheinbaren interlaminaren Scherfestigkeit(2563); 1997.

[70] ASTM International. Standard test method for measuring the curved beam strength of a fiber-reinforced polymer-matrix composite(D 6415/D 6415M).

[71] Deutsches Institut für Normung e.V. Thermal analysis (TA) - Terms(51005); 2005.

[72] Deutsches Institut für Normung e.V. Thermische Analyse Dynamische, Dynamische Differenzkalorimetrie (DKK)(53765); 1994. [April 29, 2014].

[73] Parlevliet PP, van der Werf, Wouter A.W., Bersee HE, Beukers A. Thermal effects on microstructural matrix variations in thick-walled composites. Composites Science and Technology 2008;68(3-4):896–907.

[74] Ticona. Ticona Celstran CFR-TP PPS CF60-01: Preliminary data.

[75] TenCate Advanced Composites. Product data sheet Semi-preg carbon PPS 5-harness satin. CD 0286 050 030 8538 43000.

[76] Ye L, Chen Z, Lu M, Hou M. De-consolidation and re-consolidation in CF/PPS thermoplastic matrix composites. Composites Part A: Applied Science and Manufacturing 2005;36(7):915–22.

[77] TenCate Advanced Composites. Press forming of Cetex Continuous fiber reinforced thermoplastics.

[78] TenCate Advanced Composites. Technical data CETEX Thermolite TC1100 PPS Resin System.

[79] Specht E. Grundlagen der Wärme- und Stoffübertragung: Vorlesungsmanuskript. Magdeburg; 2008.

[80] Howell JR. Catalog of radiation configuration factors: McGraw-Hill; 1982.

[81] Polifke W, Kopitz J. Wärmeübertragung: Grundlagen, analytische und numerische Methoden. 2nd ed. München: Pearson Deutschland; 2009.

[82] Hexcel. HexTow IM7 Carbon Fiber: Product data sheet.

[83] Cytec engineerd materials. CYCOM PR520 RTM resin system: Technical data sheet.

[84] Hexcel. HexPly 8551-7 Epoxy matrix: Product data sheet.

[85] TenCate Advanced Composites. CETEX TC 1200: Technical data sheet.

[86] Mitschang P, Grebel K. Zykluszeitverkürzung bei der Verarbeitung von FVK durch den Einsatz variothermer Werkzeuge. Kaiserslautern.